Geodesics and Shadows of Rotating Black Holes

By

Sumarna Haroon

(Registration No: NUST201490220PSNS7114F)

A thesis submitted to National University of Sciences and Technology, Islamabad
in partial fulfillment of the requirements for the degree of

Doctor of Philosophy in
Mathematics

Thesis Supervisor: Prof. Azad A. Siddiqui

Co-Supervisor: Dr. Mubasher Jamil

Department of Mathematics,
School of Natural Sciences,

National University of Sciences and Technology (NUST),
Islamabad, Pakistan.
(2022)

THESIS ACCEPTANCE CERTIFICATE

Certified that final copy of PhD thesis written by **Sumarna Haroon**, (Registration No. **NUST201490220PSNS7114F)**, of **School of Natural Sciences** has been vetted by undersigned, found complete in all respects as per NUST statutes/regulations/PhD policy, is free of plagiarism, errors, and mistakes and is accepted as partial fulfillment for award of PhD degree. It is further certified that necessary amendments as pointed out by GEC members and foreign/local evaluators of the scholar have also been incorporated in the said thesis.

Signature: _____

Name of Supervisor: Prof. Azad A. Siddiqui

Date: 03/02/2022

Signature (HoD): _____

Date: 03/02/2022

Signature (Dean/Principal): _____

Date: 03.02.2022

Form PhD-7 (Revised)
DOCTORAL PROGRAMME
OF STUDY
(Must be type written)

National University of Sciences & Technology
REPORT OF DOCTORAL THESIS DEFENCE

Name: Sumarna Haroon NUST Regn No: NUST201490220PSNS7114F

School/College/Centre: NUST – SCHOOL OF NATURAL SCIENCES (SNS)

DOCTORAL DEFENCE COMMITTEE

Doctoral Defence held on **03 February, 2022 (Thursday) at 1100 hrs**

	QUALIFIED	NOT QUALIFIED	SIGNATURE
GEC Member-1: Prof. Tooba Feroze	✓		
GEC Member-2: Dr. Hussain Gohar	✓		
GEC Member *(External)*: Dr. Ibrar Hussain	✓		
Supervisor: Prof. Azad A. Siddiqui	✓		
Co-Supervisor *(if appointed)*: Dr. Mubashir Jamil	✓		
External Evaluator-1: Dr. Zahid Ahmad (Local Expert)	✓		
External Evaluator-2: Prof. Muhammad Sharif (Local Expert)	✓		
External Evaluator-3: Dr. Rueda Hernadez Jorge Armando (Foreign Expert)			
External Evaluator-4: Dr. Yi-Fu Cai (Foreign Expert)			

FINAL RESULT OF THE DOCTORAL DEFENCE
(Appropriate box to be signed by HOD)

NOT PASS FAIL

The student Sumarna Haroon Regn No NUST201490220PSNS7114F is / ~~is NOT~~ accepted for Doctor of Philosophy Degree.

Dated: 03.02.2022

Dean/Commandant/Principal/DG

Distribution:
1 x copy each for Registrar, Exam Branch, Dir R&D, Dir Acad Jat HQ NUST, HoD, Supervisor, Co-Supervisor (if appointed), one for student's dossier at the School/College/Centre and copy each for members of GEC.

Note:
* Decision of External Evaluators (Foreign Experts) will be sought through video conference, if possible, on the same date and their decision will be intimated (on paper) to HQ NUST at a later date.

CERTIFICATE OF APPROVAL

This is to certify that the research work presented in this thesis entitled **"Geodesics and Shadows of Rotating Black Holes"** was conducted by **Sumarna Haroon** under the supervision of **Prof. Azad A. Siddiqui.**

No part of this thesis has been submitted anywhere else for any degree. This thesis is submitted to the **School of Natural Sciences** in partial fulfillment of the requirements for the degree of Doctor of Philosophy in Field of **Mathematics** Department of **Mathematics, School of Natural Sciences (SNS)** University of **National University of Sciences and Technology, Islamabad, Pakistan.**

Student Name: **Sumarna Haroon** Signature: _____

Examination Committee:

a)	**External Examiner:**		
	Name	Dr. Zahid Ahmad	
	Designation	Associate Professor	
	Official Address	COMSATS Institute of Information Technology, Abbottabad, Pakistan	Signature

b)	**External Examiner:**		
	Name	Dr. Muhammad Sharif	
	Designation	Professor	
	Official Address	Department of Mathematics, University of the Punjab, Lahore-54590, Pakistan	Signature

c)	**Internal Examiner:**		
	Name	Prof. Tooba Feroze	
	Designation	Professor	
	Official Address	NUST-SNS	Signature

Supervisor Name: **Prof. Azad A. Siddiqui** Signature: _____

Name of HoD: **Dr. Meraj Mustafa Hashmi** Signature: _____

AUTHOR'S DECLARATION

I, **Sumarna Haroon** hereby state that my PhD thesis titled **Geodesics and Shadows of Rotating Black Holes** is my own work and has not been submitted previously by me for taking any degree from this University

"National University of Sciences and Technology"

Or anywhere else in the country / world.

At any time if my statement is found to be incorrect even after my Graduation the university has the right to withdraw my PhD degree.

Name of Student: Sumarna Haroon

Signature: Sumarna

Date: 03-02-2022

Anx-P

PLAGIARISM UNDERTAKING

I solemnly declare that the research work presented in the thesis titled **"Geodesics and Shadows of Rotating Black Holes"** is solely my research work with no significant contribution from any other person. Small contribution/help wherever taken has been duly acknowledged and that complete thesis has been written by me.

I understand the zero-tolerance policy of the HEC and University,

National University of Sciences and Technology

towards plagiarism. Therefore I as an author of the above titled thesis declare that no portion of my thesis has been plagiarized and any material used as reference is properly referred/cited.

I undertake that if I am found guilty of any formal plagiarism in the above titled thesis even after of Ph.D. degree, the University reserves the rights to withdraw/revoke my Ph.D. degree and that HEC and the University have the right to publish my name on the HEC/University Website on which names of students are placed who submitted plagiarized thesis.

Student / Author Signature: Sumarna

Name: **Sumarna Haroon**

Dedicated

to

my Husband

Acknowledgment

Many thanks to Allah Almighty for providing me with best of his resources and opportunities which eventually led me to understand a fraction of His marvelous creation – The Universe.

I would like to present my deepest gratitude to

My Supervisor **Prof**. **Azad A**. **Siddiqui** for his suggestions and healthy criticism especially during the writeup of this thesis.

My Co-supervisor, **Dr**. **Mubasher Jamil**, for his constant guidance regarding my research work.

My Guidance and Examination Committee (GEC) members,**Prof**. **Tooba Feroze**, **Dr**. **Ibrar Hussain** and **Dr**. **Hussain Gohar** for their valuable comments and suggestions.

All those who taught me Mathematics and Physics.

My parents who always encouraged me to remain consistent no matter what hardships come in way and supported me in all ups and downs of life.

My elder sister **Shanza Haroon** for teaching me so much in life.

My brother **Faizan Haroon** for keeping me mentally insane during my stay in Canada.

My brother **Farhan Haroon** for consoling me and giving me a ray of hope with his valuable advices.

My **Mother** − **in Law** and **Father** − **in Law** for their unconditional love and support, which I cannot repay them in anyway. They introduced me to the value and strength a relationship can bring.

My **brothers** and **sisters in Law** for their never ending support and encouragement.

My best friend **Rehana Rahim** for her valuable feedback on my work.

My husband who never gave up on me even when I had lost all hope. He was the photon in my darkest time. Without his support I would never have been able to come that far.

Last but not least, my son **Arham** for making me smile in my hardest times and my daughter **Rumaysa** for waking me up at night so I could study.

Abstract

We first investigate the consequences of running gravitational coupling on certain properties of rotating black hole. We are motivated by the functional form of gravitational coupling previously investigated in the context of infra-red limit of asymptotically safe gravity theory. In this approach, the involvement of a new parameter $\tilde{\xi}$ in this solution makes it different from Schwarzschild black hole. The Killing horizon, event horizon and singularity of the computed metric is then discussed. It is noticed that the ergosphere is increased as $\tilde{\xi}$ increases. Considering the black hole in equatorial plane, the geodesics of particlesare explored. The effective potential is computed and graphically analyzed for different values of parameter $\tilde{\xi}$. Apart from the changes induced in the space-time structure of such black holes, we also study the implications to Penrose process and geodetic precession. The energy extraction from black hole is investigated via Penrose process. For the same values of spin parameter, the numerical results suggest that the efficiency of Penrose process is greater in asymptotically safe gravity than in Kerr Black Hole. At the end, a brief discussion on Lense-Thirring frequency is also done.

A black hole's spacetime is remarkably affected by presence of dark matter around it. We analyze the shadow of a new solution to Einstein Field Equations and consider the effects of dark matter on it. This solution describe a rotating

black hole in the background of perfect fluid dark matter, along with its extension to nonzero cosmological constant Λ. Working in Boyer-Lindquist coordinates, we consider the effects of the perfect fluid dark matter parameter α on the shadow cast by a black hole with respect to an observer at position (r_o, θ_o).

Global monopoles are topological defects which may have been produced during the phase transitions in the early universe. In fact, global monopoles are just one type of topological defects. Other types of topological objects are expected to exist including domain walls and cosmic strings. A metric for rotating dyonic black hole with global monopole in presence of perfect fluid is computed in this work. We then discuss its surface topology at the event horizon using Gauss-Bonnet Theorem and also the ergoregion. We investigate the shadows of the rotating dyonic black hole. Choosing certain values of parameters, such as $\omega = -1/3, 0, 1/3$, we observe the effect of dark matter, dust and radiation on the silhouette of the black hole. Our findings lead us to conclude that the presence of parameters γ and α, also deforms the shape of black hole's shadow. These results have been depicted through graphical representation. We also analyze the two observables, radius R_s and distortion δ_s, related to black hole's shadow. Energy emission rate of rotating dyonic black hole with global monopole surrounded by perfect fluid is also computed and graphically illustrated with respect to parameters.

List of Publications

As publication is one of the requirements of the Higher Education Commission of Pakistan, we give here a list of publications from the thesis:

- S. Haroon, M. Jamil, K. Lin, P. Pavlovic, M. Sossich and A. Wang, The effects of running gravitational coupling on rotating black holes, The European Physical Journal C, **78** (6) 2018.
- S. Haroon, M. Jamil, K. Jusufi, K. Lin, R. B. Mann, Shadow and deflection angle of rotating black holes in perfect fluid dark matter with a cosmological constant, Physical Review D, **99** (4) 2019.
- S. Haroon, K. Jusufi, M. Jamil, Shadow Images of a Rotating Dyonic Black Hole with a Global Monopole Surrounded by Perfect Fluid, Universe, **6** (4) 2020.

Contents

List of Figures

List of Abbreviations

ASG	Asymptotically Safe Gravity
BBH	Binary Black Hole
BH	Black Hole
DM	Dark Matter
EFE	Einstein's field Equations
GTR	General Theory of Relativity
GW	Gravitational Wave
KBH	Kerr Black Hole
PFDM	Perfect Fluid Dark Matter
RBH	Rotating Black Hole
RDBH	Rotating Dyonic Black Hole
SBH	Schwarzschild Black Hole

Chapter 1

Introduction

Black holes (BHs) are one of the strangest cosmic bodies present in outer space which have drawn immense attention from scientists due to their fascinating properties. Interestingly, a BH is formed when a massive star gravitationally collapses inwardly. Consequently, a region of great density and extremely strong gravity is formed from whose boundary, called event horizon, not even light can escape.

Indeed, formation of a BH occurs when an astronomical object having mass M gravitationally collapses and consequently contracts to a point that its size crosses gravitational radius $r_g = 2GM/c^2$, also known as Schwarzschild radius, here G is Newton's gravitational constant, and c is the speed of light. Further what happens is that the escape velocity required to break away the boundary of BH gets equals to c. Since c is the maximum limit on the propagation velocity for physical signals this leads to an obvious conclusion that neither signals nor particles are able to escape from a BH. Mass of the gravitating body characterizes as gravitational charge and vitally participates in the gravitational interaction. The particles, be it massive or massless, cannot escape from a BH instead the one bypassing it ends

up falling into it thus defining a boundary called the event horizon [1].

Conceptually, the foundations of BH's study were set by the end of 18th century when Michell and Laplace gave the possibility of existence of such objects using Newtonian theory [1,2]. But it was not until the emergence of General Theory of Relativity (GTR) , formulated by Einstein in 1915, that theorist got solid grounds to claim the physical existence of such mysterious objects.

The core idea of Einstein's GTR lies in geometry of four dimensional spacetime. It features gravitation to be the geometrical entity emerging from a curved four dimensional spacetime rather than just a force. For Einstein, gravitation was not a force defined by per square distance but a geometrical curvature of space time. Einstein defined this geometrical curvature through his famous Einstein's field Equations (EFE) :

$$\mathcal{R}_{\mu\nu} - \frac{1}{2} g_{\mu\nu}\mathcal{R} + g_{\mu\nu}\Lambda = 8\frac{\pi G}{c^4} T_{\mu\nu}, \tag{1.1}$$

where Ricci tensor is $\mathcal{R}_{\mu\nu}$, Ricci scalar is $\mathcal{R}$, the gravitational field is shown by the metric tensor $g_{\mu\nu}$, cosmological constant is Λ and $T_{\mu\nu}$ is the energy-momentum tensor. On the left of EFE lies the information about the geometry of spacetime under study while on right lies the terms having knowledge of matter distribution.

Not even a year had passed to the formulation of GTR, when Einstein received a letter from his former colleague turned soldier, Karl Schawarzschild, enclosing first ever exact solution of EFE [3]. Einstein's response to this solution was *"I had not expected that one could formulate the exact solution of the problem in such a simple way."* This solution, named after Schwarzschild himself, describes gravitational field of an uncharged non-spinning spherical body. Little was known that this solution will explain the structure of chargeless non-rotating BH, thus setting foundation for a whole new branch of Physics: Black Hole Physics.

To achieve deep understanding of physical aspects of EFE's solution, it is bene-

ficial to mathematically explore the motion of test particles and light rays in these spacetimes. Such a study has both observational and fundamental importance. From observational point of view, matter and light are two observable quantities which can give clear insight to the physical behavior of a given gravitational field. From fundamental point of view, the study of motion of light or matter around some gravitating body can not only help in classifying a given spacetime but also can highlight its characteristics and thus decode its structure.

With the discovery of Schwarzschild's solution to these EFE, the next obvious interest arose in studying motion of massless or massive particles in vicinity of the static and spherically symmetric background. In 1931, Hagihara was able to analytically compute geodesic equations in Schwarzschild spacetime [4]. He used theory of elliptic functions and carried an extensive study on timelike geodesics as well as null geodesics. In 1918, another exact solution of EFE in presence of an electrical charge of the gravitating body was derived by Reissner and Nordström [5,6]. The method adopted by Hagihara for the computation of geodesics can be used to discuss geodesics of Reissner-Nordström spacetime.

In 1918, Lense and Thiring [7], working under the framework of GTR, found an additional effect associated to slight distortion of geodesics of a rotating massive object. Not hosted by Newtonian Theory, this effect, also known as *frame dragging*, solely comes from GTR and is considered to be a prominent feature of rotating astronomical objects. In 1963, Roy Patrick Kerr was able to figure out the exact solution of a stationary and axially symmetric spacetime [8]. Later, Carter [9,10] explored the structure of Kerr solution and was able to establish a fourth constant of motion, named Carter constant, by determining the separability of the Hamilton-Jacobi equations. By eighties, extensive studies were done on geodesics of BHs, especially Kerr BH. In 1983, Chandrasekhar compiled, analyzed and enhanced the work of many authors in his book [11].

The study of geodesics for null (photon) and time-like (massive) particles, has always held a significant importance. The analysis of circular motion of particles in a curved space time exhibits its geometrical behaviour . A detail study of null, time-like and space-like geodesics is done in [12] for certain BHs. Geodesics of some BHs spacetimes with cosmological constants is comprehensively investigated by Hackmann [13]. Equatorial geodesics are studied in [14, 15].

On theoretical grounds, Einstein's GTR not only predicted the existence of BHs, but also provided mathematical tools to directly observe them. Synge was the first to propose the apparent shape of a spherically symmetric BH [16]. Synge effectively identified that a photon sphere, enclosing a compact spherical body, would cast a shadow on the observer's sky. For a circular shadow having angular radius ρ, he computed an expression given by

$$\sin^2 \rho = \frac{27}{4} \frac{(\rho_o - 1)}{\rho_o^3} \tag{1.2}$$

where for observer's radial position r_o, $\rho_o = r_o/(2m)$.

In 1973, the shadow of a KBH was first studied by Bardeen [17]. Bardeen's distant observer is suitable for describing the shape of the shadow. According to his findings, for a rotating black hole (RBH) the shadow is no longer circular but rather flattened on one side. After that Luminet [18] discussed the appearance of a SBH surrounded by an accretion disk. These initial works on shadow images of BHs not only gave theorists new grounds to extend their investigations but also arose the interest among astrophysicists to physically explore such compact objects. After seventies, the astrophysical importance of BHs became inevitable. J. P. Luminet [19] recalls in detail the struggles faced and steps taken on the road to imaging a BH, between years 1972 to 2002.

With time, the astrophysical advances also motivated many authors to invest qualitatively in theoretical analysis of BH shadows. A de Vries [20] investigated

the shapes of various Kerr Newmann spacetimes considering the geometry of the closed photon orbits. Hioki and Maeda [21] introduced two observables which characterized the apparent shape of a KBH. In same paper, they also broaden their technique to study naked singularity. A. Abdujabbarov et. al. [22] studied the shadow of a spinning BH with gravitomagnetic charge and observed that apart from angular momentum the presence of gravitomagnetic charge is also responsible for the deformation in the apparent shape of BH's shadow. L. Amarilla et. al. [23] studied the shadow casted by RBH in Chern Simons modified gravity. This model is developed by introducing to the Hilbert Einstein action a scalar field that couples to the first class Pontryagin density. It was concluded in [23] that in presence of Chern Simons parameter the shape of the shadow of RBH is thus deformed. L. Amarilla and E. F. Eiroa [24], in the Randall-Sundrum scenario, computed the shadow of a rotating braneworld BH. Their observation was that the tidal charge term does effect the shape of the BH's shadow such that an enlarged shape of the shadow is obtained in presence of the negative tidal charge while the effect is opposite when the tidal charge is positive. The same authors in [25] considered the shadow for a Kaluza-Klein rotating dilaton BH and concluded that mass and charge also play role in deforming the shape of the shadow. Wei and Liu [26] showed that parameters involved in Einstein-Maxwell-Dilaton-Axion BH significantly effect the shape of its shadow. Not only BHs but also shadow of Kerr-like wormholes as well as traversable wormholes and many more, have been of great interest for the researchers too [27–35]. Some authors have also tried to test theories of gravity by using the observations obtained from shadow of Sgr A* [36–39]. An effective overview by Cunha and Heidro [40] gives a considerable insight to the theoretical aspects of shadows of BHs in both GTR and Alternative Theories of Gravity.

The question that whether dark matter is strong enough to deform the geometry

of BH is currently revolving among inquisitive minds. The influence of dark matter halo, particularly Scalar Field Dark Matter and Cold Dark Matter models, around Sgr A* was investigated by Hou et. al. [47]. The shadow of BH in the presence of quintessence has been discussed in [48,49]. The characteristic features of the dark matter– its effective mass and non interaction with electromagnetic field–were implied by Konoplya [50]. By a robust analysis, he concluded that for a galactic BH it is unlikely for a dark matter to affect the shadow's shape unless it is highly concentrated near the BH. Another interesting dark model was consider by Jusufi et. al. [51] in M87 galactic center and images of its shadow were identified. It is anticipated that the effect of dark matter on the apparent shadow shape can shed some light in future observations as an indirect way to detect dark matter using the shadow images [51].

In 1919, Eddington successfully performed the first experiment to test the correctness of GTR. That time when Einstein was asked about what if the physical results came against his theoretical findings, Einstein's promptly replied "*I will be sorry for the good Lord but the theory is correct*". Even after hundred years, on April 10th, 2019, GTR firmly stood its ground when the first image of BH was publicly announced by Event Horizon Telescope (EHT) Collaboration.

Long had been known that our neighbouring elliptical galaxy M87 accommodates a massive and bright radio source (a BH) at its core. According to GTR, the presence of a massive body (e.g. a BH) in a spacetime generates curvature, which bends the paths of photons ultimately forming null geodesics in curved spacetime. By studying these geodesics around BHs it is observed that photons can be absorbed or escape from a BH [40]. Simply put, a boundary is defined between these two categories of light-like geodesics, giving rise to a dark region known as the *shadow*. Presence of M87 relatively less distant to our galaxy provided an excellent opportunity to capture image of BH's shadow at exquisite resolution [52,53].

The image observed by EHT [52] was consistent with Kerr BH, as predicted by GTR. Based on the information collected, the observed BH has mass $M = (6.5 \pm 0.7) \times 10^9 (\mathrm{M}_\odot)$ and spins away from us i.e. it rotates in clockwise direction. This data has unlocked new paths and eventually may enable us to test GTR in strong-field regime.

Another ground breaking discovery to be mentioned here is detection of gravitational wave (GW) signal dubbed GW150914, in 2015 [41]. This was done by a United States based observatory named Laser Interferometry Gravitational-Wave Observatory LIGO. The birth of this wave signal was due to merger of a pair of stellar mass BHs. The key features of GW150914 were in alliance to numerically generated simulations of inspiral, merger and ringdown phases of waveform templates. The data obtained from this marvelous detection acted as a compelling evidence of binary black hole (BBH) system blending to form a single BH thus giving rise to GW astronomy as an observational science. These observations not only play vital role in understanding unique properties of spacetime in strong-field regime and high velocity regime but also confirms the predictions of GTR regarding BHs dynamics.

In 2017, the LIGO- Virgo collaboration detected another GW signal(GW170817) formed by coalescing of a pair of neutron stars [54]. Approximately 1/7th of a second after the detection of GW170817 followed gamma ray burst (GRB 170817A). Through extensive observations along electromagnetic spectrum the optical transient of GRB 170817A was detected [55]. This was the first time that both gravitational and electromagnetic waves were observed from a single source-making it a first of its kind discovery in the field of multimessenger astronomy. This also gave another evidence in favour of GTR: the postulate that GW emitting from their source propagates outwards with speed of light.

Furthermore LIGO-Virgo collaboration observed in total ten GW signals during

the first two runs. Out of these ten signals, nine were concluded to be compatible with those generated by BBH system, and the other with binary neutron star (BNS) merger [56]. Recently, Advanced LIGO and Advanced Virgo have publicly released the results collected in the first half of the third observing run $(O3a)$– between 1st April 2019 to 1st October 2019 [42]. This current study has reported 39 events as a host to GW emission, showing consistency with the coalescence of BBHs, BNS and NS-BH binaries.

The images of $M87^*$ by EHT collaboration and detection of GW are altogether a break through in astrophysics. These discoveries have reignited the faith in GTR as well developed a never ending interest in gravitational physics. The images of another BH named Sagittarius A^*, this time hosted by our very own galaxy– the Milky way, is expected soon too. This and some other undergoing GW missions (e.g. KAGRA, LISA and others [57]) make us living on the verge of an inquisitive yet intriguing new era of highly precise tests related to extreme gravity and gravitational waves physics.

Mathematically, the methods used for computing shadows of BHs is more or less the same in all cases. An observer is placed at a very large distance (effectively infinity) away from the BH, and it is from the viewpoint of this observer that the shadow is determined; typically celestial coordinates are introduced. For asymptotically flat BHs these methods are fine, but in the presence of a cosmological constant there is an additional subtlety in that the position of the observer needs to be fixed.

Grenzebach et al. [64, 65] derived a promising analytical formula to deduce shadow of a BHs lying in Pleba$\tilde{n}$ski- Demia$\tilde{n}$ski class. Basically, they assumed that the observer at finite position having four-velocity as linear combination of ∂t and $\partial\phi$. The shadow can then be calculated using the standard aberration formula [66] for observers with any other four-velocities. The solution to KBH is

considered as a particular case in the work by [67] to compute an approximate formula that permits extraction of spin of the BH from the shape of its shadow. By examining the shadow of a BH and naked singularity it is now possible to distinguish between the two. This was suggested and proved by Hioki and Maeda in [21] in which they also provided a technique to measure the spin and angle of inclination by defining two observables.

We intend here to use techniques recently employed in [68] for computing the shadow of a RBH with cosmological constant. We begin by fixing the location of the observer in Boyer-Lindquist (BL) coordinates (r_0, θ_0), the respective radial and polar angular coordinates of the observer. Instead of considering photon rays coming from past, we follow them from the location (r_0, θ_0) to the past. The behaviour of light-like geodesics can be characterized into two categories: those that venture so close to the outer horizon $r = r_+$ of the BH that they are absorbed by it due to the gravitational pull, and those that ultimately escape to their original source in the past. Thus a boundary is defined, between these two categories of light-like geodesics, which encloses a dark region called the *shadow*.

With all the technological and theoretical development around us, it is now a golden time to carry on studying shadows of BHs and the effect of their parameters (especially spin) on them. The astrophysical BHs depends solely on their electrical charge Q, mass M and angular momentum $J = aM$ (which is particularly in direct relation with spin a of a BH). Astronomically, a spinning BH has tremendous importance since its spin stores enormous amount energy with a fossil record about how the BH formed and grew. For example, it is still a mystery that how supermassive BHs are formed in the early Universe, by investigating that whether these BHs are highly spinning or not enables one to differentiate between the scenarios responsible for the their formation i.e. from BH mergers or coherent disk accretion [43].

Further, the BH's spin also acts as the potent source of energy for emission of relativistic jets [60]. In Newtonian frame work, the Universal Law of Gravitation contains only mass of a body with no information on the gravitational effects if the body is spinning. Whereas in GTR, the characteristics of a rotating massive bodies is somewhat analogous to a rotating charge in electrodynamics. For example, the spin changes the position of the event horizon [46]. The spin of a BH considerably affects shape of its shadow too.

In GTR, the geometry of chargeless RBH is described by Kerr metric. The Kerr BH can be completely specified by its mass M and angular momentum J. By unlocking these two parameters, all the properties of spacetime geometry can be known. However it is a difficult task to calculate the spin of a BH since it has no effect in Newtonian gravity and therefore it is necessary to probe the spacetime close to the object [46].

BHs are formed due to the gravitational collapse of a star. In our Galaxy, the expected number of BHs is about 10 Million. However, we know of only 20 stellar mass BH candidates, living in X-ray binaries [136]. BH X-ray binaries are classified into two categories: Low mass X ray binaries have stellar companion of only few solar mass ($\lesssim 3M_{\odot}$) and High-mass X-ray binaries have massive stellar companion ($\gtrsim 10M_{\odot}$). Theoretically assuming the BH candidate satisfying characteristics of a KBH, the spin is measured nearly equal to unity. Black holes having spin close to 1 are considered a rapidly RBHs. However the reason behind such a high spin values is still not understood [46]. In [58], the authors conclude for a low-mass X-ray binary source GRS $1915+105$ is fast rotating KBH with minimum spin value $a > 0.98$. In the case of high-mass X-ray binary Cygnus X-1 the lowest spin is $a > 0.983$. The spin of supermassive BHs in active galactic nuclei evolves somewhat differently since their mass is increased by several orders from its initial value. In case of random merger of two BHs, the most probable final

product is a BH with $a \approx 0.69$ while fast rotating objects with $a > 0.9$ should be rare [59]. Accretion from a disk can potentially be a very efficient way to spin a compact object up [60] .

It is usually assumed that Einstein's GTR is valid only as an effective theory of gravity. According to this picture, GTR can be taken as a correct description of gravitational interaction only up to certain scales of energy and characteristic distances. When they get comparable to Planck scale the theory is expected to break, and to be replaced with a completely different physical model. This reasoning seems to be supported by the well known fact that the Einstein-Hilbert action, leading to the field equations of GTR, is perturbative non-renormalizable [76]. The problem of finding a consistent theory of quantum gravity remains to be the central challenge in theoretical physics. During the past decades different approaches and perspectives on this issue were developed, such as loop quantum gravity [69,70], string theory [71,72], and effective approaches of modified gravity theories [73–75]. These attempts also addressed various problems of cosmology and astrophysics, including DE and DM problem, the horizon problem, as well as the singularities of GTR. All of these problems are connected to the potential limitations of Einstein's GTR, and are therefore important motivation and reference in the investigation of quantum gravity.

However, Weinberg proposed a new nonperturbative notion of renormalizibility which is called "asymptotic safety" [77], based on the existence of a nontrivial fixed point in renormalization group, which makes the physical couplings of the theory non-divergent. The basic assumption of Weinberg's proposal was that gravity can meet this criteria, and thus its description can be considered as a consistent field theory on all scales. A review and discussion of attempts to prove the existence of this fixed point for gravity can be found in [78]. In the perspective of research on quantum gravity, it is of special interest to consider the consequences

of the asymptotically safe gravity (ASG) picture on the well known physical systems, which are in principle also accessible to observations. Black holes are a good example of such system, where the corrections to standard description of gravity could be important. Black holes in ASG were previously studied in [79–88].

In this work we continue the investigation of BHs in ASG, considering the RBH solutions, and focusing on the functional form of gravitational coupling inspired by the potential infra-red limit of the theory, due to its observational relevance. Previous to this work the quantum gravity effects in the Kerr spacetime were studied in [90], where the structure of horizons, the ergosphere, the Penrose process and the static limit surfaces were investigated considering the generalization of gravitational constant to a general function of radial coordinate, $G(r)$ – that comes as a result of quantum effects. In this work we extend the analysis performed in [90].

A rotational sphere with electric charge generates magnetic field. Similarly, it is expected that a RBH, or a massive star, also produces “magnetic effect" of gravity according to modern gravitational theory. Such phenomenon is known as Lense-Thirring effect which was firstly proposed by Lense and Thirring in 1918 [7]. In this work, we also investigate the Lense-Thirring effect for the RBH considering the varying Newtonian coupling.

The Standard model of cosmology suggests that our universe is compiled of 27% DM and 68% DE, while the rest is baryonic matter. Though DM has not been directly detected, observational evidence for its existence can be found in abundance. Examples include galactic rotation curves [91], the dynamics of galaxy clusters [92], and the measurements of cosmic microwave background anisotropies obtained through PLANCK [93]. It is therefore natural to ask how BH solutions might depend on DM. Recently a generalization of the Kerr-(A)dS solution in the presence of perfect fluid dark matter (PFDM) was obtained [99]. This solution

had a number of interesting features. The size of its ergosphere decreased with increasing $|\alpha|$, where α parameterizes the strength of the DM contribution to the metric. Null circular stable orbits were shown to exist, and the dependence of the rotational velocity on α was determined. However no observational consequences of this solution were considered. Motivated by the above, we also investigate the shadow of the rotating BH in presence of PFDM [99].

Global monopoles are topological defects which may have been produced during the phase transitions in the early universe. In fact, global monopoles are just one type of topological defects. Other types of topological objects are expected to exist including domain walls and cosmic strings (e.g. [94]). More precisely, a global monopole is a heavy object characterized by spherically symmetry and divergent mass. Such objects which may have been formed during the phase transition of a system composed of a self-coupling triplet of scalar fields ϕ^a which undergoes a spontaneous breaking of global $O(3)$ gauge symmetry down to $U(1)$. The gravitational field of a static global monopole for the first time was found by Barriola and Vilenkin and are expected to be stable against spherical as well as polar perturbations [95]. According to their model, global monopoles are configurations whose energy density decreases with the distance as r^{-2} and whose spacetimes exhibit a solid angle deficit given by $\Delta = 8\pi^2\gamma^2$, where γ is the scale of gauge-symmetry breaking. Among other things, global monopoles are expected to rotate and to carry magnetic charges. Gravitational lensing by rotating global monopoles has been investigated in Ref. [96] and more recently in Ref. [97]. Thus it is worth to explore RBHs with a global monopole.

In this thesis, firstly, some theoretical aspects of varying Newtonian coupling are analyzed [61]. While focusing on a more specific setting of infra-red limit of asymptotic safe gravity, we concentrate on a specific form of $G(r)$ function,

which enables us to obtain the concrete solutions for equatorial geodesics, Penrose process, and to analyze the Lense-Thiring effect. Secondly, shadows of a RBH in PFDM with cosmological constant are obtained [62]. Our study provides a possible tool for observation of DM via shadows, perhaps using the high resolution imaging of EHT. Lastly, a comprehensive study of the impact of the rotating global monopole BH surrounded by perfect fluid on its shadow is done. For this a new metric has been formulated, using Newman-Janis algorithm with an exception of no complexification [63] (the method is also illustrated in A). This new metric has configuration of a rotating dyonic black hole (RDBH) with global monopole having perfect fluid around it. A graphical comparison between the shadow of a new metric and its Kerr counter part and the effect of new parameters on the apparent shadow shape can shed some light in future observations as an indirect way to detect characteristics of a BH using the shadow images.

This thesis consists of **six** Chapters which are separated as follows:

- *Chapter **two*** discusses the conceptual foundation of this study. This basic information come handy in better understanding of rest of the thesis.
- *Chapter **Two*** investigates the consequences of running gravitational coupling on certain properties of an RBH in ASG theory. The horizons structure and singularity of the metric is then discussed. Considering the BH solution in equatorial plane, the geodesics of particles, both null and time like cases, are explored. The effective potential is computed and graphically analyzed for different values of parameter $\tilde{\xi}$. The energy extraction from BH is investigated via Penrose process. A brief discussion on Lense-Thirring frequency is also done in the end.
- *Chapter **Four*** is based on studying the effects of DM on the shadow of an RBH

in the background of PFDM, along with its extension to nonzero cosmological constant Λ. Working in BL coordinates, we consider the effects of the PFDM parameter α on the shadow cast by a BH with respect to an observer at position (r_o, θ_o).

- *Chapter **Five*** mainly covers the computation of shadow of an RDBH with global monopole in presence of a perfect fluid. Firstly, the surface topology at the event horizon is deduced using the Gauss-Bonnet Theorem. By choosing $\omega = -1/3, 0, 1/3$ the effect of DM, dust and radiation on the silhouette of BH are then investigated. In the end, energy emission rate with respect to parameters is analyzed.
- *Chapter **Six*** is on the results obtained. It contains the conclusive remarks regarding this study.

Chapter 2

Preliminaries

In this chapter we briefly review some basic concepts of geodesic equations, RBHs and phenomenon of their imaging.

2.1 Geodesic Equations in General Relativity

One of the most pivotal topics of this thesis is the geodesic equations of motion. A geodesic is observed as a straight line on a curve manifold. It is the curved-spacetime version of the notion of *straight path* in Euclidean space. In this section, we will formally define a geodesic and derive the geodesic equation for a four dimensional spacetime, equipped with a metric $g_{\mu\nu}$. Furthermore, we will also describe the formulation of geodesic equation using Lagrangian and Hamiltonian approach. Hamiltonian Jacobi approach for computing geodesic equations of motion will also be discussed in the end of this section.

Intrinsic Derivative

Let $\mathbf{e}_\mu(u)$ be the coordinate basis vectors, on the curve $\mathfrak{C}$, corresponding to the parameter value u [98]. Then the vector field $\mathfrak{v}$ at any point along the curve is defined as

$$\mathfrak{v}(u) = \mathfrak{v}^\mu \mathbf{e}_\mu(u). \tag{2.1}$$

On taking the derivative of the above equation, we attain the form

$$\frac{d\mathfrak{v}}{du} = \frac{d\mathfrak{v}^\mu}{du}\mathbf{e}_\mu + \mathfrak{v}^\mu \frac{d\mathbf{e}_\mu}{du}. \tag{2.2}$$

With the use of result $\partial \mathbf{e}_\mu / \partial x^\rho = \Gamma^\nu_{\mu\rho}\mathbf{e}_\nu$ and applying chain rule, lead us to

$$\frac{d\mathfrak{v}}{du} = \left(\frac{d\mathfrak{v}^\mu}{du} + \Gamma^\mu_{\nu\rho}\mathfrak{v}^\nu \frac{dx^\rho}{du}\right)\mathbf{e}_\mu. \tag{2.3}$$

Let us write the term in the parentheses separately as

$$\frac{Dv^\mu}{Du} = \frac{dv^\mu}{du} + \Gamma^\mu_{\nu\rho}v^\nu \frac{dx^\rho}{du}, \tag{2.4}$$

which is the intrinsic derivative of $\mathfrak{v}$ along the curve $\mathfrak{C}$. The intrinsic derivative is often also referred as absolute derivative.

Parallel Transport

Consider an initial point O on the curve $\mathfrak{C}$ parametrised by u. Let a vector $\mathfrak{v}$ is defined at O with parameter u_o. Then vector $\mathfrak{v}$ is parallel transported throughout the curve $\mathfrak{C}$ given that the derivative of $\mathfrak{v}$ vanishes along the curve i.e.

$$\frac{d\mathfrak{v}}{du} = 0. \tag{2.5}$$

As a consequence, we are left with a "*parallel*" field of vectors at each point along $\mathfrak{C}$, generated by the parallel transport of $\mathfrak{v}$.

Thus, carrying a vector along a path such that the vector remains parallel to itself

during its transport along the curve all the while, is a concept known as *parallel transport*.

2.1.1 Geodesic Equations

In a spacetime, for a general parameter u, a geodesic can be associated with a curve $\mathrm{Y}^\mu = \mathrm{Y}^\mu(u)$. Let the tangent vector to Y^μ be $\boldsymbol{\chi}(u)$. Then geodesic can also be described as a curve parallel transported along its tangent vector i.e.

$$\frac{d\boldsymbol{\chi}}{du} = \lambda(u)\boldsymbol{\chi}. \tag{2.6}$$

Here $\lambda(u)$ is a function. Combining (2.4) and (2.5), we see that the components χ^μ of the tangent vector must satisfy

$$\frac{D\chi^\mu}{Du} = \frac{d\chi^\mu}{du} + \Gamma^\mu_{\nu\rho}\chi^\nu\frac{dx^\rho}{du} = \lambda(u)\chi^\mu. \tag{2.7}$$

The components of the tangent vector are given by $\chi^\mu = dx^\mu/du$, using this above, we obtain a set of equations, known as *geodesic equations*, as

$$\frac{d^2x^\mu}{du^2} + \Gamma^\mu_{\nu\rho}\frac{dx^\nu}{du}\frac{dx^\rho}{du} = \lambda(u)\frac{dx^\mu}{du}. \tag{2.8}$$

Geodesics are categorize as: (i) the ones corresponding to propagation of massless particles, called null geodesics, (ii) the ones corresponding to propagation of massive particles, called non-null geodesics.

Equation (2.8) is valid for both null and non-null geodesics dependent on some general parameter u. However, if the curve is reparameterised such that $\lambda(u)$ vanishes then u is termed as an affine parameter [98]. From (2.6), we see that this corresponds to a parameterisation in which the tangent vector is the same at all points along the curve (i.e. it is parallel-transported), so that

$$\frac{d\boldsymbol{\chi}}{du} = 0 \quad \Longrightarrow \quad \frac{D\chi^\mu}{Du} = 0. \tag{2.9}$$

The equations satisfied by an affinely parameterised geodesic are thus

$$\frac{d^2x^\mu}{du^2} + \Gamma^\mu_{\nu\rho}\frac{dx^\nu}{du}\frac{dx^\rho}{du} = 0. \tag{2.10}$$

Thus, a geodesic can also be defined as a curve whose tangent vector is parallel transported along itself.

In General Theory of Relativity, the geodesic equations (2.10) stand among the most important results to study motion of a particle. But one has to put in a lot of tedious work to set up these geodesic equations. To solve them would be another tiring task. Fortunately, it is possible to set up few other, less complicated, approaches for the computation of geodesic equations. These alternative approaches are briefly discussed below.

2.1.2 Lagrangian Approach for Geodesics

Another way of driving the geodesic equations (2.10) is through calculus of variation and Hamilton's principle of least action. For a start, we consider an action S, for some fixed parameter λ, to be

$$S[x^\mu(\lambda)] = \int_{\lambda_2}^{\lambda_1} \mathcal{L} d\lambda, \tag{2.11}$$

which is the spacetime distance between two fixed endpoints λ_1 and λ_2. The action is invariant under arbitrary reparametrisations of the curve. Fulfilling the requirement that the variation of the action functional (2.11) vanishes (i.e., $\delta S = 0$) leads to Euler-Lagrange equations of motion

$$\frac{d}{d\lambda}\left(\frac{\partial \mathcal{L}}{\partial \dot{x}^\mu}\right) - \frac{\partial \mathcal{L}}{\partial x^\mu} = 0 \tag{2.12}$$

This equation gives n second order differential equations for the geodesic motion of a particle.

Inserting the Lagrangian

$$\mathcal{L} = \frac{1}{2} g_{\mu\nu} \dot{x}^\mu \dot{x}^\nu, \tag{2.13}$$

into the Euler Lagrange equations gives geodesic equation of the form (2.10). Here overdot denotes differentiation with respect to the parameter. This form of geodesic equations is non-affinely parametrised. By introducing an affine parameter to the curve, we arrive at the geodesic equations (2.10). Geodesics can thus be defined as paths in spacetime $x^\mu(\lambda)$, obtained by extrimising the action (2.11). Another point to mention here is that the Lagrangian (2.13) is not a unique function in the sense that the geodesic equation (2.10) would have also be obtained if, as an example, Lagrangian function

$$\mathcal{L} \to \mathcal{L}' = \sqrt{|g_{\mu\nu} \dot{x}^\mu \dot{x}^\nu|},$$

is chosen and inserted in action

$$S'[x^\mu(\lambda)] = \int \mathcal{L}' d\lambda. \tag{2.14}$$

The former particle Lagrangian is parametrised by the time coordinate while the second particle Lagrangian is parametrized by the arc-length. Both are easily tractable. The former equation convinces that the particle will travel along a path in the shortest time between two points while second equation tells that particle follows or chooses the shortest path in the spacetime. Naturally, the shortest path in arc-length or the path with shortest time should be same in the gravitational field. It depends how one parametrizes the problem which structures the aim of the problem. Any how, mostly the Lagrangian (2.13) is preferred since it does not feature a square root, which makes it more convenient in use.

2.1.3 Hamiltonian Approach for Geodesics

Another way of defining geodesic equations is through Hamiltonian formulation. This formulation is somewhat deduced using Lagrangian formulation, by following the standard procedure. As a first step, the Hamiltonian function $\mathcal{H}$ is defined in terms of generalized coordinates x^μ and conjugate momenta p_μ, such that

$$\mathcal{H} = \mathcal{H}(x^\mu, p_\mu, \lambda) \quad \text{and} \quad p_\mu = \frac{\partial \mathcal{L}}{\partial \dot{x}^\mu}, \tag{2.15}$$

with $\dot{x}^\mu$ being the velocities.

Since Hamiltonian function $\mathcal{H}$ is the Legendre transform of the Lagrangian $\mathcal{L}$, it is given by

$$\mathcal{H} = \dot{x}^\mu p_\mu - \mathcal{L}, \tag{2.16}$$

The Eq. (2.13) and (2.16), when combined, yields

$$\mathcal{H} = \frac{1}{2} g^{\mu\nu} p_\mu p_\nu, \tag{2.17}$$

with conjugate momenta as

$$p_\mu = g_{\mu\nu} \dot{x}^\nu. \tag{2.18}$$

Evidently, the momenta p_μ represents the covariant components of the tangent vector to the geodesic.

Following a standard method [100] leads us to Hamilton's equations

$$\dot{x}^\mu = \frac{\partial \mathcal{H}}{\partial p_\mu}, \quad \dot{p}_\mu = -\frac{\partial \mathcal{H}}{\partial x^\mu}, \tag{2.19}$$

which are different from Lagrange equation, discussed earlier, in a way that later are the second order differential equations whereas Hamilton's equations defines a system of 2n coupled first order ordinary differential equations for coordinates x^μ and their conjugate momenta p_μ in n spacetime.

Using the Hamiltonian (2.17), Hamilton's equations (2.19) become

$$\dot{x}^\mu = g^{\mu\nu} p_\nu, \quad \dot{p}_\mu = -\frac{1}{2} g^{\nu\sigma}_{,\mu} p_\nu p_\sigma. \tag{2.20}$$

The first of these is clearly equivalent to the definition of the conjugate momenta (2.18). The equations (2.20) may be combined to give the familiar geodesic equation $p^\mu \nabla_\nu p_\mu = 0$.

A freely falling massive particle follows a timelike geodesics. In this case Hamiltonian function $\mathcal{H}$ equates to $-\frac{1}{2}m^2$, m is particle's mass. The Hamiltonian vanishes for light-like geodesics i.e. $\mathcal{H} = 0$, this is also referred as null condition.

The geodesic equations can also be obtained by applying the variational principle to the integral [100]

$$\int_{\lambda_1}^{\lambda_2} \left(p_\mu \dot{x}^\mu - \mathcal{H}(x^\mu, p_\mu, \lambda) \right) d\lambda \tag{2.21}$$

2.1.4 Hamiltonian Jacobi Approach for Geodesics

Uptill now, the coordinates taken are general. This allows us to write the Lagrangian, previously defined in coordinates $\{q^\mu, \dot{q}^\mu\}$, in a new coordinate system say $\{Q^\mu, \dot{Q}^\mu\}$. The geodesic equations of motion remain the same in both coordinate systems.

In the new coordinate system the Hamiltonian and Canonical momenta, respectively, now are

$$\mathcal{K} = P_\mu \dot{Q}^\mu - \mathcal{L}' \quad \text{and} \quad P_\mu = \frac{\partial \mathcal{L}'}{\partial \dot{Q}^\mu}. \tag{2.22}$$

The Lagrangian in new coordinate system is now $\mathcal{L}' = \mathcal{L}'\left(Q^\mu, \dot{Q}^\mu, \lambda\right)$. It should be mentioned here that though $\mathcal{K} = \mathcal{K}(Q^\mu, P_\mu, \lambda)$ is the same Hamiltonian but defining it in another coordinate system makes it a distinct function from $\mathcal{H} = \mathcal{H}(x^\mu, p_\mu, \lambda)$. In this regard, a new system of coordinates assigns new coordinates to the same point in phase space A set of transformations in phase space, known

as Canonical transformations preserves the form of Hamilton equations

$$\frac{\partial \mathcal{K}}{\partial Q^{\mu}} = -\dot{P}_{\mu}, \tag{2.23}$$

$$\frac{\partial \mathcal{K}}{\partial P_{\mu}} = -\dot{Q}^{\mu}. \tag{2.24}$$

The variational principle applied to the following integrals should lead to the same geodesic motion

$$\delta \int_{\lambda_1}^{\lambda_2} \left(p_{\mu} \dot{x}^{\mu} - \mathcal{H} \right) d\lambda = \delta \int_{\lambda_1}^{\lambda_2} \left(P_{\mu} \dot{Q}^{\mu} - \mathcal{K} \right) d\lambda = 0 \tag{2.25}$$

The integrands above are not necessarily equal, though they give same geodesic equations, but can be equalized if they are expressed by the relation of the form

$$\sigma \left(p_{\mu} \dot{x}^{\mu} - \mathcal{H} \right) = P_{\mu} \dot{Q}^{\mu} - \mathcal{K} + \frac{d\mathcal{F}}{d\lambda}. \tag{2.26}$$

Here σ is a constant and can be set to unity, without any loss of generality [100]. The function $\mathcal{F}$ is coordinate dependent function having a continuous second order derivatives. Interestingly, it may depends on old coordinates $\{x^{\mu}, p_{\mu}\}$ as well as new coordinates $\{Q^{\mu}, P_{\mu}\}$ since the variation of any of the coordinates vanish at the end points, consequently making the third term vanish too.

To make function $\mathcal{F}$ works more significantly , it is better to choose half the variables from old system of coordinates and the other half from new system of coordinates. This way $\mathcal{F}$ implicilty connects the two systems of coordinates as if like a *bridge* and thus constitute the name *generating function* [100].

We further choose the generating function $\mathcal{F}$ as

$$\mathcal{F}\left(x^{\mu}, Q^{\mu}, \lambda\right) = S\left(x^{\mu}, P_{\mu}, \lambda\right) - Q^{\mu} P_{\mu}. \tag{2.27}$$

The Eq. (2.26) then yields

$$\left(\frac{\partial S}{\partial x^{\mu}} - p_{\mu} \right) \dot{x}^{\mu} + \left(\frac{\partial S}{\partial P_{\mu}} - Q^{\mu} \right) \dot{P}_{\mu} + \left(\mathcal{H} + \frac{\partial S}{\partial \lambda} - \mathcal{K} \right) = 0. \tag{2.28}$$

Following the Hamilton- Jacobi formulism, the new coordinates (Q^μ, P_μ) must correspondingly act as constants of motion. This leads to attaining the value of $x^\mu(Q^\mu, P_\mu, \lambda)$ and thus a solution to the motion of the particle is obtained.
To fulfill the above requirement, the new Hamiltonian $\mathcal{K}$ vanishes identically i.e. $\mathcal{K} = 0$. Consequently, the new equations of motion becomes

$$\frac{\partial K}{\partial Q^\mu} = -\dot{P}_\mu = 0, \tag{2.29}$$

$$\frac{\partial K}{\partial P_\mu} = \dot{Q}^\mu = 0. \tag{2.30}$$

We then obtain the equation

$$\frac{\partial S}{\partial \lambda} + \mathcal{H} = 0, \quad \text{with} \quad p_\mu = \frac{\partial S}{\partial x^\mu}. \tag{2.31}$$

It is then possible to write a differential equation for the action function $S(x^\mu, P_\mu, \lambda)$ called Hamilton-Jacobi equation:

$$\mathcal{H}\left(x^\mu, \frac{\partial S}{\partial x^\mu}, \lambda\right) = -\frac{\partial S}{\partial \lambda} \tag{2.32}$$

which is a first order non linear differential equation. The function S is called the Hamilton's principle function. This function does not appears separately in the Hamilton-Jacobi equation, only its derivatives does.

2.2 Kerr Black Hole

A BH is a mysterious cosmic body with strong gravitational field as its dominant feature. The strength of its gravitational field can be noticed from the fact that not even light can escape after coming in its influence.
Formation of a BH occurs when an astronomical object having mass M gravitationally collapse consequently contracting to a point that its size crosses gravitational

radius $r_g = 2GM/c^2$, also known as Schwarzschild radius, here G is Newton's gravitational constant, and c is the speed of light. The mass of the BH acts as gravitational charge and is directly proportional to the total energy of the system. A null surface, called event horizon, around the BH does not allow any signals to escape while the physical objects and radiation can fall into it.

The Einstein's GTR effectively meets the criteria required to describe BHs. The EFE (1.1) though appear at first glance to be complicated due to its obvious non-linearity and complexity. But fortunately, soon after the appearance of EFE, the first solution to these equations gave theorists an evidence to believe the existence of BHs. Though its astronomical observations came quite later [53].

All the geometric information of a spacetime is enclosed by metric $g_{\mu\nu}$ with n dimensions. The GTR is a four dimensional theory. Implying summation by Einstein's convention, the spacetime geometry of a BH veils itself in the solutions to EFE. A general form to represent a line element is $ds^2 = g_{\mu\nu}dx^\mu dx^\nu$.

In GTR, the unique spherically symmetric vacuum solution is the Schwarzschild solution given by metric

$$ds^2 = -\left(1 - \frac{2m}{r}\right) dt^2 + \left(1 - \frac{2m}{r}\right)^{-1} dr^2 + r^2 d\theta^2 + r^2 \sin^2\theta d\phi^2, \qquad (2.33)$$

where $m = GM/c^2$ is mass of gravitating body. This is the first ever solution to EFE and fully describes the exterior of a spherically symmetric gravitating body with zero spin. For an observer faraway $(r \to \infty)$ from the gravitational source , interprets the spacetime solution (2.33) as Minkowski flat spacetime in spherical polar coordinates. The singularities appears in Schwarzschild solution at $r = 0$ and $r = 2M$. The computation of Kretchmann invariant $R_{\mu\nu\sigma\rho}R^{\mu\nu\sigma\rho} = 48M^2/r^6$ specifies the singularity at $r = 0$ as essential singularity: this singularity can not be removed but carries physical significance. The singularity at $r = 2M$, on the other hand, is a coordinate singularity and can be avoided by change

of coordinates. Eddington Finkelstein coordinates or Kruskal coordinates are some of the coordinates use to remove this singularity. The event horizon of a Schwarzschild BH exists at $r = r_H = 2M$, which is also a null surface. The interior of Schwarzschild BH solution lies in the domain $r\epsilon\big(0, 2M]$ while exterior region starts from $r > 2M$.

The gravitational field of a rotating chargeless gravitating source is described by Kerr spacetime: solution to EFE founded by Roy Kerr in 1963. To get a clear picture of this let us assume a distant object (be it a star or a BH) rotating in space about a vertical axis through its center. In four dimensional spacetime this situation can naturally be described in terms of three spherical coordinates r, θ, ϕ on $\mathbf{R}^3$ and one time coordinate t on $\mathbf{R}$. Here r is interpreted as the distance to the centre of the rotating object, θ as colatitude and ϕ as longitude.
In BL coordinates $\{t, r, \theta, \phi\}$, the metric defining a Kerr spacetime has the form

$$\begin{aligned} ds^2 = & - \left(1 - 2m\frac{r}{\Sigma}\right) dt^2 - 4ma\frac{r}{\Sigma}\sin^2\theta dt d\phi + \frac{\Sigma}{\Delta}dr^2 \\ & + \Sigma d\theta^2 + \left((r^2 + a^2)\sin^2\theta + 2m\frac{r}{\Sigma}a^2\sin^2\theta\right) d\phi^2, \end{aligned} \tag{2.34}$$

with the expressions for Σ and Δ as

$$\Sigma = r^2 + a^2\cos^2\theta, \tag{2.35}$$

$$\Delta = r^2 - 2mr + a^2. \tag{2.36}$$

Since components of this metric are independent of t and ϕ, this makes Kerr metric a stationary and axially symmetric solution. The metric above is characterized by two parameters:

- The parameter $m = GM/c^2$, where M is mass of BH. Interestingly, m has dimension of a distance.
- If a spinnig BH has J angular momentum then parameter $a = J/(Mc)$, in the above metric, relates to the rotation of BH. As can be noticed, parameter a is

angular momentum per unit mass of BH. Physical importance of parameter a is its association to the direction and speed of rotation of a spinning BH. For a positive value of a, the direction of spin is clockwise. For a counter clockwise spinning BH, the value of a is negative. As for the speed of rotation, since a is directly proportional to angular momentum J thus greater value of J indicates faster spin of BH.

Horizons

Mathematically, the horizons of Kerr metric lies in coefficient of third term of metric (2.34) i.e. when $g^{rr} = 0$. The condition $\Delta = 0$, or equivalently $r = r_{\pm} = M \pm \sqrt{M^2 - a^2}$ gives rise to two null surfaces r_- and r_+, with $r_- \leq r_+$; the surface defined by r_+ is commonly called event horizon or outer horizon. The event horizon r_+ of Kerr BH is a null surface beyond which no event or information can be observed by an observer, located at distant position. It is a sphere-shaped surface veiling the intrinsic singularity of BH. Since no information beyond r_+ is undetectable, the event horizon apparently acts as the boundary of the BH. On the other hand, r_- is the inner horizon or Cauchy horizon.

Singularities, Symmetries and Killing Vectors

Two singularities arise in Kerr metric: coordinate singularity and curvature singularity. A coordinate singularity may simply arise due to the failure of the coordinate system. By replacing the coordiante system with some other more promising system of coordinates this singularity can be avoided. In an RBH, at $r = r_{\pm} = M \pm \sqrt{M^2 - a^2}$ there exists coordinate singularity as Δ goes to zero and coefficient of dr^2 to infinity.

The second singularity which is also an intrinsic singularity of RBH is the

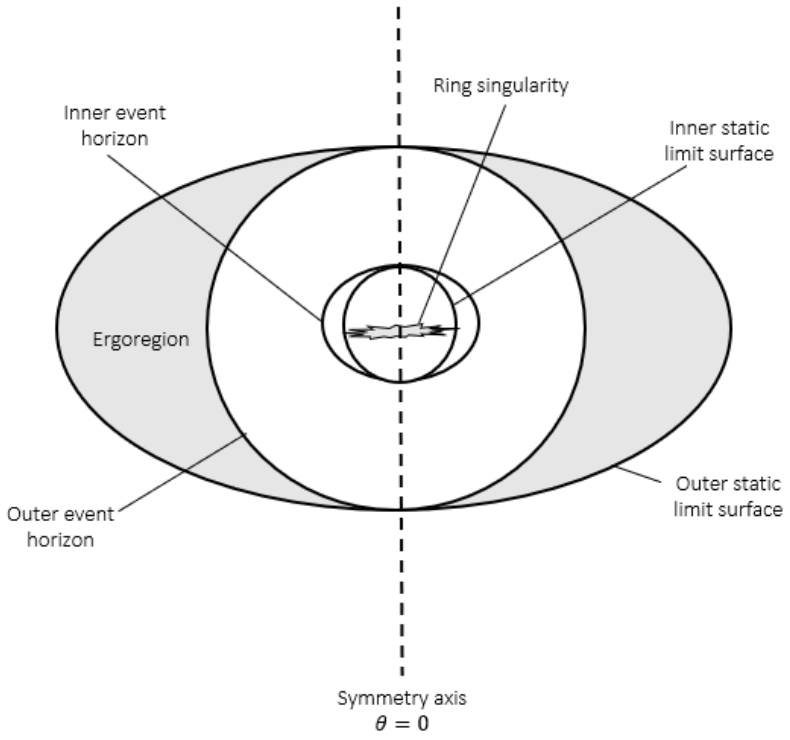

Figure 2.1: Schematic diagram showing a Kerr BH. Figure follows [98].

curvature singularity. Mathematically, this singularity is detected with the help of scalar invariant, $R_{\mu\nu\alpha\beta}R^{\mu\nu\alpha\beta}$, (also called Kretschmann scalar). The scalar invariant blows of at curvature singularity. This singularity cannot be removed by any change of coordinates and it is thus an intrinsic property of the Kerr space-time. Eq. (2.35) is sum of two nonnegative quantities. A singularity can only exist here if both terms in eq.(2.35) vanish or

$$r = 0 \quad \text{and} \quad a\cos\theta = 0, \ \text{since} \quad a \neq 0 \quad \text{thus} \quad \theta = \pi/2. \tag{2.37}$$

At a first glance this may seems an absurd result but it should be remember here that $r = 0, \theta = \pi/2$ is not a single point but forms a disk: it is rather a *ring* of unlimited gravitational forces [133]. Because of its shape *curvature* singularity is also called *ring* singularity (or even ringularity). By passing through the ring

singularity the observer exits to another realm, completely opposite to the previous one. The observer now experiences repulsion instead of attraction. The new spacetime is asymptotically flat too and is described by Kerr metric with $r < 0$. For the case of no rotation, a = 0, the ring shrinks into just a point, as in the Schwarzschild metric.

Physically, a spacetime does not depend on its coordinate system. Indeed, form of a metric is changed after employing coordinate transformation but its interpretation remains the same [135]. However, a coordinate transformation which does not change the form of the metric is called *symmetry*. Symmetries in a metric can best be described by Killing vectors.

Particularly, a Lie derivative $\mathfrak{L}$ with respect to X^μ for a metric $g_{\nu\rho}$, given by

$$\mathfrak{L}_X g_{\nu\rho} = X^\mu \partial_\mu g_{\nu\rho} + g_{\mu\rho}\partial_\nu X^\mu + g_{\nu\mu}\partial_\rho X^\mu,$$

when vanishes give us an equation of the form

$$\nabla_\mu X_\nu + \nabla_\nu X_\mu = 0.$$

The above equation is *Killing's equation* and any solutions to it are called *Killing vectors* [135]. Two Killing vectors arise in Kerr metric:

$$\xi_t = \left(\frac{\partial}{\partial t}\right)_{r,\theta,\phi} \quad \text{and} \quad \xi_\phi = \left(\frac{\partial}{\partial \phi}\right)_{t,r,\theta}, \tag{2.38}$$

with time and axial coordinate, meaning that it has two symmetries. The presence of these Killing vectors in a space time also implies that the corresponding momenta acts as constant of motion. Momenta along time and longitudinal coordinates i.e. p_t and p_ϕ, of a test particle are conserved in the Kerr spacetime.

Static Limit Surfaces and Ergoregion

For a stationary axisymmetric spacetime, static limit surfaces, r^s_+ and r^s_-, exist when the coefficient of dt^2 vanishes i.e. $g_{tt} = 0$. In Kerr space time these surfaces

occur when

$$r = r^s_{\pm} = m \pm \sqrt{m^2 - a^2 \cos^2 \theta}, \tag{2.39}$$

such that $r^s_+ > r^s_-$. Some very significant phenomenon, like Penrose process and superradiance are associated with these surfaces.
The horizons of Kerr BH

$$r_{\pm} = m \pm \sqrt{m^2 - a^2} \tag{2.40}$$

lies in the interval $[r^s_+, r^s_-]$ such that $r^s_+ > r_+ > r_- > r^s_-$. The surface r^s_+ coincides with outer horizon r_+ at $\theta = 0, \pi$, other than these points the surface r^s_+ completely encloses the outer horizon. Similarly, the surface r^s_- coincides with inner horizon r_- at $\theta = 0, \pi$ but at other points it completely confines itself in inner horizon.
The surface r^s_+ is the outer most surface of an RBH and is usually described as a boundary, outside of which the observer can be static but after crossing it, its impossible to remain static due to strong frame dragging effect. This outer surface of an RBH is also called stationary limit surface or static limit surface since the worldline changes from timelike to spacelike once this limit is crossed.
Inside the stationary limit surface, every observer, particle or photon rotates with the same direction as the rotation of the BH. The region between the stationary limit surface and the outer horizon is called the ergoregion (the stationary limit surface itself is called the ergosurface). This is the region from which particles can escape. The presence of ergosphere causes various kinds of energy extraction mechanisms for an RBH e.g Penrose process.

Spin of Kerr Black Hole

Spin of BH can be powered up by presence of a thin accretion disk. As the gas loses its angular momentum and energy it eventually falls into BH with out any

loss of considerate emission of additional radiation. This also results in increased mass and angular momentum of BH. The spin value of BH can be best evaluated from this mechanism too. In this scenario, a KBH of mass M has the value of its dimensionless spin parameter $\tilde{a} = a/M$ as [137]

$$\tilde{a} = \begin{cases} \sqrt{\frac{2}{3}}\frac{M_o}{M}\left(4 - \sqrt{18\frac{M_o^2}{M^2} - 2}\right) & \text{if} \quad M \leq \sqrt{6}M_o, \\ 1 \quad \text{if} \quad M > \sqrt{6}M_o, \end{cases} \tag{2.41}$$

where M_o is mass of the initially non-rotating BH. Now if we plot the above expression (see Figure 2.2), it is noticed that as the BH gains mass by the factor $\sqrt{6}$ then the equilibrium value of its spin is 1. As shown in Figure (2.2), initially the spin increases quite fast. Roughly speaking, the BH will have to double its mass to reach the spin $\tilde{a} = 0.99$. However, a non-negligible amount of gas is required by a BH to reach spin value 1 [46].

Special Cases:

- If the spin parameter a exceeds mass m of the RBH, a *naked singularity* appears: a singularity not veiled by horizon. Physically, such a phenomenon is not possible since it is like observing a point of infinite density. To avoid naked singularity, the value of a is restricted to interval $[-m, m]$ or $m^2 \geq a^2$.
- For the case $|a| = m$, BH gains maximum rotation. Such BHs are also named *extremal* BHs.
- The condition $\theta = \{0, \pi\}$ corresponds to the set of points in space-time along the BH's axis of rotation and the condition $\theta = \pi/2$ corresponds to the BH's equatorial plane.
- Cease the rotation by considering $a = 0$ and Ker spacetime reverts to Schwarzschild spacetime. If the mass is also then removed by setting $M = 0$

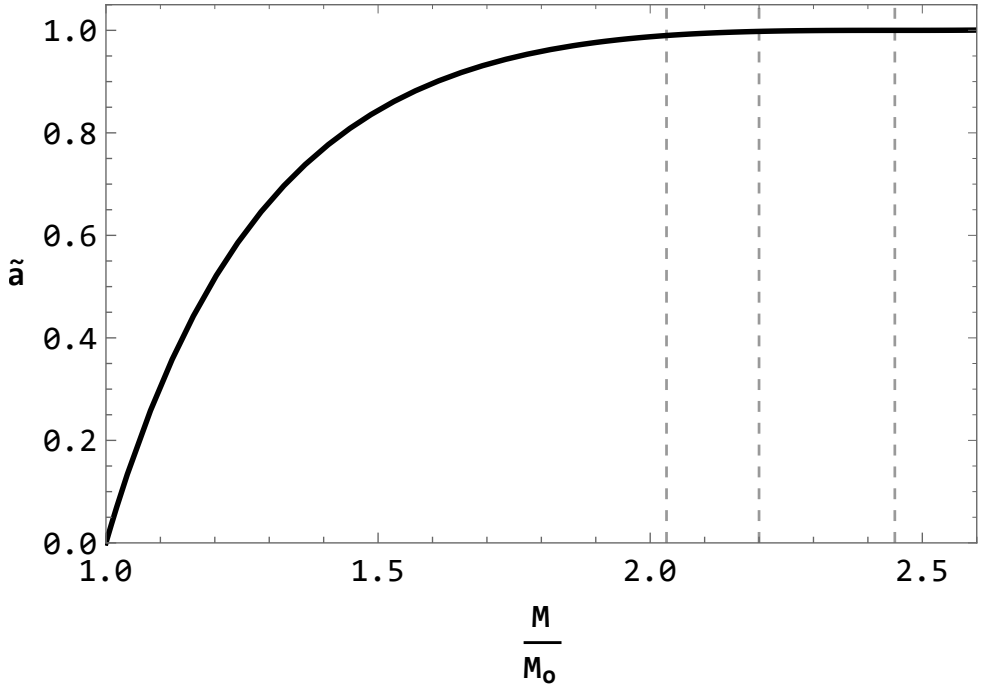

Figure 2.2: Plot showing the dimensionless spin parameter $\tilde{a}$ of a Kerr BH accreting from a thin disk, see Eq. (2.41). The three dashed vertical lines indicate when the BH spin reaches the values $\tilde{a} = 0.99(M/M_o \approx 2.03), 0.998(M/M_o \approx 2.20), and 1(M/M_o = \sqrt{6} \approx 2.45)$. Figure follows [136]

then only Minkowski spacetime is left.

For the remainder of this, and the next chapters, special units are chosen such that $c = 1$ and $G = 1$.

2.2.1 Rotating Black Hole in Asymptotically Safe Gravity Theory

Weinberg proposed a new nonperturbative notion of renormalizibility which is called "asymptotic safety" [77], based on the existence of a nontrivial fixed point

in renormalization group, which makes the physical couplings of the theory non-divergent. The key point to mention here is that when quantum corrections are applied to BH spacetime, the system is modified, such that the Newton constant G turns into a r-dependent running Newton coupling $G(r)$ i.e.

$$G \to G(r).$$

The Running Coupling in Asymptotically Safe Gravity

The solution of the renormalization group (RG) equation for the running Newton coupling, $G(p)$, of the action (2.43) is computed in [101], using the one-loop correction:

$$G(p) = \frac{G_N}{1 + \xi p^2 G_N}, \tag{2.42}$$

where G_N is Newton's constant at classical level. For simplicity, the value of G_N will be equated to unity in rest of our analysis. Here ξ is also a coupling coefficient. Cai and Easson broadened the study of BH solution in safe gravity by considering higher derivative terms in their analysis [79]. They initiated their study by introducing an effective action

$$\begin{aligned} \Gamma_p[g_{\mu\nu}] &= \int d^4x \sqrt{-g} \Big[p^4 g_o(p) + p^2 g_1(p)\mathcal{R} + g_{2a}(p)\mathcal{R}^2 \\ &+ g_{2b}(p)\mathcal{R}_{\mu\nu}\mathcal{R}^{\mu\nu} + g_{2c}(p)\mathcal{R}_{\mu\nu\sigma\rho}\mathcal{R}^{\mu\nu\sigma\rho} + \mathcal{O}(p^{-2}\mathcal{R}^3) + ... \Big], \end{aligned} \tag{2.43}$$

where $g_{\mu\nu}$ represents metric tensor with g as its determinant, Ricci scalar, Ricci tensor and Riemann tensor are denoted by $\mathcal{R}$, $\mathcal{R}_{\mu\nu}$ and $\mathcal{R}_{\mu\nu\sigma\rho}$, respectively, p is the momentum cutoff and g_i $(0, 1, 2a, ...)$ are dimensionless running couplings satisfying the renormalization group (RG) equations, for example:

$$g_0(p) = -\frac{\Lambda(p)}{8\pi G_N(p)} p^{-4}, \qquad g_1(p) = \frac{1}{8\pi G_N(p)} p^{-2}, \qquad \frac{d}{d\ln p} g_i(p) = \beta_i(g). \tag{2.44}$$

Further, it was shown that for large values of radial coordinate r, the momentum cut-off goes asymptotically small i.e. $p \sim 1/r$; it may go below the Planck scale. Under this limit (so-called Infra-red or IR), the running Newton coupling $G(r)$ takes the form

$$G(r) \simeq \left(1 - \frac{\tilde{\xi}}{r^2}\right), \tag{2.45}$$

for $r \ll l_{Planck}$, where $\tilde{\xi}$ differs from ξ by $\mathcal{O}(1)$ and has constant value, less than unity. For more understanding of this running coupling, it is recommended to see [79]. Although the main motivation of this form of $G(r)$ comes from the potential IR limit of asymptotic safe gravity, we note that the analysis performed in this work can be understood as more general and not only limited to the asymptotic safety program, since the basic assumption of its validity is only that the quantum effects can be described by the correction given in (2.45).

RG Improved Kerr Metric

The analysis of RG improved Schwarzschild metric is done in [102], and it was noticed that apart from usual Schwarzschild horizon, the presence of a new horizon was noticed which, at critical mass, coincides with the outer horizon. To understand the technique used for the computation of RG improved Schwarzschild metric it is suggested to see [102]. With the help of similar analysis an improved Kerr metric was suggested by Reuter and Tuiran [90]. In their analysis they considered Newton's coupling G to be r-dependent i.e. $G = G(r)$. With this assumption they arrived at the improved Kerr metric form as

$$\begin{aligned} ds^2 &= -\left(1 - \frac{2Mr}{\Sigma}G(r)\right)dt^2 - \frac{4aMr\sin^2\theta}{\Sigma}G(r)dtd\phi + \frac{\Sigma}{\Delta}dr^2 \\ &+ \Sigma d\theta^2 + \sin^2\theta\left[r^2 + a^2 + \frac{2a^2Mr\sin^2\theta}{\Sigma}G(r)\right]d\phi^2, \end{aligned} \tag{2.46}$$

where $\Delta = r^2 - 2MrG(r) + a^2$ and $\Sigma = r^2 + a^2\cos^2\theta$. Here a is defined as rotational parameter.

2.2.2 Rotating Black Hole in Perfect Fluid Dark Matter

There is observational evidence that our Universe is constitute of an invisible matter called dark matter (DM). Though DM covers about 27% of our Universe, but still we are unfamiliar about its nature. Some of the evidence supporting existence of DM include galactic rotation curves [91], the dynamics of galaxy clusters [92], and the measurements of cosmic microwave background anisotropies obtained through PLANCK [93]. To understand the nature of this mysterious matter a whole new physics is required possibly relying on the existence of some new species of fundamental particles. It is therefore natural to ask how BH solutions might depend on dark matter.

The action defined for BH surrounded by DM field couple to gravity is given by

$$\mathcal{S} = \int d^4x \sqrt{-g}\left(\frac{\mathcal{R}}{16\pi} + \mathcal{L}_{DM}\right), \tag{2.47}$$

where $\mathcal{L}_{DM}$ presents the DM Lagrangian density. Use of variational approach on the above action $\mathcal{S}$ leads to Einstein field equations of the form

$$\mathcal{R}_{\mu\nu} - \frac{1}{2}g_{\mu\nu}\mathcal{R} = -8\pi\left(\bar{\mathcal{T}}_{\mu\nu} + \mathcal{T}^{DM}_{\mu\nu}\right) = -8\pi T_{\mu\nu}, \tag{2.48}$$

where the ordinary matter has momentum tensor $\bar{\mathcal{T}}_{\mu\nu}$ and DM has momentum tensor $\mathcal{T}^{DM}_{\mu\nu}$. From current astrophysical observations, the dominance of dark matter and dark energy in our universe is evident. By assuming that a dark matter field in background of a BH is a perfect fluid, the energy momentum tensor then is of the form $T_{\mu\nu} = diag[-\rho, p, p, p]$ [113]. As a simplest case, it is added that for

some constant value δ,

$$p/\rho = \delta - 1.$$

Amongst the many dark matter models that have been suggested is the perfect fluid dark matter model, which was initially proposed by Kiselev [112]. An entailed construction of a new class of spherically symmetric BH metrics in the presence of PFDM was done in [113]. In the spherically symmetric case this class of BHs was distinguished by a new term in the metric function that grows logarithmically with distance from the BH. The logarithmic dependence was introduced by Kiselev [112] to account for the asymptotic behaviour of the quintessential matter at large distances, i.e. in the halo dominated region, in order to explain the asymptotic rotation curves for the dark matter (see also [113]). The metric is given by

$$ds^2 = -f(r)dt^2 + \frac{1}{f(r)}dr^2 + r^2 d\theta^2 + r^2 \sin^2\theta d\phi^2 \tag{2.49}$$

along with

$$f(r) = 1 - 2\frac{M}{r} + \frac{\alpha}{r}\ln\frac{r}{|\alpha|}.$$

The PFDM's intensity is shown by parameter α.

Only recently has this class been generalized to include rotation [99], providing a PFDM version of the Kerr-(A)dS solution. The metric is given by

$$\begin{aligned} ds^2 &= -\frac{\Delta_r}{\Xi^2\Sigma}\left(dt - a\sin^2\theta d\phi\right)^2 + \frac{\Delta_\theta \sin^2\theta}{\Xi^2\Sigma}\left(adt - (r^2+a^2)d\phi\right)^2 \\ &+ \frac{\Sigma}{\Delta_r}dr^2 + \frac{\Sigma}{\Delta_\theta}d\theta^2 \end{aligned} \tag{2.50}$$

where

$$\begin{aligned} \Delta_r &= r^2 - 2Mr + a^2 - \frac{\Lambda}{3}r^2\left(r^2+a^2\right) + \alpha r\ln\frac{r}{|\alpha|}, \\ \Delta_\theta &= 1 + \frac{\Lambda}{3}a^2\cos^2\theta, \qquad \Xi = 1 + \frac{\Lambda}{3}a^2, \\ \Sigma &= r^2 + a^2\cos^2\theta \end{aligned} \tag{2.51}$$

with the mass parameter of the BH being M. The parameter indicating the presence of perfect fluid dark matter is α. This solution reduces to a rotating BH in a PFDM background when $\Lambda = 0$, and to the Kerr-(A)dS solution for $\alpha = 0$.

2.2.3 Rotating Dyonic Black Hole with a Global Monopole in Perfect Fluid

Global monopoles are topological defects which may have been produced while the early Universe went through phase transitions. In fact, global monopoles are just one type of topological defects. Other types of topological objects are expected to exist including domain walls and cosmic strings (e.g. [94]). More precisely, a global monopole is a heavy object characterized by spherically symmetry and divergent mass.

The action, S^{EM}, for Einstein Maxwell gravity along with actions $S^{(D)}$ and $\mathcal{S}$ respectively defining presence of a global monopole and matter distribution, can be altogether written as

$$\begin{aligned} S &= S^{(EM)} + S^{(D)} + \mathcal{S} \\ &= \int \sqrt{-g}\, d^4x \left(\frac{\mathcal{R}}{2\kappa} - \frac{1}{4} F_{\mu\nu}F^{\mu\nu}\right) \\ &+ \int \sqrt{-g}\, d^4x \left(\frac{1}{2} g^{\mu\nu}\partial_\mu \Phi^{\mathbf{s}} \partial_\nu \Phi^{\mathbf{s}} - \frac{\lambda}{4}\left(\Phi^2 - \gamma^2\right)^2\right) + \mathcal{S}. \end{aligned} \tag{2.52}$$

The quantities g, $\mathcal{R}$ and $F_{\mu\nu}$ are, respectively, determinant of $g_{\mu\nu}$ associated to the gravitational field, scalar invariant and electromagnetic tensor. Also $\mu, \nu = 0, 1, 2, 3$. Now the action $S^{(D)}$ corresponds to the matter having a defect– a global monopole which is a heavy object formed in the phase transition of a system composed by a self-coupling scalar triplet field $\Phi^{\mathbf{s}}$, where s runs from 1 to 3 [95]. The corresponding EFE read

$$\mathcal{R}_{\mu\nu} - \frac{1}{2} g_{\mu\nu}\mathcal{R} = 8\pi T_{\mu\nu}. \tag{2.53}$$

While the corresponding Maxwell equations are

$$\nabla_\mu F^{\mu\nu} = 0. \tag{2.54}$$

With these equations in mind, and without loss of generality we can choose a spherically symmetric metric written as follows

$$ds^2 = -f(r)dt^2 + \frac{dr^2}{f(r)} + r^2 d\theta^2 + r^2 \sin^2\theta d\varphi^2. \tag{2.55}$$

where

$$f(r) = 1 - 8\pi\gamma^2 - \frac{2M}{r} + \frac{Q_E^2}{r^2} + \frac{Q_M^2}{r^2} - \frac{v}{r^{1+3\omega}}, \tag{2.56}$$

with the energy density in the form

$$\rho = -\frac{3\,\omega\,v}{8\pi r^{3(1+\omega)}}. \tag{2.57}$$

Note that, v is an integration constant related to the perfect fluid parameter. From the weak energy condition it follows the positivity of the energy density of the surrounding field, $\rho \geq 0$, which should satisfy the following constraint $\omega v \leq 0$. Hence the rotating spacetime metric has the form

$$\begin{aligned} ds^2 &= -\left(\frac{\Delta - a^2\sin^2\theta}{\Sigma}\right) dt^2 - 2a\sin^2\theta\left(1 - \frac{\Delta - a^2\sin^2\theta}{\Sigma}\right) dt d\varphi + \frac{\Sigma}{\Delta} dr^2 + \Sigma d\theta^2 \\ &+ \sin^2\theta\left[\Sigma + a^2\sin^2\theta\left(2 - \frac{\Delta - a^2\sin^2\theta}{\Sigma}\right)\right] d\varphi^2. \end{aligned} \tag{2.58}$$

For spin $a = 0$, perfect fluid parameter $v = 0$ and no charges, the above metric reduces to Schwarzschild BH with global monopole [128].

The vector potential computed through Newman-Janis formalism for a RDBH is given by [126]

$$A = \left(\frac{rQ_E - aQ_M\cos\theta}{\Sigma}\right) dt + \left(-\frac{ra}{\Sigma} Q_E \sin^2\theta + \frac{r^2 + a^2}{\Sigma} Q_M \cos\theta\right) d\varphi. \tag{2.59}$$

The detailed derivation of metric (2.58) is given in Chapter 5.

2.3 Shadow of a Rotating Black Hole

The path followed by light particles (photons) is straight, until they come under the influence of a strong gravitational compact object, in our case a BH. Photons are then forced to curve their path and consequently orbit around BH. The study of such photon's geodesics (also comes with the name light-like geodesics or null geodesics) leads us to some interesting optical observations.

The behaviour of null geodesics can be characterized into two categories: those that venture so close to the outer horizon $r = r_+$ of the BH that they are absorbed by it due to the gravitational pull, and those that ultimately escape to their original source in the past. Thus a boundary is defined, between these two categories of light-like geodesics, which encloses a dark region called the shadow.
In particular, the boundary of BH's shadow is composed of set of light rays that makes null orbits of constant radius around BH [40]. Such orbits are associated to a finite interval of radial positions which is referred to as a photon region. The circular orbits lying at the extremal radial positions of photon region stays on the equatorial plane and are referred to as light rings. More generally, a light ring is taken to be any planar circular photon orbit, which implies $R = 0 = dR/dr$. The existence of unstable photon orbits around compact objects is associated to multiple images of light sources, and in case of a BH, to a shadow. Thus image of a photon region is considered as BH's shadow.

Description of Method

The basic technique to compute shadow of BH was formulated, for example, in [17]. Another recent discussion was done by [132].
Using Hamiltonian-Jacobi formulasim the null geodesics of Kerr BH can be fully separated. All four geodesic equations reduce to first order differential equations

associated with four constants of motion [9]. This considerably simplifies the problem. The two constants of motion comes from Killing vectors ξ_t and ξ_ϕ. The rest mass of photon, which is zero, acts as third constant of motion and the fourth is Carter's constant which is generated due to the presence of second order Killing tensor field.

Photons emitted from a light source opt null geodesics near a BH. Possibly photons follow three trajectories:

- those absorbed by the BH appear as a dark zone (shadow) to the observer.
- those scattered away to infinity from the BH, these photons appear visible to observer's eye.
- those critical null geodesics which separate the first two orbits.

To study shadow of a BH, the observer is considered faraway $(r_o \to \infty)$ from a BH. The orthonormal basis vectors $\{e_{\hat{t}}, e_{\hat{r}}, e_{\hat{\theta}}, e_{\hat{\phi}}\}$ are useful to define the position of a local observer located faraway from a BH. The expression

$$e_{\hat{\alpha}} = e^{\mu}_{\hat{\alpha}} e_{\mu}, \tag{2.60}$$

relates orthonormal basis to coordinate basis $\{e_t, e_r, e_\theta, e_\phi\}$ of the spacetime

$$\boldsymbol{e}_{\hat{\alpha}}.\boldsymbol{e}_{\hat{\beta}} = \eta_{\hat{\alpha}\hat{\beta}}, \tag{2.61}$$

with $\eta_{\hat{\alpha}\hat{\beta}} = (-1, 1, 1, 1)$ a Minkowski metric. Let the orthonormal basis satisfying the above conditions be chosen as

$$e_{\hat{t}} = A_1\, e_t + A_2\, e_\phi, \tag{2.62}$$

$$e_{\hat{r}} = A_3\, e_r, \tag{2.63}$$

$$e_{\hat{\theta}} = A_4\, e_\theta, \tag{2.64}$$

$$e_{\hat{\phi}} = A_5\, e_\phi, \tag{2.65}$$

where A_1, A_2, A_3, A_4, A_5 are coefficients. These orthonormal basis may differ for other spacetime metrics.

Since these orthonormal basis vectors satisfy Eq. (2.61), we get

$$A_1 = \sqrt{\frac{g_{\phi\phi}}{g_{t\phi}^2 - g_{tt}g_{\phi\phi}}}, A_2 = -\frac{g_{t\phi}}{g_{\phi\phi}}\sqrt{\frac{g_{\phi\phi}}{g_{t\phi}^2 - g_{tt}g_{\phi\phi}}} \tag{2.66}$$

$$A_3 = \frac{1}{\sqrt{g_{rr}}}, \quad A_4 = \frac{1}{\sqrt{g_{\theta\theta}}}, \quad A_5 = \frac{1}{\sqrt{g_{\phi\phi}}}. \tag{2.67}$$

In the new basis, the locally measured energy and axial angular momentum are

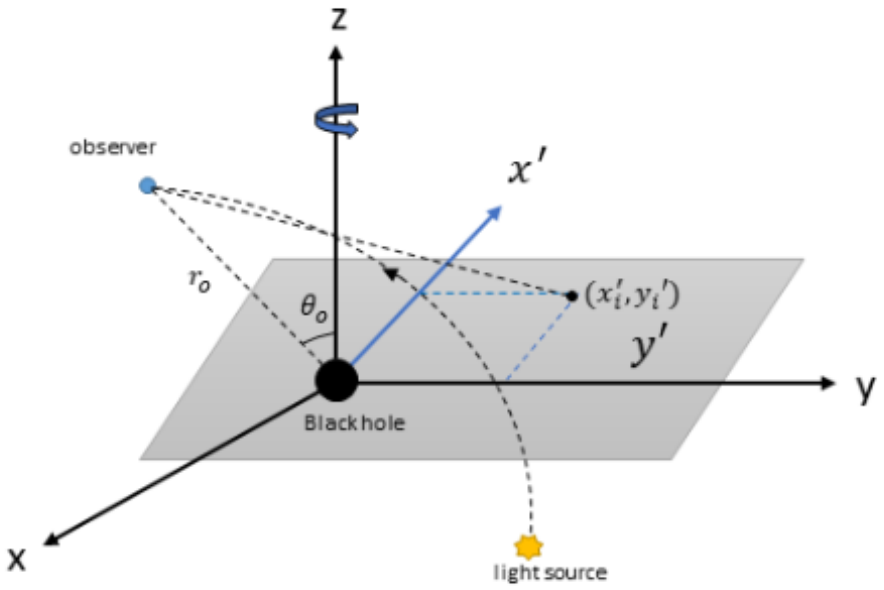

Figure 2.3: Schematic diagram of the coordinates for a distant observer.

given by the expressions [11]

$$
\begin{aligned}
p^{\hat{t}} &= A_1 E - A_2 L_z, && (2.68)\\
p^{\hat{r}} &= \frac{p_r}{\sqrt{g_{rr}}}, && (2.69)\\
p^{\hat{\theta}} &= \frac{p_\theta}{\sqrt{g_{\theta\theta}}} && (2.70)\\
p^{\hat{\phi}} &= \frac{L_z}{\sqrt{g_{\phi\phi}}}, && (2.71)
\end{aligned}
$$

Furthermore, new coordinates (x', y') are defined for the image plane of an observer. The BH is considered at the origin of the image plane (see Figure(2.3)). The observer located at $\{r = r_o, \theta = \theta_o\}$ has the coordinates on the image plane as

$$
\begin{aligned}
x' &= -r_o \frac{p^{\hat{\phi}}}{p^{\hat{t}}}, && (2.72)\\
y' &= r_o \frac{p^{\hat{\theta}}}{p^{\hat{t}}}. && (2.73)
\end{aligned}
$$

The coordinates x' and y' are the apparent perpendicular distances of the image as seen from the axis of symmetry and from its projection on the equatorial plane, respectively.

In null geodesics, the photon's motion is significantly expressed in terms of two independent impact parameters [11]

$$
\begin{aligned}
\eta &= \frac{L}{E}, && (2.74)\\
\xi &= \frac{\mathcal{K}}{E^2}.
\end{aligned}
$$

These parameters contains conserved quantities and can be explicitly expressed using location of the circular photon orbits [134].

Chapter 3

Geodesics of a Rotating Black Hole in Asymptotically Safe Gravity Theory

In this chapter we investigate the consequences of running gravitational coupling on the properties of a rotating BH, previously discussed in section (2.2.1). In this approach, the involvement of a new parameter $\tilde{\xi}$ in this solution makes it different from Schwarzschild BH. Initially, the Killing horizon, event horizon and singularity of the computed metric is discussed. It is noticed that the ergosphere is increased as $\tilde{\xi}$ increases. Considering the BH solution in equatorial plane, the geodesics of particles, both null and time like cases, are explored. The effective potential is computed and graphically analyzed for different values of parameter $\tilde{\xi}$. The energy extraction from BH is investigated via Penrose process. For the same values of spin parameter, the numerical results suggest that the efficiency of Penrose process is greater in ASG than in KBH. At the end, a brief discussion on Lense-Thirring frequency is also done.

The outline of this chapter is established as follows. In section I, a BH solution in IR regime with ASG theory is constructed, following with the comments on

event horizon and singularity of the computed rotating metric. In section II, equatorial null and time-like geodesics of this BH are taken into account along with the discussion on effective potential. Section III is on the study of Penrose process. Section VI gives a thorough description on Lense-Thirring effect.

3.1 Kerr Metric in the Infra-red limit of Asymptotically Safe Gravity Theory

Considering the running Newton parameter (2.45) in metric (2.46), we reach to the form of improved Kerr metric solution in ASG in the infra-red limit. The metric is thus given by

$$\begin{aligned} ds^2 &= -\Big(1-\frac{2Mr}{\Sigma}\Big(1-\frac{\tilde{\xi}}{r^2}\Big)\Big)dt^2 - \frac{4aMr\sin^2\theta}{\Sigma}\Big(1-\frac{\tilde{\xi}}{r^2}\Big)dtd\phi + \frac{\Sigma}{\Delta}dr^2 + \Sigma d\theta^2 \\ &+ \sin^2\theta\Big[r^2+a^2+\frac{2a^2Mr}{\Sigma}\sin^2\theta\Big(1-\frac{\tilde{\xi}}{r^2}\Big)\Big]d\phi^2, \end{aligned} \tag{3.1}$$

where $\Delta = r^2 - 2Mr + \frac{2M\tilde{\xi}}{r} + a^2$. This metric reduces to its static and spherically symmetric version when $a \to 0$. For reader's better understanding and to provide stronger grounds for the results computed in rest of the sections, a detail derivation of metric (3.1), using the technique in [89], is presented in appendix (A). In next sections we are going to take into account some other characteristic behaviours of metric (3.1).

3.1.1 Event and Killing Horizons

Modifications of the Kerr metric, that came as a result of the generalization of Lagrangian in the framework of ASG, also manifest in the properties of the BH horizons. In the Boyer-Lindquist coordinates the event horizon, r_H, is given by

the condition that at $r = r_H$ hypersurface is everywhere null, or $g^{rr} = 0$. For the standard GR case it follows that the Kerr BH will have two solutions as long as $M > a$, while the case $M < a$ leads to existence of a naked singularity. This is however changed when one considers the modifications coming from the spatial dependence of gravitational coupling. Now, the position of horizons is determined by the cubic equation

$$r^3 - 2Mr^2 + a^2 r + 2M\tilde{\xi} = 0. \tag{3.2}$$

Although the horizon equation now has three solutions, only two of them can be positive - so there are no new horizons in this case. When compared to the horizons in the standard GR it can be checked that Eq. (3.2) will tend to lead to smaller separation between the inner and outer horizon. Moreover, the structure of BH, described by its horizons, will now be changed and will depend on the value of $\tilde{\xi}$ - determining if the horizons exist.

For a general polynomial of order three, the number and type of roots is determined by its discriminant, D, so that for $D > 0$ there exist three real solutions, in the $D = 0$ case the solutions are real and two of them are identical, while for $D < 0$ one solution is real and two remaining ones are complex conjugated. The existence of horizons, which should of course be real and positive, is then determined by $\tilde{\xi}_c$ for which $D = 0$. It follows that $\tilde{\xi}_c$ is given by

$$\tilde{\xi}_c = \frac{-\left(9M^2a^2 - 8M^4\right) \pm \sqrt{M^2\left(4M^2 - 3a^2\right)^3}}{27M^2}. \tag{3.3}$$

We note that $\tilde{\xi}_c$ will be physically viable (real valued) as long as the standard GR condition $M > a$ is satisfied. Thus, for $\tilde{\xi} > \tilde{\xi}_c$ there will be no horizons, and this case leads to a naked singularity. For $\tilde{\xi} = \tilde{\xi}_c$ there will be only one horizon (two identical positive roots), but this case is unstable since addition of some small

amount of matter will violate this condition. Finally, for $\tilde{\xi} < \tilde{\xi}_c$ the Kerr BH will have one inner and one outer horizon. Since $\tilde{\xi}_c$ is given in general by theoretical consideration of asymptotic correction to the GR, this discussion constraints possible space of parameters for Kerr BH that leads to physically realistic solutions.

The Killing horizon, being defined as the set of points where norm of the Killing vector becomes null, $K^\mu K_\mu = 0$, in the case of running gravitational coupling is given by the solution of the following cubic equation

$$r^3 - 2Mr^2 + a^2\cos^2(\theta)r + 2M\tilde{\xi} = 0. \tag{3.4}$$

The discussion for event horizons structure depending on parameter $\tilde{\xi}$ given above can also be applied to the study of Killing horizons, with the replacement

$$\tilde{\xi}_c = \frac{-\left(9M^2a^2\cos^2\theta - 8M^4\right) \pm \sqrt{M^2\left(4M^2 - 3a^2\cos^2\theta\right)^3}}{27M^2}. \tag{3.5}$$

The ergosphere, being the region between the outer event horizon and Killing horizon, is a region of particular interest since it is related to potentially observable processes related to the Kerr BH, such as the extraction of energy via the Penrose process. It is therefore of special interest to investigate what are the effects of the IR gravity modifications on the ergosphere surface. It follows that the IR asymptotic safe modification typically increases the ergosphere region when compared to the one in the standard GR, as we show in Figure (3.1–3.3). It can be seen that the ergosphere surface tends to increase with the increase of parameter $\tilde{\xi}$. This in principle means that the region from where it is possible to extract energy from BH by axial accretion of particles, via Penrose process, is bigger then in the GR for the equal parameters characterizing the BH. However, the practical significance of this result is limited by the fact that $\tilde{\xi}$ needs to be a small parameter.

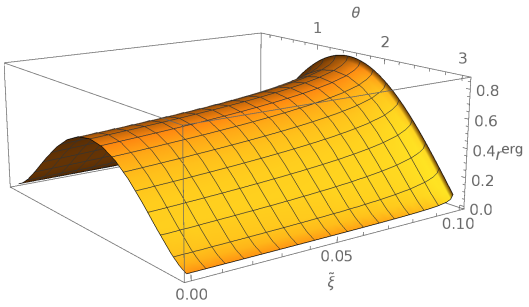

Figure 3.1: Difference between the Killing horizon and outer event horizon, r^{erg}, in the IR limit of quantum corrected gravitational coupling, for the BH defined by $a = 0.9$ and $M = 1$.

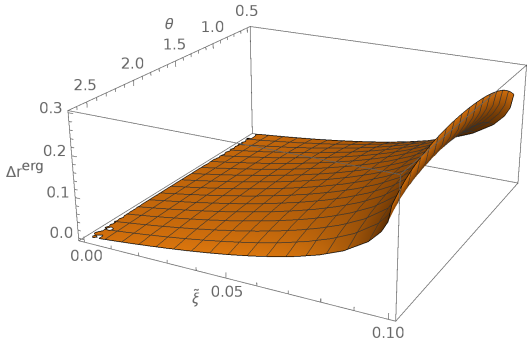

Figure 3.2: Difference between r^{erg} in the IR limit of quantum corrected gravitational coupling and GR which we label as Δr^{erg}. The BH is defined by $a = 0.9$ and $M = 1$.

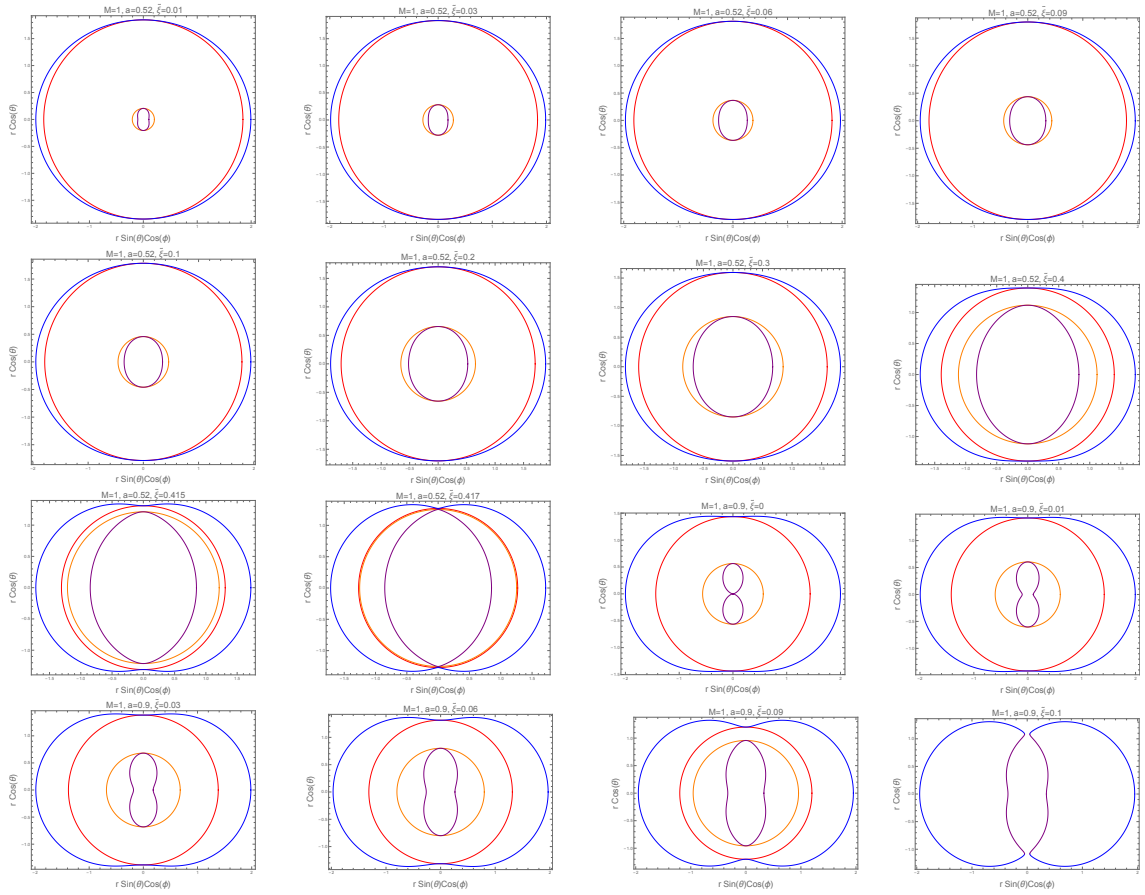

Figure 3.3: Graphs showing change in shape of inner/outer horizons (Red/Orange) and inner/outer ergo-spheres (Blue/Purple) while the value of rotational parameter is $a = 0.52, 0.9$. Note that ergosphere increases as $\tilde{\xi}$ increases.

3.1.2 Curvature Singularity

An interesting characteristic of a BH is its singularity, which can be defined mathematically when Kretschmann scalar K tends to infinity. For metric given by Eq. (3.1) the Kretschmann scalar is

$$K = \frac{M^2 \mathcal{Z}(r, \theta, a, \tilde{\xi})}{8(r\Sigma)^6}, \tag{3.6}$$

where

$$\begin{aligned} \mathcal{Z} &= 384r^{12} - 2560r^{10}\tilde{\xi} - a^8\tilde{\xi}^2 + 5888r^8\tilde{\xi}^2 + 4a^2\left(-1440r^{10} + 4864r^8\tilde{\xi} + a^6\tilde{\xi}^2 - 1632r^6\tilde{\xi}^2\right)\cos^2\theta \\ &- 2a^4\left(-2880r^8 + 1280r^6\tilde{\xi} + 3a^4\tilde{\xi}^2 - 64r^4\tilde{\xi}^2\right)\cos^4\theta + 4a^6\left(-96r^6 + a^2\tilde{\xi}^2 + 96r^2\tilde{\xi}^2\right)\cos^6\theta \\ &+ 127a^8\tilde{\xi}^2\cos^8\theta + a^8\tilde{\xi}^2\sin^8\theta. \end{aligned}$$

We observe poles at $r = 0$ and $\Sigma = r^2 + a^2\cos^2\theta = 0$ from where we interpret that the singularity exists at these points. This further constitutes a ring singularity analogous to that of Kerr BH [11].

3.2 Geodesic Equations in Equatorial Plane

This section is on equatorial geodesics of rotating BH solution in ASG, including the effects of corrected gravitational coupling. The Lagrangian, for this metric, in the equatorial plane $(\theta = \frac{\pi}{2}, \dot{\theta} = 0)$ is written as [11]

$$\begin{aligned} 2\mathcal{L} = &- \left[1 - \frac{2M}{r}\left(1 - \frac{\tilde{\xi}}{r^2}\right)\right]\dot{t}^2 - \frac{4aM}{r}\left(1 - \frac{\tilde{\xi}}{r^2}\right)\dot{t}\dot{\phi} \\ &+ \frac{r^2}{\Delta}\dot{r}^2 + \left[r^2 + a^2 + \frac{2a^2M}{r}\left(1 - \frac{\tilde{\xi}}{r^2}\right)\right]\dot{\phi}^2. \end{aligned} \tag{3.7}$$

The generalized momenta are given by

$$p_t = -\left[1-\frac{2M}{r}\left(1-\frac{\tilde{\xi}}{r^2}\right)\right]\dot{t}-\frac{2aM}{r}\left(1-\frac{\tilde{\xi}}{r^2}\right)\dot{\phi}=-E, \tag{3.8}$$

$$p_\phi = -\frac{2aM}{r}\left(1-\frac{\tilde{\xi}}{r^2}\right)\dot{t}+\left[r^2+a^2+\frac{2a^2M}{r}\left(1-\frac{\tilde{\xi}}{r^2}\right)\right]\dot{\phi}=L, \tag{3.9}$$

$$p_r = \frac{r^2}{\Delta}\dot{r}, \tag{3.10}$$

where dots over r, t and ϕ denote derivatives with respect to affine parameter τ. It can be easily seen that Lagrangian does not depend on t and ϕ, therefore p_t and p_ϕ are conserved quantities.

The Hamiltonian is given by

$$\mathcal{H} = p_t\dot{t}+p_\phi\dot{\phi}+p_r\dot{r}-\mathcal{L}. \tag{3.11}$$

It takes the form

$$2\mathcal{H} = \left[-\left(1-\frac{2M}{r}\left(1-\frac{\tilde{\xi}}{r^2}\right)\right)\dot{t}-\frac{2aM}{r}\left(1-\frac{\dot{\xi}}{r^2}\right)\dot{\phi}\right]\dot{t} \tag{3.12}$$

$$+\left[-\frac{2aM}{r}\left(1-\frac{\tilde{\xi}}{r^2}\right)\dot{t}+\left(r^2+a^2+\frac{2a^2M}{r}\left(1-\frac{\tilde{\xi}}{r^2}\right)\dot{\phi}\right)\right]\dot{\phi}+\frac{r^2}{\Delta}\dot{r}^2,$$

$$2\mathcal{H} = -E\dot{t}+L\dot{\phi}+\frac{r^2}{\Delta}\dot{r}=\delta=constant, \tag{3.13}$$

where Hamiltonian is constant as it is t independent and $\delta=-1,0,1$ gives timelike, null and spacelike geodesics respectively. Solving Eq. (3.8) and Eq. (3.9) yield:

$$\dot{t} = \frac{1}{\Delta}\left[\left(r^2+a^2+\frac{2a^2M}{r}\left(1-\frac{\tilde{\xi}}{r^2}\right)\right)E-\frac{2aM}{r}\left(1-\frac{\tilde{\xi}}{r^2}\right)L\right], \tag{3.14}$$

$$\dot{\phi} = \frac{1}{\Delta}\left[\frac{2aM}{r}\left(1-\frac{\tilde{\xi}}{r^2}\right)E+\left(1-\frac{2M}{r}\left(1-\frac{\tilde{\xi}}{r^2}\right)\right)L\right]. \tag{3.15}$$

On substituting Eq. (3.14) and Eq. (3.15) in Eq. (3.13), we get the radial equation of motion

$$r^2\dot{r}^2=\Delta\delta+r^2E^2+\frac{2M}{r}\left(1-\frac{\tilde{\xi}}{r^2}\right)(aE-L)^2+\left(a^2E^2-L^2\right). \tag{3.16}$$

In the limit $\tilde{\xi}\to 0$, Eq. (3.16) takes the form of radial equation in the Kerr BH case.

3.2.1 Null Geodesics

In equatorial plane, the null geodesics are rendered when δ gets zero in Eq. (3.16), which then becomes

$$r^2\dot{r}^2 = r^2E^2 + \frac{2M}{r}\left(1 - \frac{\tilde{\xi}}{r^2}\right)(aE - L)^2 + \left(a^2E^2 - L^2\right). \tag{3.17}$$

For convenience, introduce an impact parameter $D = L/E$ in Eq. (3.17). Through this parameter the angular momentum can be expressed in terms of energy. Two cases may arise here: either $D = a$ or $D \neq a$.

CASE (I); when D=a

As a particular case, consider $D = a$ or $L = aE$. As a result of which Eq. (3.14), Eq. (3.15) and Eq. (3.17) imply

$$\dot{t} = \frac{r^2 + a^2}{\Delta}E, \tag{3.18}$$

$$\dot{\phi} = \frac{aE}{\Delta}, \tag{3.19}$$

$$\dot{r} = \pm E. \tag{3.20}$$

Notice here that when $\Delta = 0$ (at horizon), both $\dot{t}$ and $\dot{\phi}$ go to infinity. This implies that t and ϕ operate as 'bad coordinates' in the vicinity of horizon, but this singularity vanishes in Eq. (3.20), the expression for $\dot{r}$. Using above equations, the differentials of t and ϕ, with respect to r, are computed as

$$\frac{dt}{dr} = \pm\frac{\left(r^2 + a^2\right)}{\Delta}, \tag{3.21}$$

$$\frac{d\phi}{dr} = \pm\frac{a}{\Delta}, \tag{3.22}$$

where $+$ and $-$ signs in Eq.s (3.20-3.22) stand respectively for the trajectory of outgoing and ingoing photon. The trajectory for outgoing photon is numerically solved and plotted in Figure (3.4) and Figure (3.5) where the initial condition

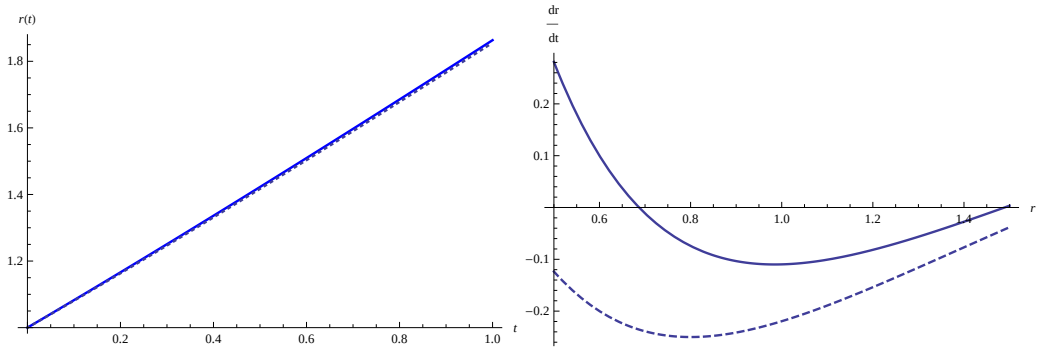

Figure 3.4: The left panel represents the outgoing trajectory of photons with respect to time t. The solid line represents when $\tilde{\xi} = 0.09$ and dashed line is when $\tilde{\xi} = 0$ i.e Kerr case. The values of parameters are $a = 0.1$ and $M = 0.1$ with the initial condition $r(0) = 10M$. On the right panel the phase portret is depicted for the same parameters, where again the solid line represents the case when $\tilde{\xi} = 0.09$ and dashed line is when $\tilde{\xi} = 0$. The fixed points are getting closer in the ASG, as opposed to the GR case where the fixed points are at maximum distance.

$r(0) = 10M$ is imposed. It can be seen that there are no high deviation from the GR counterpart in the trajectory $r(t)$ as expected from small $\tilde{\xi}$, but from the phase portrait, when dr/dt is considered as a function of r, the fixed points are getting closer to each other by increasing $\tilde{\xi}$. Same are the results for the photon trajectory with respect to angle ϕ. To get a qualitative description of equations (3.21) and (3.22) one can also easily analyze them in the phase space for different values of $\tilde{\xi}$. It can be seen that there exists a bifurcation point for which the two real fixed points vanish, and for this parameters the solution leads to a naked singularity, the phase spaces are plotted in Figure (3.6).

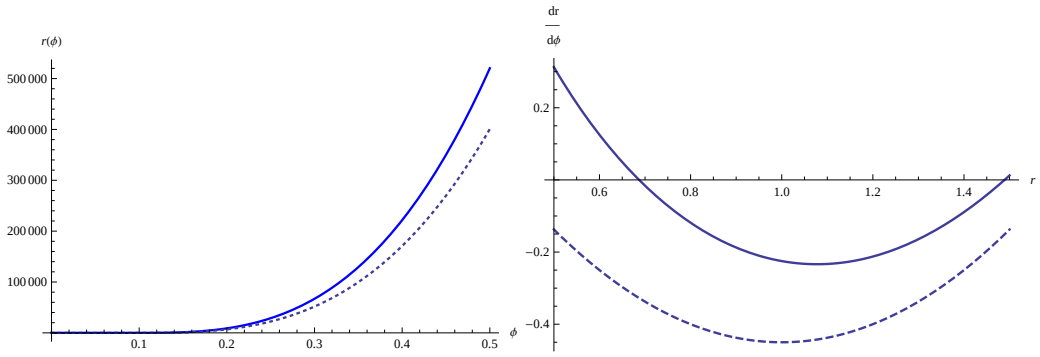

Figure 3.5: The left panel represents the outgoing trajectory of photons with respect to angle ϕ. The solid line represents when $\tilde{\xi} = 0.09$ and dashed line is when $\tilde{\xi} = 0$ i.e Kerr case for the values of parameters $a = 0.1$ and $M = 0.1$ with the initial condition $r(0) = 10M$. On the right panel the phase portrait is depicted for the same parameters, where again the solid line represents the case when $\tilde{\xi} = 0.09$ and dashed line is the GR case $\tilde{\xi} = 0$. The fixed points are again getting closer in the ASG, in the contrast to the GR case where the distance between them is maximal.

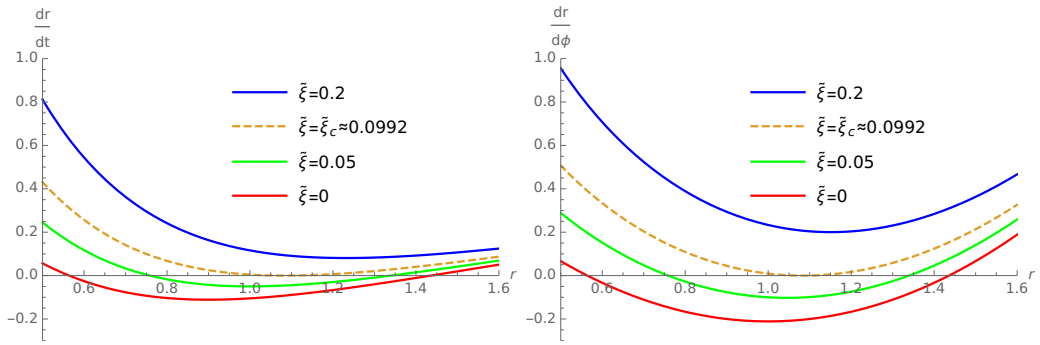

Figure 3.6: Phase space portrait, dr/dt on the left panel and $dr/d\phi$ on the right, for different values of $\tilde{\xi}$, but for fixed parameters $M = 1$ and $a = 0.9$. Clearly, the critical value for $\tilde{\xi} = \tilde{\xi}_c$ represent the bifurcation point for which the fixed points do not exist anymore.

CASE(II); when $D \neq a$

As a general case consider $D \neq a$, which consequently gives circular orbit $r = r_c$ of photon. Introduce an impact parameter $D_c = L_c/E_c$. The radial equation (3.17) along with its derivative takes the following form

$$r_c^2 + \frac{2M}{r_c}\left(1 - \frac{\tilde{\xi}}{r_c^2}\right)(a - D_c)^2 + \left(a^2 - D_c^2\right) = 0, \tag{3.23}$$

$$r_c - \frac{M}{r_c^2}\left(1 - \frac{3\tilde{\xi}}{r_c^2}\right)(a - D_c)^2 = 0. \tag{3.24}$$

Combining above two equations implies the following result

$$r_c^2 - 3Mr_c + \frac{5M\tilde{\xi}}{r_c} \pm 2a\sqrt{Mr_c\left(1 - \frac{3\tilde{\xi}}{r_c^2}\right)} = 0. \tag{3.25}$$

The real positive solution of the above equation will give circular photon orbit. For $\tilde{\xi} = 0$, it matches with circular photon orbit for Kerr BH.

3.2.2 Time-like Geodesics

To investigate time-like geodesics, take $\delta = -1$. Notice that equations for $\dot{\phi}$ and $\dot{t}$ remain unchanged, while Eq. (3.16) becomes

$$r^2\dot{r}^2 = -\Delta + r^2E^2 + \frac{2M}{r}\left(1 - \frac{\tilde{\xi}}{r^2}\right)(aE - L)^2 + \left(a^2E^2 - L^2\right), \tag{3.26}$$

where E is now described as the energy per unit mass of the particle moving in a trajectory. Two cases arise here, either $L = aE$, a special case, or $L \neq aE$, a general case which can lead us to circular and associated orbits.

Special Case: when $L = aE$

Consider $L = aE$, Eq. (3.26) gives

$$r^2\dot{r}^2 = r^2\left(E^2 - 1\right) + 2Mr\left(1 - \frac{\tilde{\xi}}{r^2}\right) - a^2, \tag{3.27}$$

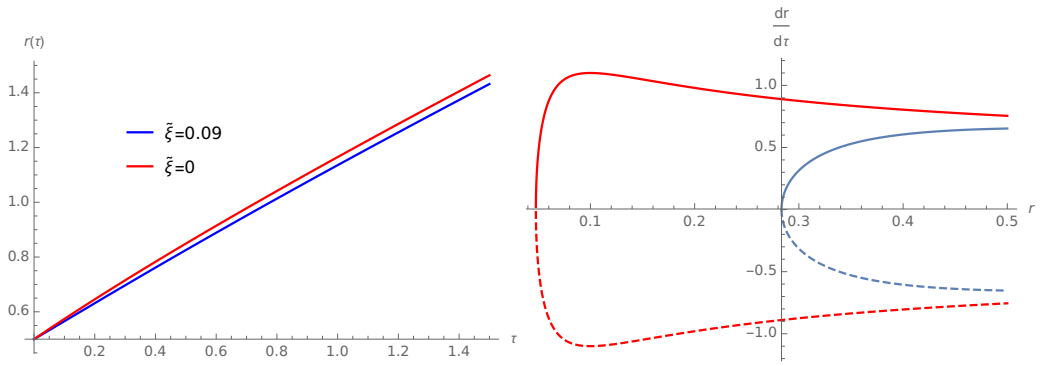

Figure 3.7: The left panel represents the trajectory of a particle $r(t)$, where the blue line represents the ASG case with $\tilde{\xi} = 0.09$ and the red line represents the GR case $\tilde{\xi} = 0$ i.e Kerr case. The values of parameters are $a = 0.1$, $M = 0.1$ and $E = 1.1$ with the initial condition $r(0) = 10M$. On the right panel the phase portrait is depicted for the same parameters, where the blue line is the phase diagram for $\tilde{\xi} = 0.09$ and the red line is the GR case where $\tilde{\xi} = 0$, the solid line represents the positive square root and dashed line the negative for each case. The fixed point is increased in the ASG $(r_* \approx 0.285)$ from the GR case $(r_* \approx 0.05)$.

while $\dot{t}$ and $\dot{\phi}$ are the same as for null geodesics. Integrate Eq. (3.27)

$$\tau = \int \frac{rdr}{\sqrt{r^2\left(E^2-1\right)+2Mr\left(1-\frac{\tilde{\xi}}{r^2}\right)-a^2}}. \tag{3.28}$$

The above equation is somewhat hideous to solve analytically. Its numerical solution is plotted in Figure (3.7). Again, as there are no high deviations from the GR case it could be more interesting to analyze the phase portrait for each case. It can be seen that the fixed point is higher in the ASG from the GR counterpart, also the phase space shows higher deviations near the fixed point but asymptotically as $r \to \infty$ the phase spaces coincide in the two cases. The phase space diagram is also plotted in Figure (3.7) but on the right panel.

General Case: when $L \neq aE$

To investigate the general case, again take into account the radial Eq. (3.26). By introducing the reciprocal radius $u = 1/r$, the equation takes the form

$$\begin{aligned} \mathcal{F}(u) = u^{-4}\dot{u}^2 &= E^2 + 2Mu^3\left(1-\tilde{\xi}u^2\right)(aE-L)^2 + \left(a^2E^2 - L^2\right)u^2 \\ &- \left(1 - 2Mu\left(1-\tilde{\xi}u^2\right) + a^2u^2\right), \end{aligned} \tag{3.29}$$

where u is the independent variable.

The task now is to compute the values of E and L for the circular orbit at the reciprocal radius $u = 1/r$. Circular orbits exist when $\mathcal{F}(u) = 0$ and $\mathcal{F}'(u) = 0$. Also, assume $x = L - aE$ in Eq. (3.29), to get

$$E^2 - \left(1 - 2Mu\left(1-\tilde{\xi}u^2\right) + a^2u^2\right) + 2Mu^3\left(1-\tilde{\xi}u^2\right)x^2 - \left(x^2 + 2xaE\right)u^2 = 0, \tag{3.30}$$

$$M\left(1-3\tilde{\xi}u^2\right) - a^2u + 3Mu^2x^2\left(1 - \frac{5}{3}\tilde{\xi}u^2\right) - \left(x^2 + 2xaE\right)u = 0. \tag{3.31}$$

Solve Eq. (3.30) and Eq. (3.31), to reach to the following form

$$E^2 = Mu^3x^2\left(1-3\tilde{\xi}u^2\right) + 1 - Mu\left(1+\tilde{\xi}u^2\right), \tag{3.32}$$

$$2xaEu = 3Mu^2x^2\left(1 - \frac{5}{3}\tilde{\xi}u^2\right) + M\left(1-3\tilde{\xi}u^2\right) - x^2u - a^2u.qz \tag{3.33}$$

Using Eq. (3.32) and Eq. (3.33), E is eradicated and the quadratic equation in x is obtained as

$$\begin{aligned} x^4 \quad & u^2\left[3Mu\left(1 - \frac{5}{3}\tilde{\xi}u^2 - 1\right)^2 - 4Ma^2u^3\left(1-3\tilde{\xi}u^2\right)\right] \\ - \quad & 2x^2u\left[\left(3Mu(1-\frac{5}{3}\tilde{\xi}u^2) - 1\right)\left(a^2u - M(1-3\tilde{\xi}u^2) + 2a^2u(1-Mu(1+\tilde{\xi}u^2))\right)\right] \\ + \quad & \left[a^2 - M(1-3\tilde{\xi}u^2)\right]^2 = 0. \end{aligned} \tag{3.34}$$

The discriminant of the above equation is given by

$$\mathcal{D} = 16a^2 M u^3 {\Delta_u}^2, \tag{3.35}$$

where $\Delta_u = 1 + a^2u^2 - 2Mu\left(1 - \tilde{\xi}u^2\right)$. The calculations can be eased by considering

$$1 - 3Mu\left(1 - \frac{5}{3}\tilde{\xi}u^2\right) - 4Ma^2u^3\left(1 - 3\tilde{\xi}u^2\right) = \mathcal{F}_+\mathcal{F}_-,$$

where

$$\mathcal{F}_\pm = 1 - 3Mu\left(1 - \frac{5}{3}\tilde{\xi}u^2\right) \pm 2a\sqrt{Mu^3\left(1 - 3\tilde{\xi}u^2\right)}.$$

The solution of Eq. (3.34) is then simply computed as

$$x^2u^2 = \frac{\Delta_u\mathcal{F}_\pm - \mathcal{F}_+\mathcal{F}_-}{\mathcal{F}_+\mathcal{F}_-} = \frac{\Delta_u - \mathcal{F}_\mp}{\mathcal{F}_\mp}, \tag{3.36}$$

where

$$\Delta_u - \mathcal{F}_\mp = u\left[a\sqrt{u} \pm \sqrt{M\left(1 - 3\tilde{\xi}u^2\right)}\right]^2.$$

Finally, we get

$$x = -\frac{a\sqrt{u} \pm \sqrt{M\left(1 - 3\tilde{\xi}u^2\right)}}{u\mathcal{F}_\mp}. \tag{3.37}$$

Put Eq. (3.37) in Eq. (3.31), to get energy of the circular orbit

$$E = \frac{1}{\sqrt{\mathcal{F}_\mp}}\left[1 - 2Mu\left(1 - \tilde{\xi}u^2\right) \mp au\sqrt{Mu\left(1 - 3\tilde{\xi}u^2\right)}\right], \tag{3.38}$$

where upper and lower signs are respectively interpreted as prograde and retrograde orbits. Angular momentum associated to the circular orbit is thus given by

$$L = \frac{\mp\sqrt{M\left(1 - 3\tilde{\xi}u^2\right)}}{\sqrt{u\mathcal{F}_\mp}}\left[1 + a^2u^2 \pm 2au\left(1 - \tilde{\xi}u^2\right)\sqrt{\frac{Mu}{\left(1 - 3\tilde{\xi}u^2\right)}}\right]. \tag{3.39}$$

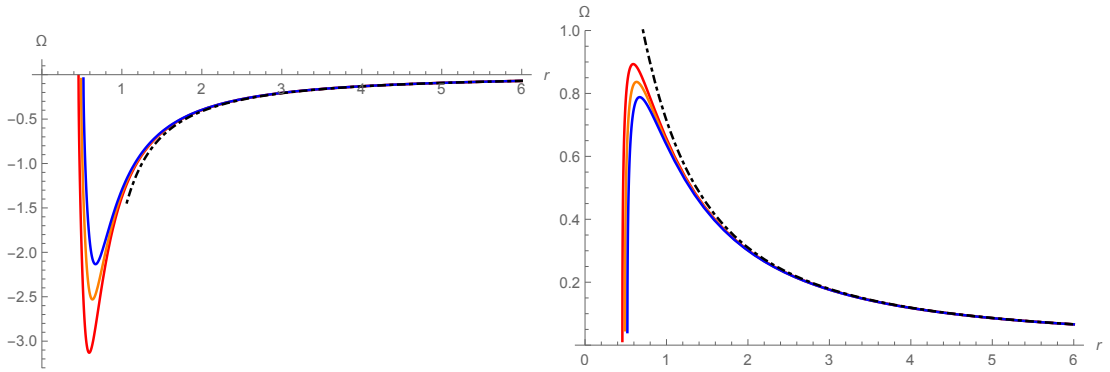

Figure 3.8: Angular velocity of prograde (left panel) and retrograde (right panel) motion of particles orbiting in the equatorial plane of rotating BH in ASG, for the values of the parameters as: M=1, $\tilde{\xi} = 0.07$ (Red), 0.08 (Orange), 0.09 (Blue) and $a = 0.4$. Black (DotDashed) line shows $\tilde{\xi} = 0$ i.e Kerr case.

The angular velocity is computed using Eq. (3.14) and Eq. (3.15)

$$\Omega = \frac{\dot{\phi}}{\dot{t}} = \frac{\frac{2aM}{r}\left(1-\frac{\tilde{\xi}}{r^2}\right)E + \left(1-\frac{2M}{r}\left(1-\frac{\tilde{\xi}}{r^2}\right)\right)L}{\left(r^2+a^2+\frac{2a^2M}{r}\left(1-\frac{\tilde{\xi}}{r^2}\right)\right)E - \frac{2aM}{r}\left(1-\frac{\tilde{\xi}}{r^2}\right)L},$$

which, by using reciprocal radius, can be reduce to the form

$$\Omega = \frac{\left[L - 2Mux\left(1-\tilde{\xi}u^2\right)\right]u^2}{\left(1+a^2u^2\right)E - 2aMu^3\left(1-\tilde{\xi}u^2\right)}.$$

This can be simplified to the form

$$\Omega = \frac{\mp\sqrt{Mu^3\left(1-3\tilde{\xi}u^2\right)}}{1 \mp au\sqrt{Mu\left(1-3\tilde{\xi}u^2\right)}}.$$

Thus the angular velocity in terms of r can be written, by using $r = \frac{1}{u}$, as

$$\Omega = \frac{\mp\sqrt{M\left(r-\frac{3\tilde{\xi}}{r}\right)}}{r^2 \mp a\sqrt{M\left(r-\frac{3\tilde{\xi}}{r}\right)}}.$$

The graphical representation of angular velocity of particles is shown in Figure (3.8). The value of Ω, for corotating (prograde) motion, first decreases but it increases with the increase in $\tilde{\xi}$ and r. But for counter rotating (retrograde) motion, the particle's angular velocity declines when $\tilde{\xi}$ is increased.
The time period is given by

$$T = \frac{2\pi}{\Omega} = 2\pi \frac{r^2 \mp a\sqrt{M\left(r - \frac{3\tilde{\xi}}{r}\right)}}{\mp\sqrt{M\left(r - \frac{3\tilde{\xi}}{r}\right)}}. \tag{3.40}$$

3.2.3 Effective Potential

To check the stability (or instability) of circular orbit of particles around the rotating BH in ASG in IR regime, the effective potential is determined. Thus the equation governing the effective potential of circular orbits, both for photons and time-like particles, is given by [105]

$$\frac{E^2 - 1}{2} = \frac{\dot{r}^2}{2} + V_{\text{eff}},$$

where effective potential is represented by V_{eff}. The extreme value $r = r_o$ of the effective potential is the solution of the equation

$$\frac{dV_{\text{eff}}}{dr}|_{r=r_o} = 0.$$

There must be present a minimum at the second derivative of effective potential i.e $\frac{d^2V_{eff}}{dr^2} > 0$ which gives stable circular orbits along with the condition that at circular orbit $r = r_o$ the particles initial velocity must vanish i.e $\dot{r} = 0$. Following is the discussion on the effective potential of null and time-like geodesics.

For Null Geodesics

For $L = aE$, the null geodesics is governed by radial equation $\dot{r} = \pm E$, so the case sufficient to consider here is when $L \neq aE$. In this case, the effective potential is

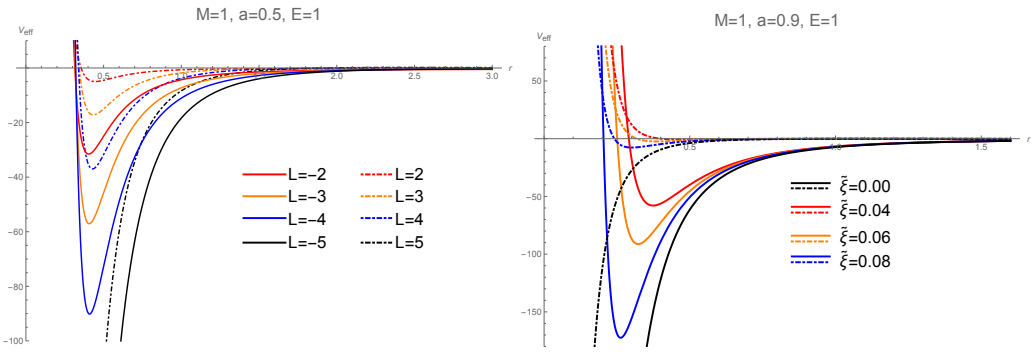

Figure 3.9: Plots showing behaviour of effective potential, for null geodesics, with respect to r. Here co-rotating (counter-rotating) particles are shown by solid (dot-dashed) lines.

thus given by

$$V_{\text{eff}} = \frac{1}{2r^3}\Big[-2M\Big(1-\frac{\tilde{\xi}}{r^2}\Big)\Big(aE-L\Big)^2+\Big(L^2-a^2E^2\Big)r-r^3\Big].$$

This effective potential is graphically presented in Figure (3.9). As one can easily see the presence of minimum values in these plots which corresponds to the existence of stable points. Also note that the behavior of V_{eff} for both co-rotating and counter-rotating particles is quite different from the Kerr case. Namely, the effective potential for Kerr BH approaches negative infinity when $r \to 0$, while the effective potential for the rotating BH with running gravitational coupling approaches positive infinity when $r \to 0$. This comes as a result of sign change for the leading order in the potential for small r, which comes as a consequence of introducing the asymptotic correction parameter $\tilde{\xi}$. However, it should be stressed that at very small distances IR will no longer be valid, and the proper description should now be given using the UV limit of ASG.

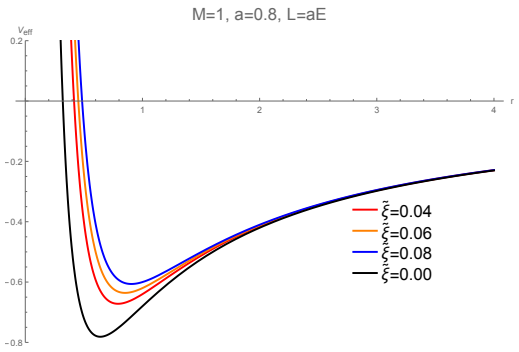

Figure 3.10: Behaviour of effective potential for time-like geodesics, with respect to r, when $L = aE$. Black line shows $\tilde{\xi} = 0$ i.e Kerr case.

For Time-like Geodesics

By the use of Eq. (3.26), the effective potential for the time-like geodesics, both when $L = aE$ and $L \neq aE$, is computed respectively as

$$V_{\text{eff}} = \frac{a^2}{2r^2} - \frac{M}{r}\left(1 - \frac{\tilde{\xi}}{r^2}\right)$$

and

$$V_{\text{eff}} = \frac{-M}{r^3}\left(1 - \frac{\tilde{\xi}}{r^2}\right)\left(aE - L\right)^2 + \frac{L^2 - a^2\left(E^2 - 1\right)}{2r^2} - \frac{M}{r}\left(1 - \frac{\tilde{\xi}}{r^2}\right).$$

For time like geodesics, when $L = aE$, the affect of $\tilde{\xi}$ on effective potential is shown in Figure (3.10). These plots show existence of stable points for different values of $\tilde{\xi}$. Figure (3.11) shows variation of $\tilde{\xi}$ and angular momentum L in effective potential. Here it is noted that for co-rotating motion of the particle the depth of the potential well increases with increase in L while for counter rotating motion, it decreases for increase in L. These graphs also show the existence of stable points. As in the case of null geodesics, discussed previously, Kerr and the IR asymptotic safe solution lead to different qualitative features of the effective potential when $r \to 0$.

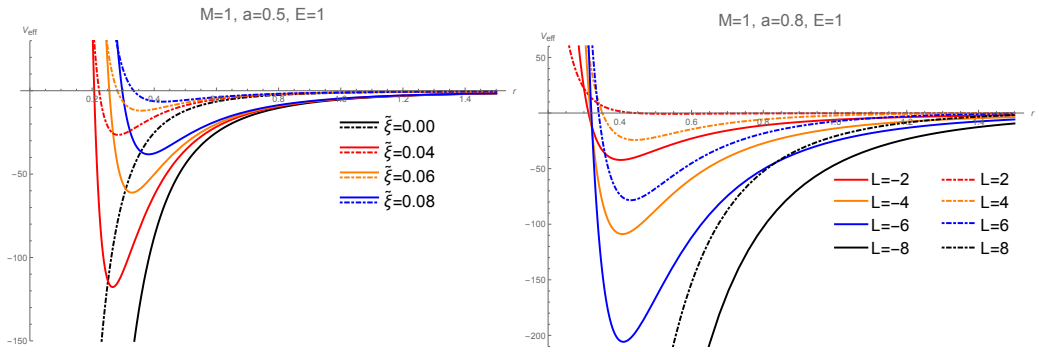

Figure 3.11: Behaviour of effective potential for time-like geodesics, with respect to r, when $L \neq aE$. Solid lines show counter-rotating while dot-dashed lines show co-rotating particles. Black (solid/dot-dashed) line shows $\tilde{\xi} = 0$ i.e Kerr case. In left panel L is kept fixed ($L = -2$ and 2 for counter-rotating and co-rotating particles) while in right panel $\tilde{\xi} = 0.09$ for different values of L

3.3 Penrose Process

Energy is a conserved quantity on the spacetime of stationary rotating BH, due to the existence of associated Killing vector, $K_\mu = \partial_t$, so that $E = -K^\mu u^\mu$, where u^μ is a four-velocity defined on some geodesic. At the asymptotic infinity both K^μ and u^μ are timelike, so that energy is always positive. However, Killing vector becomes null at the Killing horizon, and spacelike inside the region known as ergosphere – which represents the space between the outer event horizon and the Killing horizon of a BH. It is therefore possible that energy becomes negative quantity in the ergosphere of a stationary rotating BH. This fact was used by Penrose, who proposed a mechanism of extraction of energy from Kerr BH. Starting from a particle falling into a BH, which is defined by the positive energy, one can consider the case where it decays in the ergosphere, into one particle carrying positive energy, and the other particle carrying negative energy. Since the total energy needs to be conserved, if we assume that the negative energy particle crosses the

event horizon and the positive energy particle leaves the ergosphere reaching the observer, its energy will be higher than the energy of the initial particle (since it is the difference of the initial energy and the negative energy of the second particle).

We now analyze the Penrose process, taking into account the corrections of ASG. Let us first note, that the modifications coming from the quantum effects leading to a r-dependent gravitational coupling were previously considered in the context of the Penrose process in [90], where the running coupling of the following form was considered

$$G(r) = \frac{G_0 r^2}{r^2 + \omega G_0}, \tag{3.41}$$

where G_0 is the classical Newton constant, and ω a positive constant. In [90] authors studied the functional dependencies of tangential and dragging velocities in the Penrose process and concluded that there exists a lowest possible mass for the Penrose mechanism when such running gravitational coupling is considered. In our analysis this is related to the mass corresponding to $\tilde{\xi}_c$ which enters in equation (3.3). In this work we will perform a similar analysis of the Penrose process in the context of varying gravitational coupling, and further extend it by investigating the efficiency of Penrose process in this setting and comparing it with the classical limit.

As already discussed, utilizing the fact that energy in the ergoregion can be negative, it is under suitable conditions possible to extract energy from the rotating BH. In this discussion we concentrate on the scenario where we have a massive particle entering the ergosphere, and which moves along a timelike geodesic, carrying positive energy. This particle then decays into two particles which are massless, one carrying negative energy, and the second one with positive energy. The negative energy particle then falls into event horizon, while the particle with a positive energy eventually leaves the ergosphere and reaches the observer. If

this decay happened at the turning point of the geodesic, where $\dot{r} = 0$, then from the radial equation for equatorial geodesic it follows that

$$E = \frac{1}{r\left(r^2+a^2\right)+2a^2M\left(1-\frac{\tilde{\xi}}{r^2}\right)}\left[2aM\left(1-\frac{\tilde{\xi}}{r^2}\right)L\pm \sqrt{r^2\Delta L^2-\left(r\left(r^2+a^2\right)+2a^2M\left(1-\frac{\tilde{\xi}}{r^2}\right)\right)\delta r}\right], \tag{3.42}$$

and alternatively angular momentum can be expressed as

$$L = \frac{1}{r-2M\left(1-\frac{\tilde{\xi}}{r^2}\right)}\left[-2aM\left(1-\frac{\tilde{\xi}}{r^2}\right)\pm \sqrt{\Delta r^2E^2+\left(1-\frac{2M}{r}\left(1-\frac{\tilde{\xi}}{r^2}\right)\right)\Delta\delta r^2}\right], \tag{3.43}$$

where the following identity was used

$$\left[r^2\left(r^2+a^2\right)+2a^2Mr\left(1-\frac{\tilde{\xi}}{r^2}\right)\right]\left(1-\frac{2M}{r}\left(1-\frac{\tilde{\xi}}{r^2}\right)\right)=r^2\Delta-4a^2M^2\left(1-\frac{\tilde{\xi}}{r^2}\right)^2 \tag{3.44}$$

Now we can determine the condition under which energy and angular momentum will be negative. In order that $E < 0$, $L < 0$ it follows

$$4a^2M^2\left(1-\frac{\tilde{\xi}}{r^2}\right)^2L^2>\Delta\left[r^2L^2-\left(r\left(r^2+a^2\right)+2a^2M\left(1-\frac{\tilde{\xi}}{r^2}\right)\right)\delta r\right] \tag{3.45}$$

Using eq. (3.44) this can be written as

$$\left[r\left(r^2+a^2\right)+2a^2Mr\left(1-\frac{\tilde{\xi}}{r^2}\right)\right]\left[\left(1-\frac{2M}{r}\left(1-\frac{\tilde{\xi}}{r^2}\right)\right)L^2-\Delta\delta r\right]<0. \tag{3.46}$$

It follows that $E < 0 \Longleftrightarrow L < 0$ requires the condition

$$r \leq 2M\left(1-\frac{\tilde{\xi}}{r^2}\right)+\frac{\Delta\delta r^2}{L^2}, \tag{3.47}$$

so we confirm that this can happen only in the ergosphere.

We now come back to discussion of the decay of one initial massive particle to

two massless particles, carrying the energy of opposite signs. We take that initial energy is $E^{(0)} = 1$, and energy of two particles is $E^{(1)}$ and $E^{(2)}$ respectively. Let then

$$L^{(0)} = \frac{-2aM\left(1-\frac{\tilde{\xi}}{r^2}\right) + \sqrt{2Mr\left(1-\frac{\tilde{\xi}}{r^2}\right)\Delta}}{r-2M\left(1-\frac{\tilde{\xi}}{r^2}\right)} = \alpha^{(0)}, \tag{3.48}$$

$$L^{(1)} = \frac{-2aM\left(1-\frac{\tilde{\xi}}{r^2}\right) - \sqrt{r^2\Delta}}{r-2M\left(1-\frac{\tilde{\xi}}{r^2}\right)}E^{(1)} = \alpha^{(1)}E^{(1)}, \tag{3.49}$$

$$L^{(2)} = \frac{-2aM\left(1-\frac{\tilde{\xi}}{r^2}\right) + \sqrt{r^2\Delta}}{r-2M\left(1-\frac{\tilde{\xi}}{r^2}\right)}E^{(2)} = \alpha^{(2)}E^{(2)}. \tag{3.50}$$

Here α's are some arbitrary functions relating angular momentum and energy. According to conservation of energy and momentum

$$E^{(1)} + E^{(2)} = E^{(0)} = 1 \tag{3.51}$$

and

$$L^{(1)} + L^{(2)} = \alpha^{(1)}E^{(1)} + \alpha^{(2)}E^{(2)} = L^{(0)} = \alpha^{(0)}. \tag{3.52}$$

Solving these equations we can obtain the energies of two created particles as

$$E^{(1)} = \frac{1}{2}\Big[1 - \sqrt{\frac{2M}{r}(1-\frac{\tilde{\xi}}{r^2})}\Big] \tag{3.53}$$

$$E^{(2)} = \frac{1}{2}\Big[1 + \sqrt{\frac{2M}{r}(1-\frac{\tilde{\xi}}{r^2})}\Big]. \tag{3.54}$$

Then, if $E^{(2)}$ reaches the observer outside the BH, and $E^{(1)}$ crosses the event horizon, the gain in energy with respect to the original particle, as measured by the observer is

$$\Delta E = \frac{1}{2}\Big[\sqrt{\frac{2M}{r}(1-\frac{\tilde{\xi}}{r^2})} - 1\Big] = -E^{(1)}. \tag{3.55}$$

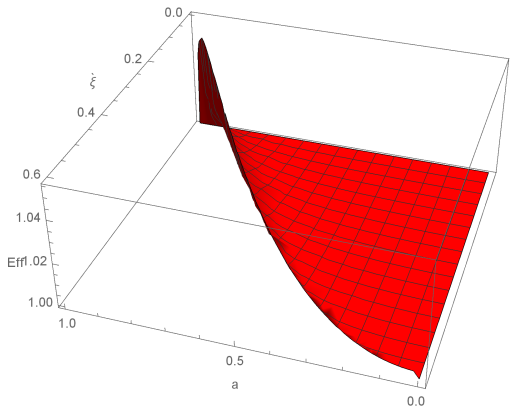

Figure 3.12: Ratio between the efficiency of Penrose process in the IR limit of quantum corrected gravitational coupling and general relativity, as a function of a and $\tilde{\xi}$, with $M = 1$.

In order to study the maximal possible efficiency of Penrose process one should consider the case with respect to which any reasonable physical realization will lead to smaller values. The gain in energy will be bigger if the radial distance is smaller, so we consider the extreme case of the event horizon $r = r_H$. For simplicity, we can use for example BH defined by $r_H = M = 1$. For such BH from the horizon equation it follows that $\tilde{\xi} = \frac{1}{2}(1 - a^2)$. We get that the maximal efficiency of Penrose process in this case is then given by

$$E_{\mathrm{ff}_{max}} = \frac{E^{(0)} + \Delta E}{E^{(0)}}_{max} = \frac{1}{2}[1 + \sqrt{2(1 - \tilde{\xi})}] < 1.207, \tag{3.56}$$

so we see that for a given BH with the same fixed parameters r_H and M in general relativity and ASG, the efficiency of Penrose process will be smaller in ASG. However, as noted earlier, in ASG the outer event horizon tends to be located at smaller r than in the standard general relativity, for all other parameters staying the same. This fact can thus compensate the direct loss coming from the corrective term in Eq. (3.55), and can even increase the efficiency above the one characteristic for Kerr BH in general relativity. We should stress that, from the astrophysical

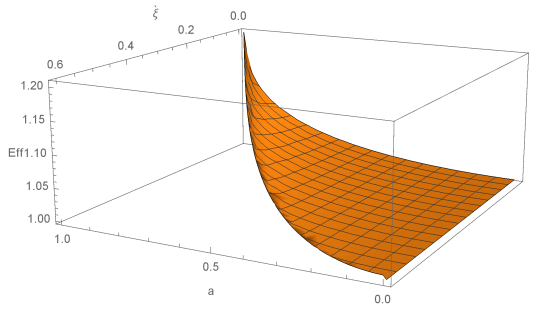

Figure 3.13: Efficiency of Penrose process in the IR limit of quantum corrected gravitational coupling as a function of a and $\tilde{\xi}$, with $M = 1$.

perspective, a and M should be considered as real independent quantities defining the BH – actually given as initial conditions during the collapse of matter leading to BH formation – and that position of event horizon should be considered as a dependent quantity. Therefore, it is more proper to compare rotating BHs in ASG and general relativity for the same values of M and a, rather than r_H. Taking $M = 1$ for simplicity, we show that – in accord with the previous reasoning – for the same values of a the efficiency of Penrose process will be greater in ASG. This is demonstrated in Figure 3.12 where we show the ratio of efficiency of Penrose process in asymptotically safe gravity and general relativity as a function of a and $\tilde{\xi}$. However, it can be seen in Figure 3.13 – where we plot the efficiency of Penrose process in ASG, that the maximal possible efficiency still basically stays confined within the region estimated in Eq. (3.56).

3.4 Lense-Thirring Frequency

The forms of electromagnetic equations and gravitational equations are very similar, so that the gravito-electromagnetism [106] summarizes the weak field gravitational equations as the “Maxwell Equations". As we all know, a rotating sphere with electric charge can produce magnetic field, so it is reasonable to believe that “magnetic effect" of gravitational field can be found in spacetime with rotating massive sphere. In 1918, Lense and Thirring theoretically proposed Lense-Thirring effect to describe the “magnetic effect" in gravitational field [7]. According to [107–110], the precession frequency vector of rotating BH is given by

$$\Omega_{LT} = \frac{1}{2}\frac{\epsilon_{ijl}}{\sqrt{-g}}\left[g_{0i,j}\left(\partial_l - \frac{g_{0l}}{g_{00}}\partial_0\right) - \frac{g_{0i}}{g_{00}}g_{00,j}\partial_l\right]. \tag{3.57}$$

From our metric, above result is rewritten as

$$\Omega_{LT} = \frac{1}{2\sqrt{-g}}\left[\left(g_{0\phi,r} - \frac{g_{0\phi}}{g_{00}}g_{00,r}\right)\partial_\theta - \left(g_{0\phi,\theta} - \frac{g_{0\phi}}{g_{00}}g_{00,\theta}\right)\partial_r\right] \tag{3.58}$$

$$\begin{aligned}\Omega_{LT} &= \Omega^\theta\partial_\theta + \Omega^r\partial_r, \\ \Omega_{LT}^2 &= g_{rr}\left(\Omega^r\right)^2 + g_{\theta\theta}\left(\Omega^\theta\right)^2.\end{aligned} \tag{3.59}$$

While in polar coordinates (where $\hat{r}$ is the unit vector of direction r and $\hat{\theta}$ is angular coordinate), Ω_{LT} is given by

$$\vec{\Omega}_{LT} = \sqrt{g_{rr}}\Omega^r\hat{r} + \sqrt{g_{\theta\theta}}\Omega^\theta\hat{\theta}. \tag{3.60}$$

Therefore, for our BH spacetime

$$\begin{aligned}\Omega^\theta &= \frac{2aM\left(r^2-\tilde{\xi}\right)\left(a^2r - 2Mr^2 + r^3 + 2M\tilde{\xi}\right)\cos(\theta)}{r\left(r^2 + a^2\cos\left(\theta\right)^2\right)^2\left(r^3 - 2Mr^2 + 2M\tilde{\xi} + a^2r\cos\left(\theta\right)^2\right)}, \\ \Omega^r &= \frac{aM\left[r^2\left(r^2 - 3\tilde{\xi}\right)\sin\left(\theta\right) - a^2\left(r^2+\tilde{\xi}\right)\cos\left(\theta\right)^2\sin\left(\theta\right)\right]}{r\left(r^2 + a^2\cos\left(\theta\right)^2\right)^2\left(r^3 - 2Mr^2 + 2M\tilde{\xi} + a^2r\cos\left(\theta\right)^2\right)}.\end{aligned} \tag{3.61}$$

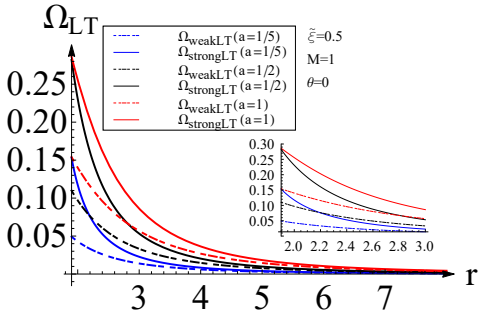

Figure 3.14: Ω_{strongLT} and Ω_{weakLT} as functions of r for $a = 1/5, 1/2, 1$, where $\tilde{\xi} = 0.5$, $M = 1$, $\theta = 0$

Therefore the magnitude of Ω_{LT} is given by

$$\Omega_{LT} = \Omega_{\text{StrongLT}} = J\frac{\sqrt{4r^2\left(r^2-\tilde{\xi}^2\right)^2\Delta\cos(\theta)^2+\left(r^4-3\tilde{\xi}r^2-a^2\left(r^2+\tilde{\xi}\right)\cos(\theta)^2\right)^2\sin(\theta)^2}}{r^2\left(\Delta-a^2\sin(\theta)^2\right)\Sigma^{3/2}}$$

According to [107], in the weak field limit (which means $r \gg M$), we expand above formula by M, so Ω_{LT} in weak field is:

$$\begin{aligned}\Omega_{\text{weakLT}} &= \frac{J}{r^2\Sigma^{5/2}}\left\{r^2\cos(\theta)^2\left[4\left(r^3-r\tilde{\xi}\right)^2+a^2\left(3r^4-8\tilde{\xi}r^2+7\tilde{\xi}^2\right)+a^2\left(r^4-3\tilde{\xi}^2\right)\cos(2\theta)\right]\right.\\ &\left.+a^4\left(r^2+\tilde{\xi}\right)^2\cos(\theta)^4\sin(\theta)^2+r^4\left[\left(r^2-3\tilde{\xi}\right)^2+4a^2\tilde{\xi}\cos(\theta)^2\right]\sin(\theta)^2\right\}^{1/2}+\mathcal{O}\left(M^2\right)\end{aligned}$$

We show the $\Omega_{LT} = \Omega_{LT}(r)$ with various parameters in Figure (3.14), Figure (3.15) and Figure (3.16).

The Figure (3.14) shows that Lense-Thirring effect is significantly increased as a is increased because it is a rotating effect. On the other hand, according to the Figure (3.15), it is interesting that the effect of Ω_{strongLT} is more outstanding at equator $\theta = \pi/2$ than the pole $\theta = 0$, but the effect of Ω_{weakLT} is more outstanding at the pole $\theta = 0$ than equator $\theta = \pi/2$. Finally, from Figure (3.16), we find that Lense-Thirring effect in our rotating BH spacetime is weaker than Kerr spacetime

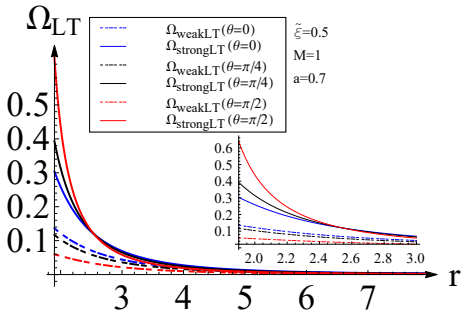

Figure 3.15: Ω_{strongLT} and Ω_{weakLT} as functions of r for $\theta = \pi/2, \pi/4, 0$, where $\tilde{\xi} = 0.5$, $M = 1$, $a = 0.7$

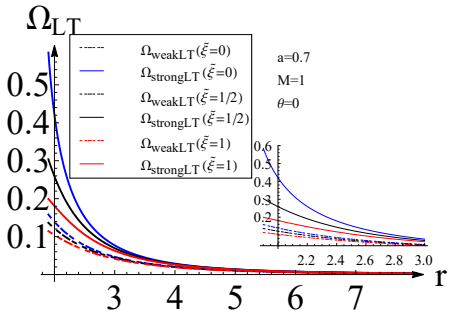

Figure 3.16: Ω_{strongLT} and Ω_{weakLT} as functions of r for $\tilde{\xi} = 0, 1/2, 1$, where $a = 0.7$, $M = 1, \theta = 0$

as $\tilde{\xi}$ increases, so it means that it is more difficult to measure this effect in our metric, but we can compare the results of experiment to determine the value of $\tilde{\xi}$, and rotating spacetime won't be Kerr spacetime if $\tilde{\xi} \neq 0$.

Chapter 4

Shadow of Rotating Black Holes in Perfect Fluid Dark Matter with a Cosmological Constant

The presence of dark matter around a BH remarkably affects its spacetime. In this chapter we consider the effects of dark matter on the shadow of a new solution to the EFEs that describes a rotating BH in the background of PFDM, along with its extension to nonzero cosmological constant Λ. Working in Boyer-Lindquist coordinates, we consider the effects of the PFDM parameter α on the shadow cast by a BH with respect to an observer at position (r_o, θ_o).

This chapter is separated in three main sections. In first section the BH' metric under consideration has been briefly reviewed. In second section, null geodesics have been computed and photon orbits have been discussed. The shadow of the BH in PFDM are investigated in detail in third section.

4.1 Black Holes in Perfect Fluid Dark Matter Background

Amongst the many dark matter models that have been suggested is the perfect fluid dark matter model, which was initially proposed by Kiselev [112], and entailed construction of a new class of spherically symmetric BH metrics in the presence of PFDM [113]. Only recently has this class been generalized to include rotation [99], providing a PFDM version of the Kerr-AdS solution. The metric is given by

$$\begin{aligned} ds^2 &= -\frac{\Delta_r}{\Xi^2\Sigma}\left(dt - a\sin^2\theta d\phi\right)^2 + \frac{\Delta_\theta \sin^2\theta}{\Xi^2\Sigma}\left(adt - (r^2+a^2)d\phi\right)^2 \\ &+ \frac{\Sigma}{\Delta_r}dr^2 + \frac{\Sigma}{\Delta_\theta}d\theta^2 \end{aligned} \tag{4.1}$$

where

$$\begin{aligned} \Delta_r &= r^2 - 2Mr + a^2 - \frac{\Lambda}{3}r^2\left(r^2+a^2\right) + \alpha r \ln\frac{r}{|\alpha|}, \\ \Delta_\theta &= 1 + \frac{\Lambda}{3}a^2\cos^2\theta \qquad \text{and} \qquad \Xi = 1 + \frac{\Lambda}{3}a^2, \qquad \Sigma = r^2 + a^2\cos^2\theta \end{aligned} \tag{4.2}$$

with the mass parameter of the BH being M. The parameter indicating the presence of perfect fluid dark matter is α. This solution reduces to a rotating BH in a PFDM background when $\Lambda = 0$, and to the Kerr-AdS solution for $\alpha = 0$. The PDFM stress-energy tensor in the standard orthogonal basis of the Kerr-AdS metric can be written in diagonal form $[\rho, p_r, p_\theta, p_\phi]$, where

$$\rho = -p_r = \frac{\alpha r}{8\pi\Sigma^2} \qquad p_\theta = p_\phi = \frac{\alpha r}{8\pi\Sigma^2}\left(r - \frac{\Sigma}{2r}\right) \tag{4.3}$$

For $\Lambda \neq 0$, the solution can either be a Kerr-Anti-de Sitter ($\Lambda < 0$) or Kerr-de Sitter ($\Lambda > 0$) metric. The horizons of the BH are the solutions of $\Delta_r = 0$ i.e.

$$\frac{\Lambda}{3}r^4 + \left(\frac{\Lambda}{3}a^2 - 1\right)r^2 + 2Mr - a^2 + \alpha r \log\left(\frac{r}{\mid \alpha \mid}\right) = 0. \tag{4.4}$$

In general there are inner and outer horizons for Kerr and Kerr anti-de Sitter BHs, with an additional cosmological horizon for Kerr-de Sitter BHs. Imposing the requirement that PDFM does not change the number of horizons as compared to its Kerr counterpart, the parameter α is constrained such that [99]

$$\alpha \in \begin{cases} (-7.18M, 0) \cup (0, 2M) & \text{if} \quad \Lambda = 0, \\ (\alpha_{min}, 0) \cup (0, \alpha_{max}) & \text{if} \quad \Lambda \neq 0 \end{cases} \tag{4.5}$$

where α_{max} and α_{min} respectively satisfy

$$\begin{aligned} \alpha_{min} \quad + \quad \alpha_{min} \log(\frac{2M}{-\alpha_{min}}) = 2M + H(\Lambda) \\ \alpha_{max} \quad + \quad \alpha_{max} \log(\frac{2M}{\alpha_{max}}) = 2M + H(\Lambda) \end{aligned} \tag{4.6}$$

and

$$H(\Lambda) = -\text{sgn}(\Lambda) \left(\frac{32}{3\Lambda} M^3 + \frac{2}{3} \Lambda a^2 \right) \tag{4.7}$$

and we see if $a = 0$ that $H > 0$ for $\Lambda < 0$ and $H < 0$ for $\Lambda > 0$.

4.2 Photon Region

For the spacetime (4.1), geodesic motion is governed by the Hamilton Jacobi equation [11]:

$$-\frac{\partial S}{\partial \tau} = \frac{1}{2} g^{\mu\nu} \frac{\partial S}{\partial x^\mu} \frac{\partial S}{\partial x^\nu}, \tag{4.8}$$

where τ is an affine parameter, x^μ represents the four-vector (t, r, θ, ϕ) and S is Hamilton's principal function, which can be made separable by introducing an ansatz such that

$$S = \frac{1}{2}\delta\tau - Et + L\phi + S_r(r) + S_\theta(\theta),$$

where energy E and angular momentum L are constants of motion related to the associated Killing vectors $\partial/\partial t$ and $\partial/\partial\phi$. For timelike geodesics $\delta = 1$ and for null geodesics $\delta = 0$. Thus by solving Eq. (4.8) the resulting equations describing the propagation of a particle are

$$\Sigma\dot{t} = \Xi^2\frac{\left((r^2+a^2)E - aL\right)(r^2+a^2)}{\Delta_r} - \frac{a\Xi^2\left(aE\sin^2\theta - L\right)}{\Delta_\theta}, \tag{4.9}$$

$$\Sigma^2\dot{r}^2 = \Xi^2\left(\left(r^2+a^2\right)E - aL\right)^2 - \Delta_r r^2\delta - \mathcal{C}\Delta_r = R(r), \tag{4.10}$$

$$\Sigma^2\dot{\theta}^2 = -\frac{\Xi^2}{\sin^2\theta}\left(aE\sin^2\theta - L\right)^2 - a^2\delta\cos^2\theta + \mathcal{C}\Delta_\theta = \Theta(\theta), \tag{4.11}$$

$$\Sigma\dot{\phi} = \frac{a\Xi^2\left((r^2+a^2)E - aL\right)}{\Delta_r} - \frac{\Xi^2\left(aE\sin^2\theta - L\right)}{\Delta_\theta\sin^2\theta} \tag{4.12}$$

for both null and time-like geodesics. In the above equations, besides the two constants of motion E and L, we also have the Carter constant $\mathcal{C}$ [114]. As we are interested in BH's shadows, henceforth we consider only null geodesics, for which $\delta = 0$. To reduce the number of parameters we write $\xi = L/E$ and $\eta = \mathcal{C}/E^2$, and rescale $R/E^2 \to R$ and $\Theta/E^2 \to \Theta$. Then Eq. (4.10) and (4.11) respectively yield

$$R = \Xi^2\left((r^2+a^2) - a\xi\right)^2 - \Delta_r\eta \tag{4.13}$$

and

$$\Theta = \eta\Delta_\theta - \frac{\Xi^2}{\sin^2\theta}\left(a\sin^2\theta - \xi\right)^2. \tag{4.14}$$

The photon region is defined as the region of space where gravity is strong enough that photons are forced to travel in orbits. Circular photon orbits only exist in the equatorial plane for rotating Kerr BHs, and there are two such types, retrograde and prograde. To this end, we note that there are other solutions such as the rotating dyonic BHs in Kaluza-Klein and Einstein-Maxwell-dilaton theory, for which circular photon orbits do not exist on the equatorial plane. Note that Schwarzschild is another counter-example, albeit static, that contains non-equatorial circular photon orbits due to spherical symmetry. To determine the

photon region we require that the radial coordinate remains constant such that $\dot{r} = 0 = \ddot{r}$ or

$$R(r) = 0 \quad \text{and} \quad \frac{dR(r)}{dr} = 0, \tag{4.15}$$

along with the condition that

$$\Theta(\theta) \geq 0 \quad \text{for} \quad \theta \in [0, \pi]. \tag{4.16}$$

By solving (4.15) we obtain the value of ξ and η to be

$$a\xi(r) = r^2 + a^2 - 4r\frac{\Delta_r}{\Delta_r'}, \tag{4.17}$$

$$\eta(r) = \frac{16r^2\Xi^2\Delta_r}{(\Delta_r')^2}. \tag{4.18}$$

By inserting Eqs (4.17) and (4.18) in condition (4.16) we find

$$\left(4r\Delta_r - \Sigma\Delta_r'\right)^2 \leq 16a^2r^2\Xi^2\Delta_r\Delta_\theta \sin^2\theta \tag{4.19}$$

that describes the photon region. For $\Lambda = \alpha = 0$, eq. (4.19) yields in the equatorial plane the Kerr result $r = 2m\left(1 + \cos\left(\frac{2}{3}\cos^{-1}\left(\pm\frac{|a|}{m}\right)\right)\right)$. Photon orbits can be stable or unstable. The unstable photon orbit at $r = r_s$ exists when $\frac{d^2R(r_s)}{dr^2} > 0$, which also defines the boundary of the BH shadow. Thus the positive solution of

$$\frac{R''(r_s)}{8E^2\Xi^2} = r_s^2 + 2r_s\Delta_{r_s}\Delta_{r_s}{}' - 2r_s^2\frac{\Delta_{r_s}\Delta_{r_s}''}{(\Delta_{r_s}')^2} \tag{4.20}$$

determines the contour of the shadow. Here we have restored the factor of E and $'$ denotes the derivative with respect to r.

4.3 Shadows of the PFDM Black Hole

As noted above, in the presence of a cosmological constant the position of the observer needs to be fixed, employing the technique recently introduced in [68].

So we fix the observer in Boyer-Lindquist coordinates (r_0, θ_0), where r_0 is the radial coordinate and θ_0 is angular coordinate of observer. We also assume that the observer is in domain of outer communication i.e. $\Delta_r > 0$ and we consider the trajectories of light rays sent from position (r_0, θ_0) to the past. We now define orthonormal tetrads (e_0, e_1, e_2, e_3) at the observer's position (r_0, θ_0) such that

$$e_0 = \frac{\Xi^2}{\sqrt{\Delta_r \Sigma}} \left(\left(r^2 + a^2 \right) \partial_t + a \partial_\phi \right) \Big|_{(r_0, \theta_0)}, \tag{4.21}$$

$$e_1 = \sqrt{\frac{\Delta_\theta}{\Sigma}} \partial_\theta \Big|_{(r_0, \theta_0)}, \tag{4.22}$$

$$e_2 = -\frac{\Xi^2}{\sqrt{\Delta_\theta \Sigma} \sin\theta} \left(\partial_\phi + a \sin^2\theta \partial_t \right) \Big|_{(r_0, \theta_0)}, \tag{4.23}$$

$$e_3 = -\sqrt{\frac{\Delta_r}{\Sigma}} \partial_r \Big|_{(r_0, \theta_0)}, \tag{4.24}$$

where e_0 is observer's four velocity, $e_0 \pm e_3$ are tangent to the direction of principal null congruences and e_3 is along the spatial direction pointing towards the centre of the BH. Let the coordinates of the light ray are described as $\lambda(s) = (r(s), \theta(s), \phi(s), t(s))$, then a vector tangent to $\lambda(s)$ is given by

$$\dot{\lambda} = \dot{r}\partial_r + \dot{\theta}\partial_\theta + \dot{\phi}\partial_\phi + \dot{t}\partial_t. \tag{4.25}$$

This tangent vector can also be described in terms of orthonormal tetrads and celestial coordinates ρ and σ as

$$\dot{\lambda} = \beta \left(-e_0 + \sin\rho \cos\sigma e_1 + \sin\rho \sin\sigma e_2 + \cos\rho e_3 \right), \tag{4.26}$$

where the scalar factor β is obtained from Eq. (4.25) and (4.26) such that

$$\beta = g(\dot{\lambda}, e_0) = \Xi^2 \frac{aL - E(r^2 + a^2)}{\sqrt{\Delta_r \Sigma}} \Big|_{(r_0, \theta_0)} \tag{4.27}$$

Our next aim is to define the celestial coordinates, ρ and σ in terms of parameters ξ and η. To do so we compare the coefficients of ∂_r and ∂_ϕ in Eq. (4.25) and (4.26)

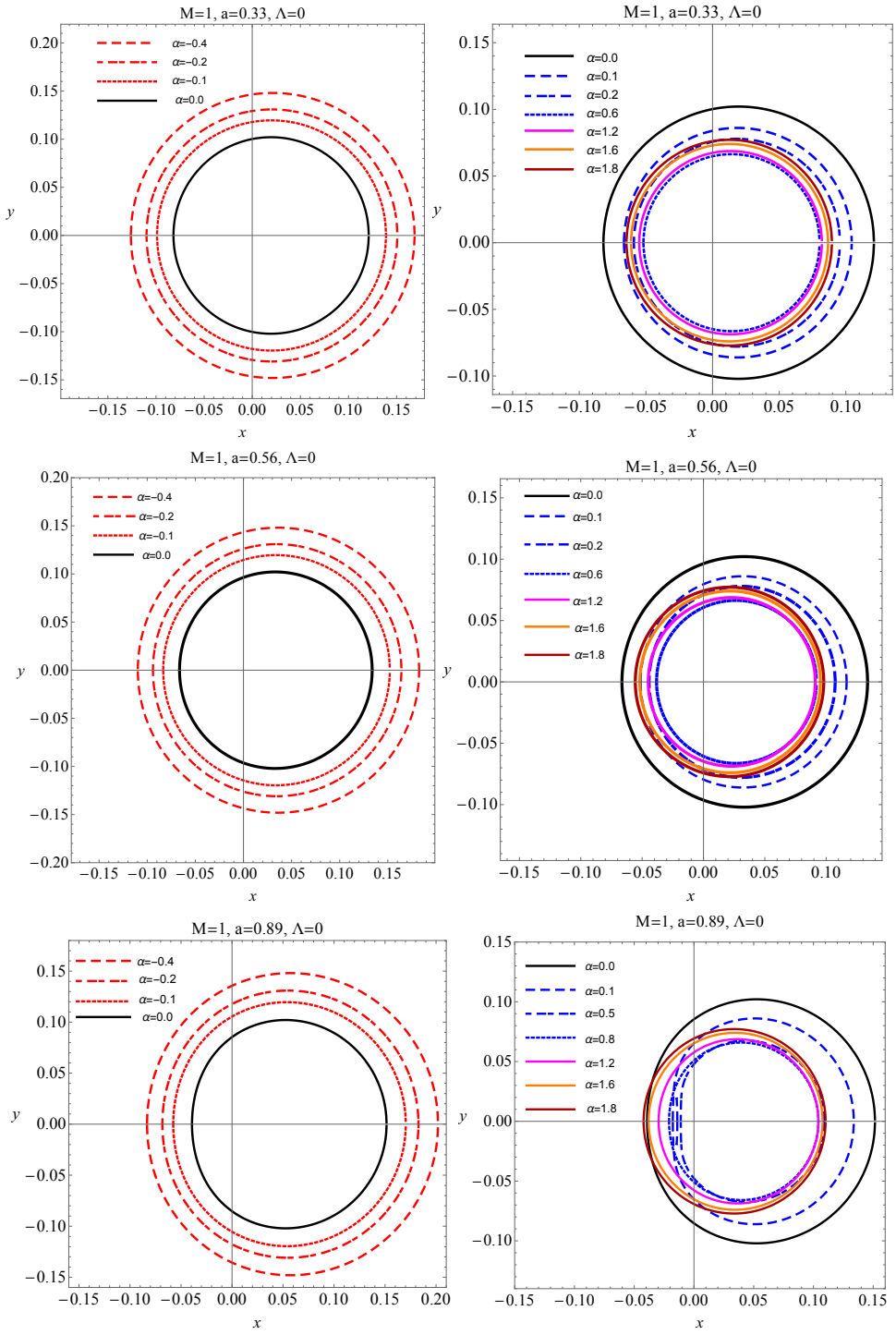

Figure 4.1: Shadows cast by a rotating BH in PFDM background for different values of α; all quantities are in units of M. The observer is positioned at r_0 and $\theta_0 = \pi/2$.

and thus we obtain

$$\sin\rho = \left.\sqrt{1-\frac{\dot{r}^2\Sigma^2}{\Xi^4\left(\left(r^2+a^2\right)E-aL\right)^2}}\right|_{(r_0,\theta_0)}. \tag{4.28}$$

and

$$\sin\sigma = \left.\frac{\sqrt{\Delta_\theta}\sin\theta}{\sqrt{\Delta_r}\sin\rho}\left(\frac{\Sigma\Delta_r}{\Xi^2\left(\left(r^2+a^2\right)E-aL\right)}\dot{\phi}-a\right)\right|_{(r_0,\theta_0)} \tag{4.29}$$

Using Eqs. (4.10) and (4.12), we can present the above two equations in terms of parameter ξ and η as

$$\sin\rho = \left.\frac{\pm\sqrt{\Xi^2\left(\Xi^2-1\right)\left(\left(r^2+a^2\right)-a\xi\right)^2+\Delta_r\eta}}{\Xi^2\left(r^2+a^2-a\xi\right)}\right|_{(r_0,\theta_0)} \tag{4.30}$$

and

$$\sin\sigma = \left.\frac{\sqrt{\Delta_r}\sin\theta}{\Xi^2\sqrt{\Delta_\theta}\sin\rho}\left[\frac{a-\xi\csc^2}{a\xi-\left(r^2+a^2\right)}\right]\right|_{(r_0,\theta_0)}. \tag{4.31}$$

The boundary of shadow of the BH can be presented graphically by projecting a stereographic projection from the celestial sphere onto to a plane with the Cartesian coordinates

$$x = -2\tan\left(\frac{\rho}{2}\right)\sin(\sigma), \tag{4.32}$$

$$y = -2\tan\left(\frac{\rho}{2}\right)\cos(\sigma). \tag{4.33}$$

Figure 4.1 allows us to distinguish the silhouette cast by a rotating BH in presence of perfect fluid dark matter ($\alpha \neq 0$) from that of Kerr BH ($\alpha = 0$). For $\alpha < 0$ we find that the shadow of the BH gets larger and more circular as α becomes increasingly negative. However for $\alpha > 0$ the effect on the shadow is no longer monotonic. For small $\alpha > 0$ the shadow shrinks whilst maintaining its asymmetric shape. However once $\alpha \gtrsim 0.8$, the shadow begins to grow, becoming increasingly circular and shifting leftward relative to its $\alpha = 0$ Kerr counterpart.

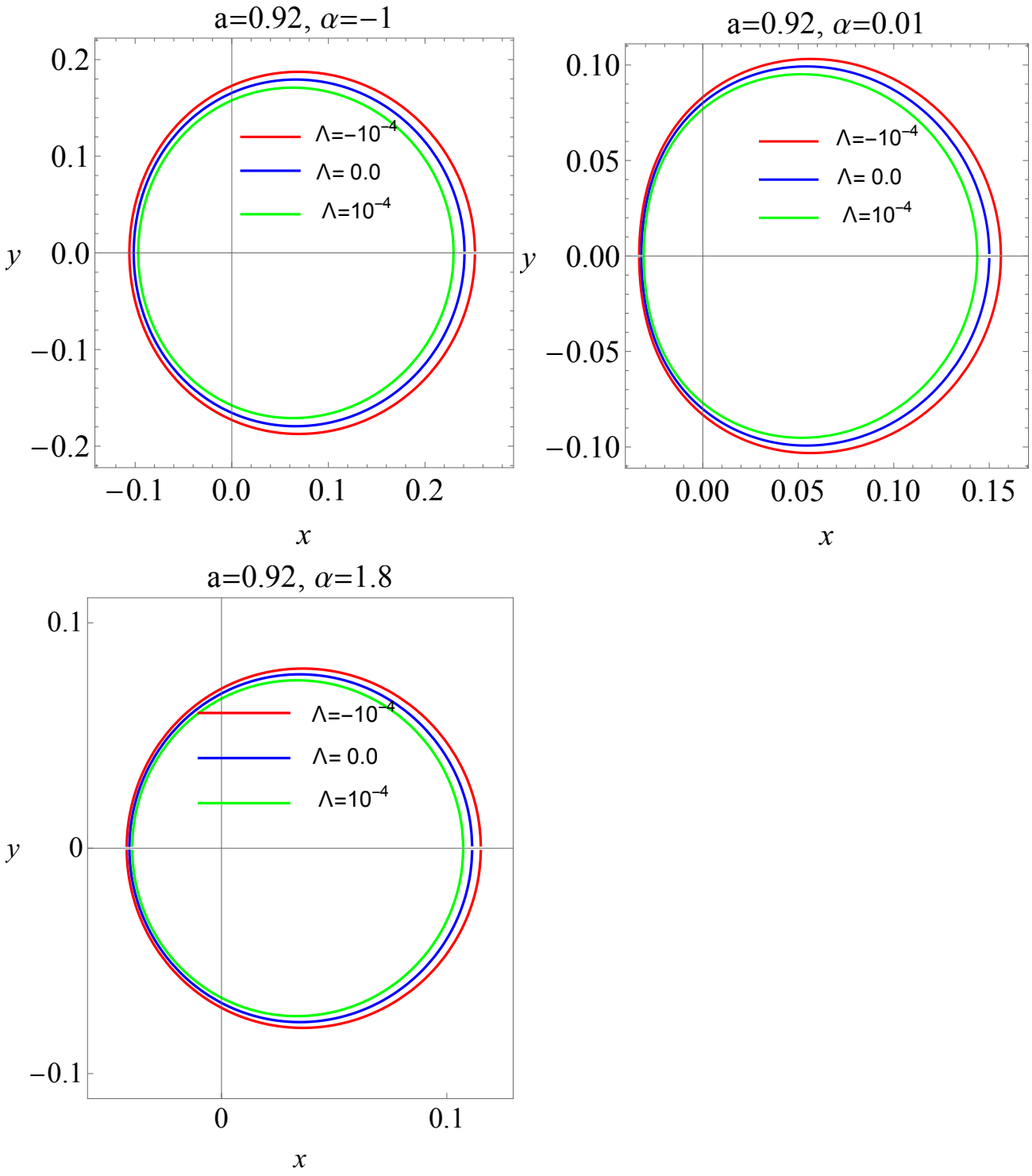

Figure 4.2: Variation in shadow of a rotating BH in PFDM background w.r.t cosmological constant, when the observer is at position $r_0 = 50$ and $\theta_0 = \pi/2$. All quantities are in units of M.

Our study thus indicates that presence of perfect fluid dark matter can have considerable effects on a BH silhouette. The rotational distortion of a Kerr BH is diminished for sufficiently large $|\alpha|$, even for large spin $(a = 0.84)$. The next effect is that the PFDM 'cancels out' the rotational distortion of the shadow.

Figure 4.2 shows the effects of cosmological constant on the shadow for different values of parameter α. We see that for small $|\Lambda|$ the shadow maintains its shape for a given α, increasing for the AdS case $\Lambda < 0$ and decreasing for the dS case $\Lambda > 0$.

Chapter 5

Shadow Images of a Rotating Dyonic Black Hole with a Global Monopole Surrounded by Perfect Fluid

Global monopoles are topological defects which may have been produced during the phase transitions in the early universe. In fact, global monopoles are just one type of topological defects. Other types of topological objects are expected to exist including domain walls and cosmic strings. A metric for rotating dyonic black hole (RDBH) with global monopole in presence of perfect fluid is computed in this work. We then discuss its surface topology at the event horizon using Gauss-Bonnet Theorem and also the ergoregion. We investigate the shadows of the RDBH. Choosing certain values of parameters, such as $\omega = -1/3, 0, 1/3$, we observe the effect of dark matter, dust and radiation on the silhouette of the black hole. Our findings lead us to conclude that the presence of parameters γ and α, also deforms the shape of BH's shadow. These results have been depicted through graphical representation. In the end we analyze the two observables, radius R_s

and distortion δ_s, related to BH's shadow. Energy emission rate of RDBH with global monopole surrounded by perfect fluid is also computed and graphically illustrated with respect to parameters.

In Section (5.1), we consider the the gravitational field of a static dyonic black hole (SDBH) with a global monopole surrounded by perfect fluid. In Section (5.2), by applying a complex coordinate transformation known as the Newman-Janis method [127] we find the spacetimes of a RDBH with a global monopole surrounded by perfect fluid. In Section (5.3), we consider the null geodesics using Hamilton-Jacobi equation. Circular orbits are discussed in (5.4). In Section (5.5) we study the impact of dark matter, dust and radiation on the shape of global monopole shadow. The observables, radius distortion, related to shape and size of shadow and energy emission rate of the BH has also been discussed in this same section.

5.1 A SDBH with a Global Monopole in Perfect Fluid

The action, S^{EM}, for Einstein Maxwell gravity along with actions S^D and $\mathcal{S}$ respectively defining presence of a global monopole and matter distribution, can be altogether written as

$$S = S^{(EM)} + S^{(D)} + \mathcal{S}. \tag{5.1}$$

The Einstein-Maxwell action $S^{(EM)}$ is given by

$$S^{(EM)} = \int \sqrt{-g}\, d^4x \left(\frac{\mathcal{R}}{2\kappa} - \frac{1}{4} F_{\mu\nu} F^{\mu\nu} \right). \tag{5.2}$$

The quantities g, $\mathcal{R}$ and $F_{\mu\nu}$ are, respectively, the determinant of the metric $g_{\mu\nu}$ associated to the gravitational field, the scalar invariant and the electromagnetic tensor. Also $\mu, \nu = 0, 1, 2, 3$.

The EFE (1.1), with $\Lambda = 0, G = 1, c = 1$, now reads

$$\mathcal{R}_{\mu\nu} - \frac{1}{2} g_{\mu\nu} \mathcal{R} = 8\pi T_{\mu\nu}. \tag{5.3}$$

While the corresponding Maxwell equations are

$$\nabla_\mu F^{\mu\nu} = 0. \tag{5.4}$$

Here $T_{\mu\nu}$ is the total stress energy tensor which we discuss later in this section. Since we are considering a dyonic black hole, which means that it is comprise of both electric charge Q_E and magnetic charge Q_M, the electromagnetic potential has two non zero terms i.e. [126, 131]

$$A = \frac{Q_E}{r} dt - Q_M \cos\theta d\varphi. \tag{5.5}$$

The only non-vanishing components of the electromagnetic tensor

$$F_{tr} = -F_{rt} = \frac{Q_E}{r^2}, \;\; F_{\theta\varphi} = -F_{\varphi\theta} = Q_M \sin\theta. \tag{5.6}$$

Now the action $S^{(D)}$ corresponds to the matter having a defect– a global monopole which is a heavy object formed in the phase transition of a system composed by a self-coupling scalar triplet field $\Phi^{\mathbf{s}}$, where s runs from 1 to 3. Thus the action in presence of a matter field $\Phi^{\mathbf{s}}$ coupled to gravity that characterizes a global monopole [95]

$$S^D = \int \sqrt{-g}\, d^4x \left(\frac{1}{2} g^{\mu\nu} \partial_\mu \Phi^{\mathbf{s}} \partial_\nu \Phi^{\mathbf{s}} - \frac{\lambda}{4} \left(\Phi^2 - \gamma^2 \right)^2 \right), \tag{5.7}$$

where $\Phi^2 = \Phi^{\mathbf{s}} \Phi^{\mathbf{s}}$, while λ is the self-interaction term and γ is the scale of a gauge-symmetry breaking. The monopole can be described through the field configuration $\Phi^{\mathbf{s}} = \frac{\gamma h(r) x^{\mathbf{s}}}{|\bar{\mathbf{x}}|}$, in which $x^{\mathbf{s}} = \{ r\sin\theta\, \cos\varphi, r\sin\theta\, \sin\varphi, r\cos\theta \}$, such that $|\bar{\mathbf{x}}| = r^2$, and $h(r)$ is a function of radial coordinate r.

The field equations for the scalar field $\Phi^{\mathbf{s}}$ reduces to a single equation for $h(r)$ given as

$$f(r)h''(r)+\left[\frac{2f(r)}{r}+\frac{1}{2f(r)}(f^2(r))'\right]h'(r)-\frac{2h(r)}{r^2}-\lambda\gamma^2h(r)\left(h^2(r)-1\right)=0. \tag{5.8}$$

With these equations in mind, and without loss of generality we can choose a spherically symmetric metric written as follows

$$ds^2=-f(r)dt^2+\frac{dr^2}{f(r)}+r^2d\theta^2+r^2\sin^2\theta d\varphi^2. \tag{5.9}$$

In our case the total energy momentum tensor reads

$$T_{\mu\nu}=T^{(EM)}_{\mu\nu}+T^{(D)}_{\mu\nu}+\mathcal{T}_{\mu\nu} \tag{5.10}$$

in which

$$T^{(EM)}_{\mu\nu}=\frac{1}{4\pi}\left(F_{\mu\sigma}F_{\nu}{}^{\sigma}-\frac{1}{4}g_{\mu\nu}F_{\rho\sigma}F^{\rho\sigma}\right), \tag{5.11}$$

$$T^{(D)}_{\mu\nu}=\partial_\mu\phi^a\partial_\nu\phi^a-\frac{1}{2}g_{\mu\nu}g^{\rho\sigma}\partial_\rho\phi^a\partial_\sigma\phi^a-\frac{g_{\mu\nu}\lambda}{4}\left(\phi^2-\gamma^2\right)^2, \tag{5.12}$$

and $\mathcal{T}_{\mu\nu}$ is the energy momentum tensor of the surrounding matter.
Outside the core $h\to 1$ and the energy momentum tensor of the monopole has the following components [95]

$$T^{(D)}{}^{t}_{t}=T^{(D)}{}^{r}_{r}=-\gamma^2\left[\frac{h^2}{r^2}+f(r)\frac{(h')^2}{2}+\frac{\lambda\gamma^2}{4}(h^2-1)^2\right]\to-\frac{\gamma^2}{r^2}, \tag{5.13}$$

$$T^{(D)}{}^{\theta}_{\theta}=T^{(D)}{}^{\varphi}_{\varphi}=-\gamma^2\left[f(r)\frac{(h'(r))^2}{2}+\frac{\lambda\gamma^2}{4}(h^2(r)-1)^2\right]\to 0. \tag{5.14}$$

The surrounding matter, whose action is denoted by $\mathcal{S}$ in Eq. (5.1), can generally be a dust, radiation, quintessence, cosmological constant, phantom field or even any combination of them. The energy momentum tensor of the surrounding fluid has the following components [130]

$$\mathcal{T}^{t}{}_{t}=\mathcal{T}^{r}{}_{r}=-\rho, \tag{5.15}$$

and

$$\mathcal{T}^{\theta}{}_{\theta} = \mathcal{T}^{\varphi}{}_{\varphi} = \frac{1}{2}(1+3\omega)\rho. \tag{5.16}$$

Thus, the Einstein's field equations yield

$$\frac{rf'(r)+f(r)-1}{r^2} + \frac{8\pi\gamma^2}{r^2} + \frac{Q_E^2}{r^4} + \frac{Q_M^2}{r^4} + 8\pi\rho = 0, \tag{5.17}$$

$$\frac{rf''(r)+2f'(r)}{2r} - \frac{Q_E^2}{r^4} - \frac{Q_M^2}{r^4} - 4\pi\rho(3\omega+1) = 0. \tag{5.18}$$

Now by solving the set of differential equations (18) and (19) one obtains the following general solution for the metric

$$f(r) = 1 - 8\pi\gamma^2 - \frac{2M}{r} + \frac{Q_E^2}{r^2} + \frac{Q_M^2}{r^2} - \frac{v}{r^{1+3\omega}}, \tag{5.19}$$

with the energy density in the form

$$\rho = -\frac{3\,\omega\,v}{8\pi r^{3(1+\omega)}}. \tag{5.20}$$

Note that, v is an integration constant related to the perfect fluid parameter. From the weak energy condition it follows the positivity of the energy density of the surrounding field, $\rho \geq 0$, which should satisfy the following constraint $\omega v \leq 0$.

5.2 An RDBH with a Global Monopole in Perfect Fluid

We now extend the study of static global monopole solution and obtain its rotating counterpart. For this we apply Newman-Janis formalism to the metric (5.9) along with (5.19), see Appendix (A).

The form of the metric we obtain is

$$\begin{aligned} ds^2 &= -\left(1 - \frac{r^2(1-f(r))}{\Sigma}\right) dt^2 - 2a\sin^2\theta \left(\frac{r^2(1-f(r))}{\Sigma}\right) dt d\varphi + \frac{\Sigma}{\Delta} dr^2 + \Sigma d\theta^2 \\ &+ \sin^2\theta \left[\frac{(r^2+a^2)^2 - a^2\Delta\sin^2\theta}{\Sigma}\right] d\varphi^2. \end{aligned} \tag{5.21}$$

where in order to simplify the notation we introduce the following quantity

$$\Delta = r^2 f(r) + a^2 = r^2 + a^2 - 2Mr - 8\pi r^2\gamma^2 + Q_E^2 + Q_M^2 - \frac{v}{r^{3\omega-1}}, \quad (5.22)$$

here $f(r)$ is given by Eq. (5.19). In this work, we consider three different cases of $\omega = -1/3$ dark matter dominant, 0 (dust dominant) and $1/3$ (radiation dominant). For spin $a = 0$, perfect fluid parameter $v = 0$ and no charges, the above metric reduces to Schwarzschild BH with global monopole [128].

The electromagnetic field of a BH is defined by its vector potential. As already mentioned, in case of a static BH the vector potential is given by Eq. (5.5). For the rotating case, the Newman-Janis method can also be applied on Eq. (5.5) using a guage transformation such that $g_{rr} = 0$ and $A_r = 0$. For the detailed procedure the authors refers the readers to consider [126]. The vector potential computed through Newman-Janis formalism for a RDBH is thus given by [126]

$$A = \left(\frac{rQ_E - aQ_M\cos\theta}{\Sigma}\right)dt + \left(-\frac{ra}{\Sigma}Q_E\sin^2\theta + \frac{r^2+a^2}{\Sigma}Q_M\cos\theta\right)d\varphi. \quad (5.23)$$

It has been shown in [89] that metric similar to (5.21) satisfies the EFE. For the Einstein tensor $G_{\mu\nu}$ and energy momentum tensor $T_{\mu\nu}$, the EFE (1.1), with $\Lambda = 0, G = 1, c = 1$ are given by $G_{\mu\nu} = R_{\mu\nu} - 1/2 g_{\mu\nu}\mathcal{R} = 8\pi T_{\mu\nu}$. For simplicity let $f(r) = 1 - 2F(r)/r^2$, where $F(r) = 4\pi\gamma^2 r^2 + Mr - (Q_E^2 + Q_M^2)/2 + v\, r^{1-3\omega}/2$, then the nonvanishing components of $G_{\mu\nu}$ are

$$\begin{aligned}
G_{tt} &= \frac{2}{\Sigma^3}\left(2F(r) - \left((r^2+a^2) + a^2\sin^2\theta\right)\right)\left(F(r) - rF'(r)\right) - \frac{a^2\sin^2\theta}{\Sigma^2}F''(r),\\
G_{rr} &= \frac{2}{\Sigma\Delta}\left(F(r) - rF'(r)\right),\\
G_{\theta\theta} &= \frac{-2}{\Sigma}\left(F(r) - rF'(r)\right) - F''(r), \qquad (5.24)\\
G_{t\varphi} &= \frac{4a\sin^2\theta}{\Sigma^3}\left((r^2+a^2) - F(r)\right)\left(F(r) - rF'(r)\right) + \frac{a}{\Sigma^2}\left(r^2+a^2\right)\sin^2\theta F''(r),\\
G_{\varphi\varphi} &= \frac{\sin^2\theta}{\Sigma^3}\left(4a^2\sin^2\theta F(r) - (r^2+a^2)\left(2(r^2+a^2) + a^2\sin^2\theta\right)\right)\left(F(r) - rF'(r)\right)\\
&- \frac{(r^2+a^2)\sin^2\theta}{\Sigma^2}F''(r).
\end{aligned}$$

In terms of the orthogonal basis, for the metric (5.21),

$$\begin{aligned} e_t^\mu &= \frac{1}{\sqrt{\Sigma\Delta}}\left(r^2+a^2,0,0,a\right), \quad e_r^\mu = \frac{1}{\sqrt{\Sigma}}\left(0,1,0,0\right), \\ e_\theta^\mu &= \frac{1}{\sqrt{\Sigma}}\left(0,0,1,0\right), \quad e_\varphi^\mu = \frac{1}{\sqrt{\Sigma\Delta}}\left(a\sin^2\theta,0,0,1\right). \end{aligned} \tag{5.25}$$

and the Einstein tensor $G_{\mu\nu}$, the energy momentum tensor is expressed as

$$\begin{aligned} p_t &= \frac{1}{8\pi} e_t^\mu\, e_t^\nu\, G_{\mu\nu}, \quad p_r = \frac{1}{8\pi} e_r^\mu\, e_r^\nu\, G_{\mu\nu}, \\ p_\theta &= \frac{1}{8\pi} e_\theta^\mu\, e_\theta^\nu\, G_{\mu\nu}, \quad p_\varphi = \frac{1}{8\pi} e_\varphi^\mu\, e_\varphi^\nu\, G_{\mu\nu}. \end{aligned} \tag{5.26}$$

Using Eqs. (5.21-5.26) gives the components for energy momentum tensor as

$$\begin{aligned} p_t &= \frac{1}{8\pi\Sigma^2}\left(8\pi\gamma^2 r^2 - 3v\omega r^{1-3\omega} + (Q_E^2+Q_M^2)\right) = -p_r, \\ p_\theta &= -p_r - \frac{1}{8\pi\Sigma}\left(8\pi\gamma^2 - \frac{3v\omega(1-3\omega)}{2r^{1+3\omega}}\right) = p_\varphi. \end{aligned} \tag{5.27}$$

Analogous to KBH, a ring singularity harbors inside the BH defined by metric 5.21. This can be demonstrated by computing the points at which the Kretschmann scalar $\mathcal{K}_s = R_{\mu\nu\sigma\rho}R^{\mu\nu\sigma\rho}$ turns to infinity. For the metric (5.21), the Kretschmann scalar has the value

$$\mathcal{K}_s = \frac{Z(r,a,\theta,Q_E,Q_M,\omega,v,\gamma)}{r^{2(1+3\omega)}(r^2+a^2\cos^2\theta)^2}. \tag{5.28}$$

where $Z(r,a,\theta,Q_E,Q_M,\omega,v,\gamma)$ is a tedious function. From the above expression, we observe that for $\omega = -1/3, 0, 1/3$ the poles are at the ring $r^2 + a\cos^2\theta = 0$ or when $r = 0$ and $\theta = \pi/2$. This leads us to the interpretation that a test particle moving in an equatorial plane $\theta = \pi/2$ will hit the singularity at $r = 0$.

5.2.1 Surface Topology

It is interesting to determine the surface topology of the global monopole spacetime at the event horizon. At a fixed moment in time t, and a constant $r = r_+$, the

metric (5.21) reduces to

$$ds^2 = \Sigma(r_+,\theta)d\theta^2 + \left(2Mr_+ + 8\pi r_+^2\gamma^2 - Q_E^2 - Q_M^2 + \frac{v}{r_+^{3\omega-1}}\right)^2 \frac{\sin^2\theta}{\Sigma(r_+,\theta)}d\varphi^2,$$

The above metric has the following determinant

$$\det g^{(2)} = \left(2Mr_+ + 8\pi r_+^2\gamma^2 - Q_E^2 - Q_M^2 + \frac{v}{r_+^{3\omega-1}}\right)^2 \sin^2\theta. \tag{5.29}$$

Theorem: *Let $\mathcal{M}$ be a compact orientable surface with metric $g^{(2)}$, and let $\mathcal{K}$ be the Gaussian curvature with respect to $g^{(2)}$ on $\mathcal{M}$. Then, the Gauss-Bonnet theorem states that*

$$\iint_{\mathcal{M}} \mathcal{K}dA = 2\pi\chi(\mathcal{M}). \tag{5.30}$$

Note that dA is the surface line element of the 2-dimensional surface and $\chi(\mathcal{M})$ is the Euler characteristic number. It is convenient to express sometimes the above theorem in terms of the Ricci scalar, in particular for the 2-dimensional surface there is a simple relation between the Gaussian curvature and Ricci scalar given by

$$\mathcal{K} = \frac{\mathcal{R}}{2}. \tag{5.31}$$

Yielding the following from

$$\frac{1}{4\pi}\iint_{\mathcal{M}} \mathcal{R}dA = \chi(\mathcal{M}). \tag{5.32}$$

A straightforward calculation using the metric (42) yields the following result for the Ricci scalar

$$\mathcal{R} = \frac{2(r_+^2 + a^2)(r_+^2 - 3a^2\cos^2\theta)}{\left(r_+^2 + a^2\cos^2\theta\right)^3} \tag{5.33}$$

From the GBT we find

$$\chi(\mathcal{M}) = \frac{1}{4\pi}\int_0^{2\pi}\int_0^{\pi}\left[\frac{2(r_+^2 + a^2)(r_+^2 - 3a^2\cos^2\theta)}{\left(r_+^2 + a^2\cos^2\theta\right)^3}\right]\sqrt{\det g^{(2)}}d\theta d\varphi. \tag{5.34}$$

Finally, solving the integral we find

$$\chi(\mathcal{M}) = 2. \tag{5.35}$$

Hence the surface topology of the RDBH with global monopole is a 2-sphere at the event horizon, since we know that $\chi(\mathcal{M})_{sphere} = 2$.

5.2.2 Configuration of Ergoregion

Let us now proceed to study the shape of the ergoregion of a RDBH with a global monopole. We do so by plotting the silhouette of ergoregion in the xz-plane. The horizons of a BH exists at the solutions of $\Delta = 0$, which in our case has the form

$$r^2 + a^2 - 2Mr - 8\pi r^2\gamma^2 + Q_E^2 + Q_M^2 - \frac{v}{r^{3\omega-1}} = 0. \tag{5.36}$$

The static limit, on the other hand, has an inner and outer ergosurface which exists when

$$g_{tt} = r^2 + a^2\cos^2\theta - 2Mr - 8\pi r^2\gamma^2 + Q_E^2 + Q_M^2 - \frac{v}{r^{3\omega-1}} = 0. \tag{5.37}$$

There is an interesting process which relies on the presence of an ergoregion, namely from such a RBH energy can be extracted, and this process is known as the Penrose process. In Figure (5.1) we plot the shape of ergoregion for different values of a, ω, γ, and v. One can observe that the event horizon and static limit surface meet at poles while the region lying between them is the ergoregion which supports negative energy orbits. Furthermore the shape of ergoregion, depends on the spin a, however due to the small values of v we observe small changes related to the value of ω.

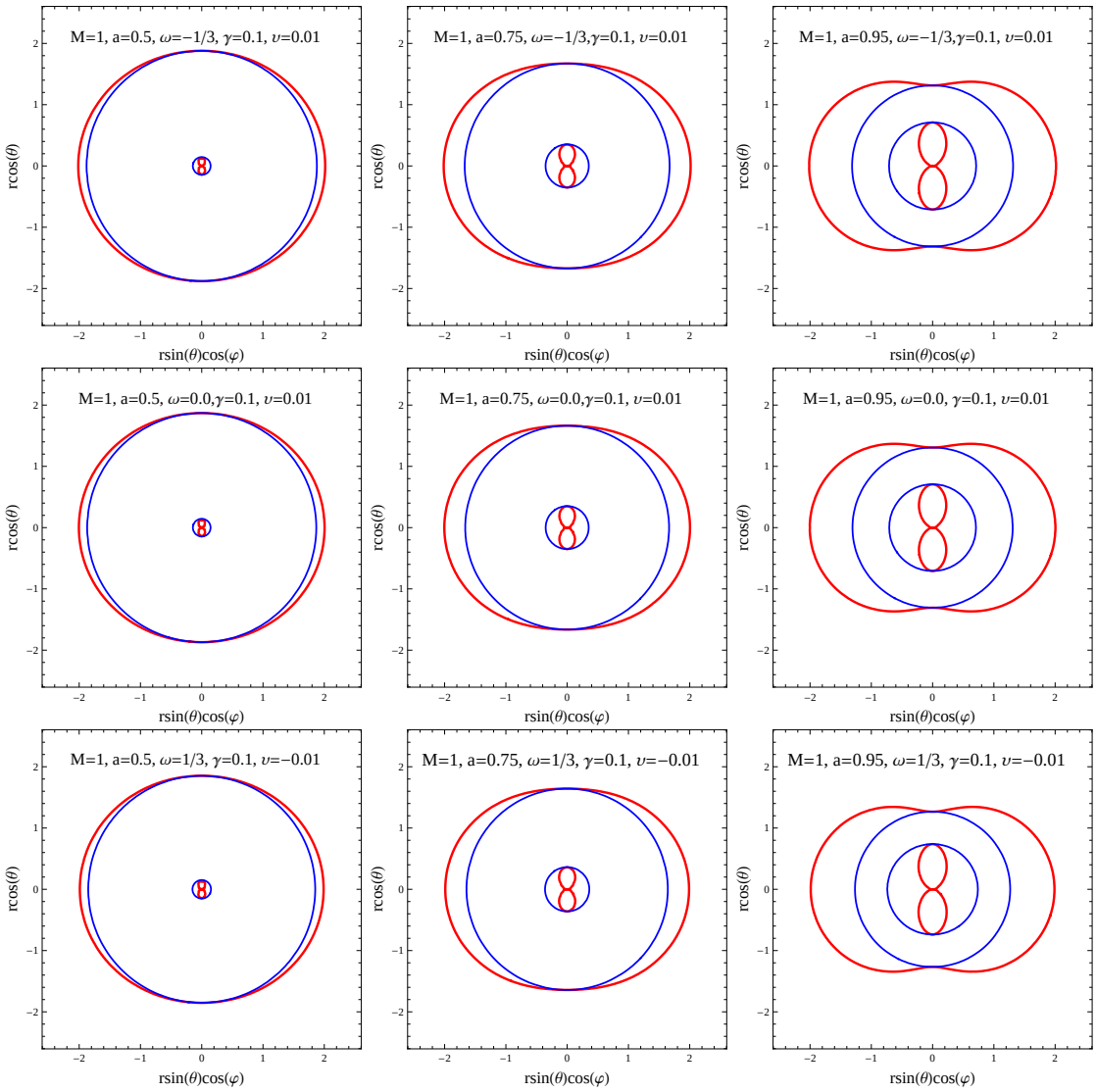

Figure 5.1: Plots showing shape of ergoregion (red) and horizons (blue) in xz-plane for different values of a, ω, and v. We have chosen $Q_E = Q_M = 0.1$.

5.3 Null Geodesics

Our main objective is to investigate the shadow casted by the BH defined by metric (5.21). To do so, we first need to analyze the geodesics structure of photons moving around the compact gravitational source. This will enable us to detect the unstable photon orbits. The boundary of the BH's shadow is defined where the unstable photon orbits exist.

For the RDBH with global monopole present in perfect fluid, the presence of null geodesics can be observed by following the Hamilton-Jacobi method. The Hamilton-Jacobi equation is given by

$$\partial_\tau \mathcal{J} = -\mathcal{H}. \tag{5.38}$$

In the above equation

On Left Side $\mathcal{J}$ is the Jacobi action, defined as the function of affine parameter τ and coordinates x^μ i.e. $\mathcal{J} = \mathcal{J}(\tau, x^\mu)$.

On Right Side $\mathcal{H}$ is the Hamiltonian of test particle's motion and is equivalent to $g^{\mu\nu}\partial_\mu \mathcal{J}\ \partial_\nu \mathcal{J}$.

In the spacetime under consideration, along the photon geodesics the energy E and momentum L, defined respectively by Killing fields $\xi_t = \partial_t$ and $\xi_\phi = \partial_\phi$, are conserved. The mass $m = 0$ of the photon is also constant. Using these constants of motion we can thus separate the Jacobi function as

$$\mathcal{J} = \frac{1}{2}m^2\tau - Et + L\phi + \mathcal{J}_r(r) + \mathcal{J}_\theta(\theta) \tag{5.39}$$

where the functions $\mathcal{J}_r(r)$ and $\mathcal{J}_\theta(\theta)$ respectively depends on coordinates r and θ. Combining Eq. (5.38) and Eq. (5.39) yields a set of equations, which describes the

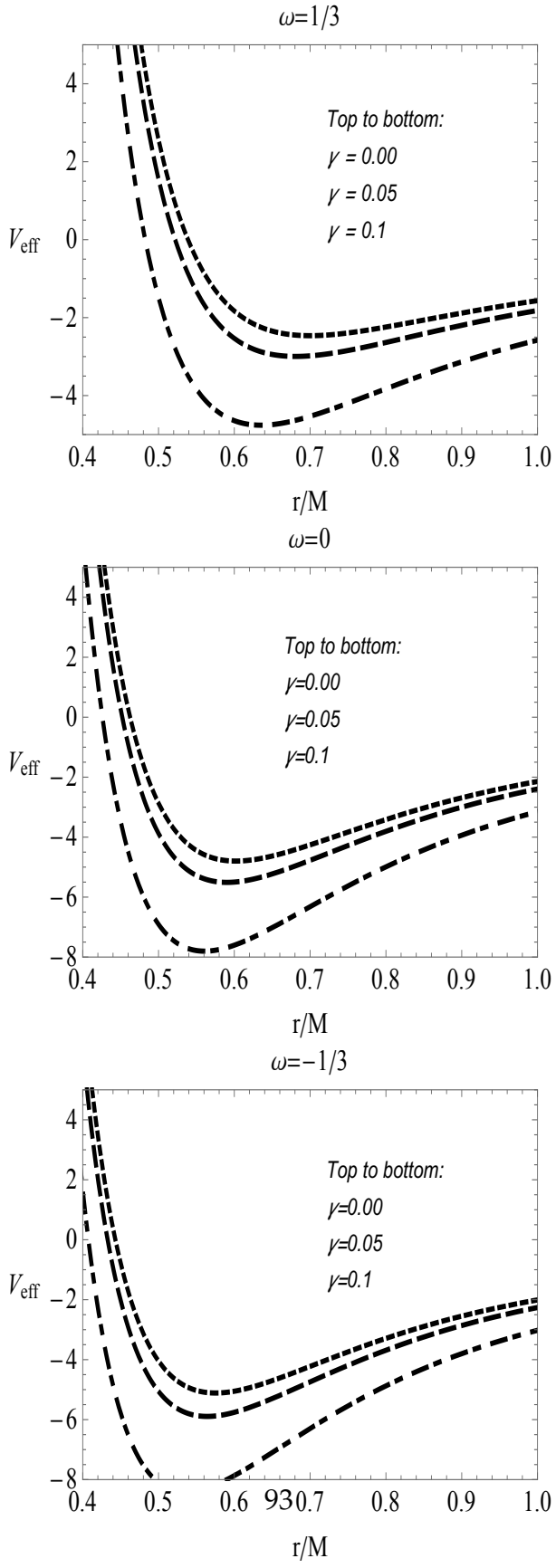

Figure 5.2: Plot showing V_{eff} of a photon w.r.t its radial motion: $\omega = 1/3$ for radiation, $\omega = 0$ for dust and $\omega = -1/3$ for dark matter.

dynamics of a test particle around the RBH in perfect fluid matter, as:

$$\Sigma\frac{dt}{d\tau} = \frac{r^2+a^2}{\Delta}[E(r^2+a^2)-aL]-a(aE\sin^2\theta-L), \tag{5.40}$$

$$\Sigma\frac{dr}{d\tau} = \sqrt{\mathcal{R}(r)}, \tag{5.41}$$

$$\Sigma\frac{d\theta}{d\tau} = \sqrt{\Theta(\theta)}, \tag{5.42}$$

$$\Sigma\frac{d\varphi}{d\tau} = \frac{a}{\Delta}[E(r^2+a^2)-aL]-\left(aE-\frac{L}{\sin^2\theta}\right), \tag{5.43}$$

where $\mathcal{R}(r)$ and $\Theta(\theta)$ read as

$$\mathcal{R}(r) = [E(r^2+a^2)-aL]^2-\Delta[m^2r^2+(aE-L)^2+\mathcal{K}], \tag{5.44}$$

$$\Theta(\theta) = \mathcal{K}-\left(\frac{L^2}{\sin^2\theta}-a^2E^2\right)\cos^2\theta, \tag{5.45}$$

with $\mathcal{K}$ the Carter constant.

5.4 Circular Orbits

Now we consider a gravitational source placed between a light emitting source and an observer at infinity. The photons emitted from the light source will form two kinds of trajectories: the ones which eventually fall into the BH and the ones which scatter away from it. The region separating these trajectories, contains unstable circular orbits. These unstable circular orbits form a dark region in sky thus forming the contour of the shadow. In this section we intend to discuss the presence of unstable circular orbits around the BH under consideration. For this we consider photon as a test particle and hence take $m = 0$. We can express the radial geodesic equation in terms of effective potential V_{eff} of photon's radial motion as

$$\Sigma^2\left(\frac{dr}{d\tau}\right)^2+V_{\text{eff}} = 0.$$

At this point, for mere convenience, we introduce two independent parameters ξ and η [11] as

$$\xi = L/E, \qquad \eta = \mathcal{K}/E^2. \tag{5.46}$$

The effective potential in terms of these two parameters is then expressed as

$$V_{\text{eff}} = \Delta((a-\xi)^2 + \eta) - (r^2 + a^2 - a\,\xi)^2, \tag{5.47}$$

where we have replaced V_{eff}/E^2 by V_{eff}. Figure (5.2) shows the variation in effective potential associated with the radial motion of photons. From the figure we observe that in all three cases the value of effective potential decreases with increase in parameter γ. Now the circular photon orbits exists when at some constant $r = r_c$ the conditions

$$V_{\text{eff}}(r) = 0, \qquad \frac{dV_{\text{eff}}(r)}{dr} = 0 \tag{5.48}$$

are satisfied. We then use Eq. (5.47) in Eq. (5.48) and thus obtain

$$[\eta + (\xi - a)^2]\Delta - (r^2 + a^2 - a\xi)^2 = 0, \tag{5.49}$$

$$4(r^2 + a^2 - a\xi) - [\eta + (\xi - a)^2]\mathcal{A}(r) = 0, \tag{5.50}$$

where

$$\mathcal{A}(r) = 1 - 8\pi\gamma^2 - \frac{M}{r} + (\frac{3\omega - 1}{2})\frac{v}{r^{1+3\omega}}. \tag{5.51}$$

Combining Eqs. (5.49-5.50) results in

$$a\,\xi = r^2 + a^2 - \frac{2\,\Delta}{\mathcal{A}(r)}\,, \tag{5.52}$$

$$\eta = \frac{4\Delta}{\mathcal{A}(r)^2} - \frac{1}{a^2}\left(r^2 - \frac{\Delta}{\mathcal{A}(r)^2}\right)^2 \tag{5.53}$$

It is worth mentioning here that impact parameters, ξ and η, will be affected not just by radial coordinate r, spin parameter a and mass of BH M but also by electric charge Q_E, magnetic charge Q_M, monopole parameter γ and perfect

fluid parameter v. The unstable circular orbits are located at local maxima of the potential curves i.e. when $V''_{\text{eff}} < 0$ or

$$\left(\Delta'^2 + 2\Delta\Delta''\right) r + 2\Delta\Delta' > 0 \tag{5.54}$$

5.5 Silhouette of a Black Hole

We now extend our calculations to observe shadow of RDBH with global monopole surrounded by perfect fluid. To gain the optical image we specify the observer at position (r_o, θ_o), where $r_o = r \to \infty$ and θ_o is the angular coordinate at infinity, on observer's sky. The new coordinates, also widely known as celestial coordinates, α and β are then introduced. These coordinates are selected such that α and β correspond to the apparent perpendicular distance of the image from axis of symmetry and its projection on the equatorial plane, respectively.Due to the presence of global monopole we have asymptotically non flat solutions due to the global nontrivial topology. Now we obtain the proper celestial coordinates for the asymptotically non-flat solution by abopting [**?**]

$$\alpha = \lim_{r\to\infty} -r\frac{p^{(\phi)}}{p^{(t)}} \tag{5.55}$$

$$\beta = \lim_{r\to\infty} r\frac{p^{(\theta)}}{p^{(t)}} \tag{5.56}$$

where $(p^{(t)}, p^{(r)}, p^{(\theta)}, p^{(\phi)})$ are the tetrad components of the photon momentum with respect to locally nonrotating reference frame. So basically one can define the observerâĂŹs sky as the usual cases in which the observer bases $e^{\mu}_{(\nu)}$ can be expanded as a form in the coordinate bases. In the limit $r \to \infty$ can relate the above coordinates to parameters ξ and η, which then yield

$$\alpha = -\sqrt{1-8\pi\gamma^2}\,\frac{\xi}{\sin\theta} \tag{5.57}$$

$$\beta = \pm\sqrt{1-8\pi\gamma^2}\,\sqrt{\eta + a^2\cos^2\theta - \xi^2\cot^2\theta}\,, \tag{5.58}$$

for the case $\omega = 0$ and $\omega = 1/3$. And similarly

$$\alpha = -\sqrt{1-8\pi\gamma^2-\upsilon}\,\frac{\xi}{\sin\theta} \tag{5.59}$$

$$\beta = \pm\sqrt{1-8\pi\gamma^2-\upsilon}\,\sqrt{\eta + a^2\cos^2\theta - \xi^2\cot^2\theta} \tag{5.60}$$

for the case $\omega = -1/3$. We observe that in the dark matter case there is a similar contribution term compared to the global monopole. In the limit $\gamma \to 0$ and $\upsilon \to 0$ we obtain the usual relations for celestial coordinates for the asymptotically flat solution.

We expect that the parameters involve in RDGM in presence of a perfect fluid will effect the shape of its shadow. This can be clearly confirmed through Eq. 5.60 as it depends not only on spin parameter a and angular coordinate θ_o but also on γ, ω and perfect fluid parameter υ. Later, we will justify our results also through graphical interpretations.

As our observer is placed in the equatorial plane ($\theta = \pi/2$), α and β reduce to

$$\alpha = -\sqrt{1-8\pi\gamma^2}\;\xi \tag{5.61}$$

$$\beta = \pm\sqrt{1-8\pi\gamma^2}\;\sqrt{\eta}, \tag{5.62}$$

for the case $\omega = 0$ and $\omega = 1/3$. And

$$\alpha = -\sqrt{1-8\pi\gamma^2-\upsilon}\;\xi \tag{5.63}$$

$$\beta = \pm\sqrt{1-8\pi\gamma^2-\upsilon}\;\sqrt{\eta} \tag{5.64}$$

for the case $\omega = -1/3$. Figure (5.3) and (5.4) show deformation in shapes of the shadow with respect to monopole parameter γ and and perfect fluid parameter υ, respectively. It is a well known observation now that the rotational effect in a black hole distorts its shape. That being said, we notice in Figure (5.3) that for small spin parameter, a, the shadow of the black hole maintains a circular shape along with the increase in its size with the inclination of γ. As for larger spin value,

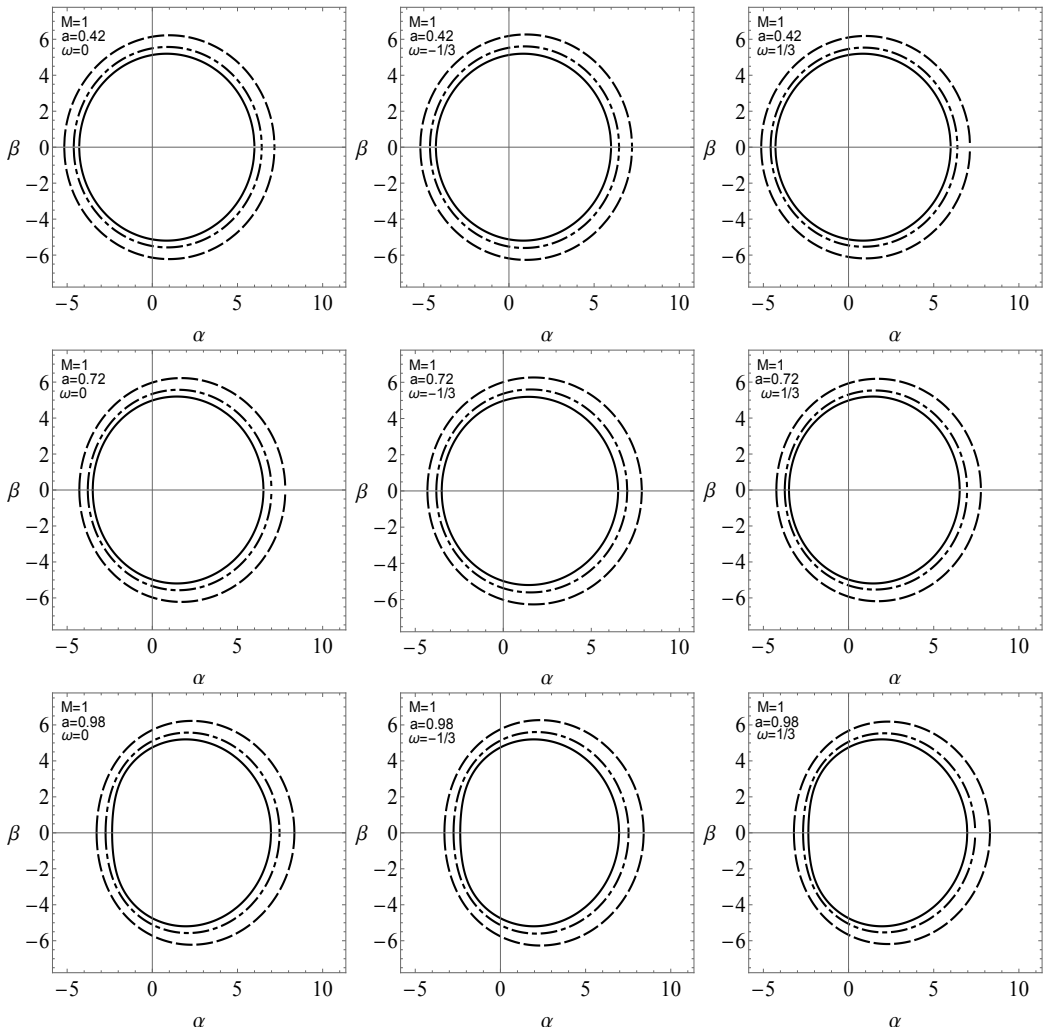

Figure 5.3: Variation in shape of a rotating dyonic global monopole surrounded by a perfect fluid. Magnetic and electric charges are kept constant such that $Q_E = 10^{-2} = Q_M$. In each graph the Kerr case i.e. $\gamma = 0$ and $v = 0$, is represented by solid line, $\gamma = 0.05$ by dotdashed and $\gamma = 0.08$ by dashed lines. For dark matter $(\omega = -1/3)$ and dust $(\omega = 0)$ case $v = 0.01$, whereas $v = -0.01$ in case of radiation $(\omega = 1/3)$.

the shadow is clearly distorted and matches with its Kerr counter part in perfect fluid [125] for $\gamma = 0$. Figure (5.4) shows the effect of parameter v on the rotating

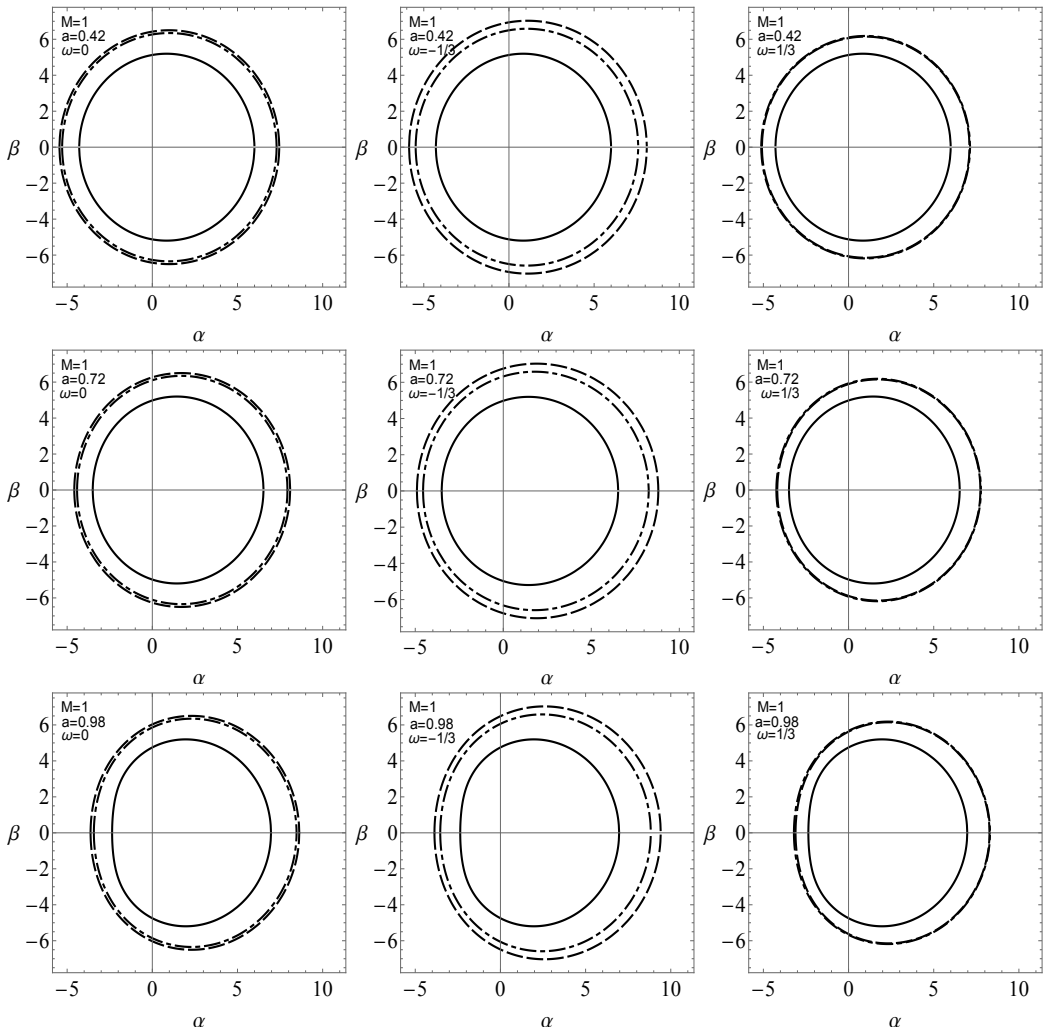

Figure 5.4: Variation in shape of a rotating dyonic black hole with global monopole surrounded by a perfect fluid, for different values of perfect fluid parameter v. Magnetic and electric charges along with the global monopole parameter are kept constant such that: $Q_E = 10^{-2} = Q_M$ and $\gamma = 0.08$. For dark matter and dust case $v = 0$ (Solid), 0.05 (DotDashed) and 0.1 (Dashed). In case of radiation $v = 0$ (Solid), -0.01 (DotDashed) and -0.05 (Dashed).

dyonic black hole with a global monopole present in perfect fluid. It is noticed in figure 5.4 that as perfect fluid parameter, v, increases the size of the shadow also

increases. A distortion is noticed in shape of the shadow when the spin parameter a is increased. Also, in case of dark matter and dust, there is significant change in the size of the shadow with respect to v. On the other hand, in case of radiation we do not observe any significant effect of perfect fluid parameter v, in fact the effect is negligibly small.

In [21], the authors introduces two observables, radius R_s and distortion δ_s, to analyze the size and form of the shadow. The first observable R_s is the approximate radius of the shadow. It is defined by considering a reference circle passing through three points on the boundary of the shadow, such that $(\alpha_{\text{tp}}, \beta_{\text{tp}})$ is the top most point on the shadow, $(\alpha_{\text{bm}}, \beta_{\text{bm}})$ is the bottom most point on the shadow and $(\alpha_{\text{r}}, 0)$ is the point corresponding to unstable circular orbit seen by an observer on reference frame. Thus

$$R_s = \frac{(\alpha_{\text{tp}} - \alpha_r)^2 + \beta_{\text{tp}}^2}{2|\alpha_{\text{tp}} - \alpha_r|}. \tag{5.65}$$

The second observable δ_s is the distortion parameter. Let D_{CS} be the difference between the contour of shadow and reference circle. Then for the point $(\tilde{\alpha}_p, 0)$ lying on the reference circle and the point $(\alpha_p, 0)$ lying on the contour of the shadow, $D_{CS} = |\tilde{\alpha}_p - \alpha_p|$. Thus

$$\delta_s = \frac{\tilde{\alpha}_p - \alpha_p}{R_s}.$$

For our case, we consider the points $(\tilde{\alpha}_p, 0)$ and $(\alpha_p, 0)$ to be on the equatorial plane, opposite to the point $(\alpha_{\text{r}}, 0)$. The variations in these observables with respect to monopole parameter γ are graphically presented in Figure (5.5). The dependence of R_s on parameter γ is such that as γ increases the radius R_s also increases. Thus the size of the shadow increases with increase in monopole parameter γ. Whereas the distortion δ_s decreases monotonically with an increase in γ. This tells us that with respect to circumference of reference circle, the shadow of the rotating black hole is significantly distorted for $\gamma \in [0, 0.1]$ but for $\gamma > 0$ it may not show any

distortion and thus we may obtain a perfect circle. As we have considered our

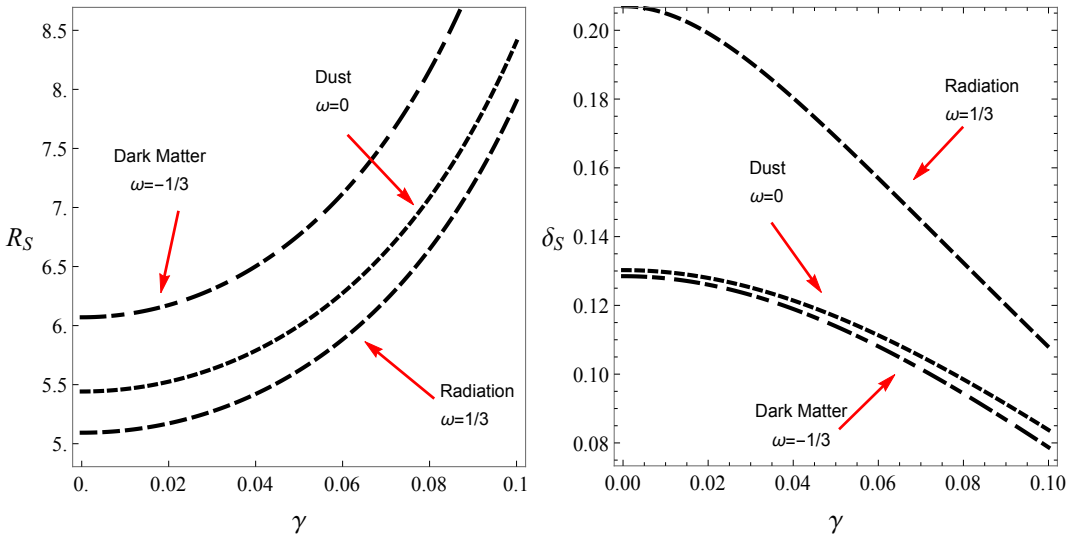

Figure 5.5: The quantities R_s and δ_s with respect to parameter γ

observer to be at infinity so in this case the area of the black hole shadow will be approximately equal to high energy absorption cross section as discussed in [26]. For a spherically symmetric black hole the absorption cross section oscillates around Π_{ilm}, a limiting constant value. For a black hole shadow with radius R_s, we adopt the value of Π_{ilm} as calculated by [26]

$$\Pi_{ilm} \cong \pi R_s^2.$$

The energy emission rate of the black hole is thus defined by

$$\frac{d^2E(\sigma)}{d\sigma dt} = 2\pi^2 \frac{\Pi_{ilm}}{e^{\sigma/T}-1}\sigma^3,$$

where σ is the frequency of the photon and T represents the temperature of the black hole at outer horizon i.e. r_+, given by

$$\begin{aligned} T(r_+) &= \lim_{r\to r_+} \frac{\partial_r \sqrt{g_{tt}}}{2\pi\sqrt{g_{rr}}} \\ &= \left(2a^2\left(f(r)-1\right)+r(r^2+a^2)f'(r)\right)\frac{r}{4\pi\left(r^2+a^2\right)^2} \end{aligned}$$

For all three cases, radiation, dust and dark matter, the energy emission rate is graphically presented in Figure (5.6) where we notice that the energy emission rate decreases with increase in parameter γ. A slight shift to the lower frequency is also observed while γ increases. The spin parameter a also effects the shape of the energy emission rate as an abrupt decrease in energy emisiion rate is noticed for higher spin value.

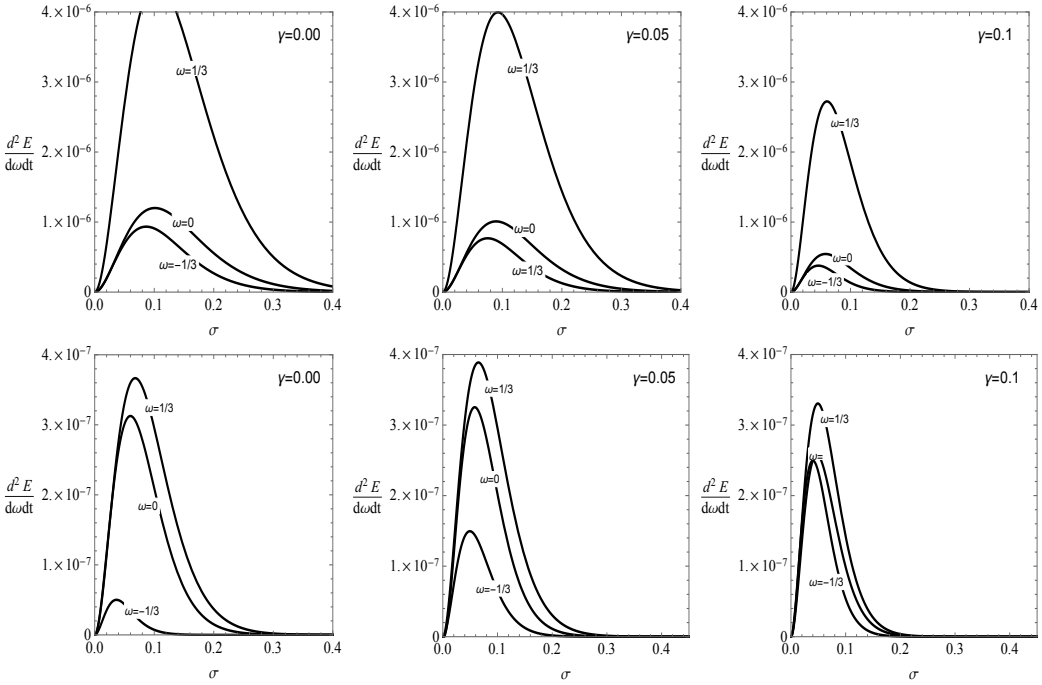

Figure 5.6: The figure shows the energy emission rate when $a = 0.46$ (upper panel) and $a = 0.92$ (lower panel).

Chapter 6

Conclusion

The detection of gravitational waves and BH images obtained by EHT are altogether a break through in astrophysics. These discoveries have just not reignited the faith in Einstein's GTR but also opened doors to test other theories of gravity too. Certainly we are living in an intriguing new era of research and development regarding both theoretical and astrophysical aspects.

From astrophysical point of view, RBHs are of significant importance. Since the spin of a BH carries all the information about its formation and growth. It is also potent source of energy to power relativistic jets. As per finding of EHT collaboration, the BHs hosted by our neighbor galaxy (M87) and our own galaxy are spinning. All these reasons set a path for an intriguing mind to look into dynamics of these mysterious objects not only in GTR but also in its alternatives. The recent interest in studying particle (particularly photon) motion around a BH to eventually obtain its image is a motivation for us to play our part.

To conclude this study we now summarize the results obtained in previous chapters.

In Chapter **TWO** we have discussed in detail the properties of a RBH solution

considering the variation of gravitational coupling. This new metric is characterized by three parameters: rotational parameter a, mass of BH M and constant parameter $\tilde{\xi}$, describing the quantum corrections. We have first discussed the consequences of the asymptotically safe gravity correction on the structure of event and Killing horizons. While doing so we noted that ergosphere is significantly increased when $\tilde{\xi}$ increases, which also depicts that the region of the BH from which energy can be extracted, through Penrose process, is bigger as compared to standard GR. Further, particle's motion is investigated by studying geodesics for both null and time-like particles. For the case $L = aE$, the equations for outgoing photon trajectory are numerically solved. By plotting these results, it is observed that,for small $\tilde{\xi}$, the photon trajectory with respect to both time t and angle ϕ shows no high deviation from its GR counterpart. The presence of a bifurcation point is also numerically analyzed, which leads us to existence of naked singularity. Expressions of energy and angular momentum for time-like geodesics, depending on r, are derived. Angular velocity Ω is computed and it is observed that for prograde motion Ω increases when $\tilde{\xi}$ is increased but for retrograde motion it decreases with $\tilde{\xi}$. A detailed discussion is made on effective potential also. It is graphically shown that the shape of potential barrier is changed for different values of $\tilde{\xi}$. The extraction of energy is discussed by taking into account the Penrose process. We have demonstrated that for the same values of a the efficiency of Penrose process will be greater in asymptotically safe gravity, while the maximum possible efficiency of Penrose process will not be significantly changed. In the end, another effect called Lense-Thirring effect is also explored. It is noted that this effect, being a rotational effect, depends on the rotational parameter a. With the increase in the value of a Lense-Thirring effect shows notable change when plotted. It should be kept in mind here that to avoid the whole system to get strongly coupled, Cai and Easson [79] considered the value of coupling parameter

$\tilde{\xi}$ to be less than unity, which limitized the practical significance of our result.

The existence of dark matter around BHs located at the centers of most of large galaxies plays an important role in many astrophysical phenomena. Motivated by this fact, in Chapter **THREE** we have studied the effects of perfect fluid dark matter and a cosmological constant on the shadow of a RBH. Our work provides a possible tool for observation of dark matter via shadows, perhaps using the high resolution imaging of the Event Horizon Telescope.

We have shown that the different shadow shapes are found by varying the PFDM parameter, mass, spin parameter, and the cosmological constant. Through graphs we have demonstrated that size of shadow of our BH decreases for $\alpha < 1$ but after that we see an increase in its size.

In Chapter **FOUR** we have used the complex transformations pointed out by Newman and Janis to obtain an RDGM solution in presence of a perfect fluid dark matter. Using the Gauss-Bonnet theorem we have shown that the surface topology of a RDBH with a global monopole is indeed a 2-sphere. Furthermore by choosing $\omega = -1/3, 0, 1/3$ we have explored the impact of dark matter, dust, radiation, as well as the global monopole parameter γ, and perfect fluid parameters α, on the silhouette of BH. We have found that a RDBH with a global monopole retains a circular shape for small spin parameter. Whereas for high spin like $a = 0.98M$ the shadow of RDBH with global monopole is distorted. Also as monopole parameter γ increases, a slight shift towards the right is also noticed in shape of shadow of BH under consideration. The two observables, R_s and δ_s, are also being discussed. In the end we analyze energy emission rate of RDBH with global monopole surrounded by perfect fluid with respect to parameters.

Appendix A

Newman-Janis Algorithm

The method given in [89] is subsequently being adapted here. We first consider a static and spherically symmetric metric as

$$ds^2 = -A_1(r)dt^2 + \frac{dr^2}{A_2(r)} + h(r)\left(r^2 d\theta^2 + r^2 \sin^2\theta d\phi^2\right), \tag{A.1}$$

The algorithm, for metric's computation, begins by transforming BL to EF coordinates i.e. $(t, r, \theta, \phi) \to (u, r, \theta, \phi)$. So with the use of the following coordinate transformation, in Eq. (A.1),

$$dt = du + \frac{dr}{\sqrt{A_1(r)A_2(r)}},$$

a line element of the form

$$ds^2 = -A_1(r)du^2 - 2\sqrt{\frac{A_1(r)}{A_2(r)}}dudr + h(r)d\Omega^2,$$

is obtained. This metric in terms of null tetrads is written as

$$g^{\mu\nu} = -l^\mu n^\nu - l^\nu n^\mu + m^\mu \bar{m}^\nu + m^\nu \bar{m}^\mu, \tag{A.2}$$

where null tetrads are

$$\begin{aligned} l^{\mu} &= \delta^{\mu}_{r}, \\ n^{\mu} &= \sqrt{\frac{A_2(r)}{A_1(r)}}\,\delta^{\mu}_{u} - \frac{A_2(r)}{2}\delta^{\mu}_{r}, \\ m^{\mu} &= \frac{1}{\sqrt{2h(r)}}\left(\delta^{\mu}_{\theta} + \frac{i}{\sin\theta}\delta^{\mu}_{\phi}\right), \\ \bar{m^{\mu}} &= \frac{1}{\sqrt{2h(r)}}\left(\delta^{\mu}_{\theta} - \frac{i}{\sin\theta}\delta^{\mu}_{\phi}\right). \end{aligned}$$

The first two null tetrads, l and m, are real vectors while m is complex and $\bar{m}$ is conjugate of vector m. These vectors are orthogonal, isotropic and normalized i.e they satisfy the following conditions

$$\begin{aligned} l^{\mu}l_{\mu} = n^{\mu}n_{\mu} = m^{\mu}m_{\mu} = \bar{m}^{\mu}\bar{m}_{\mu} = 0, \\ l^{\mu}m_{\mu} = l^{\mu}\bar{m}_{\mu} = n^{\mu}m_{\mu} = n^{\mu}\bar{m}_{\mu} = 0, \\ l^{\mu}n_{\mu} = -m^{\mu}\bar{m}_{\mu} = 1. \end{aligned}$$

Introducing complex coordinate transformations

$$\begin{aligned} u' &\rightarrow u - ia\cos\theta, \\ r' &\rightarrow r + ia\cos\theta, \end{aligned}$$

where a is the rotational parameter. It is also assumed that due to these transformations the functions $A_1(r)$, $A_2(r)$ and $h(r)$ shift to $F_1 = F_1(r, a, \theta)$, $F_2 = F_2(r, a, \theta)$ and $\Sigma = \Sigma(r, a, \theta)$ respectively.

This leads to new null tetrads (dropping primes) as

$$\begin{aligned} l^{\mu} &= \delta^{\mu}_{r}, \\ n^{\mu} &= \sqrt{\frac{F_2}{F_1}}\,\delta^{\mu}_{u} - \frac{F_2}{2}\delta^{\mu}_{r}, \\ m^{\mu} &= \frac{1}{\sqrt{2\Sigma}}\left[\left(\delta^{\mu}_{u} - \delta^{\mu}_{r}\right) ia\sin\theta + \delta^{\mu}_{\theta} + \frac{i}{\sin\theta}\delta^{\mu}_{\phi}\right], \\ \bar{m^{\mu}} &= \frac{1}{\sqrt{2\Sigma}}\left[-\left(\delta^{\mu}_{u} - \delta^{\mu}_{r}\right) ia\sin\theta + \delta^{\mu}_{\theta} - \frac{i}{\sin\theta}\delta^{\mu}_{\phi}\right]. \end{aligned} \tag{A.3}$$

With the help of Eq. (A.2) and Eq. (A.3), contravariant components of new metric are computed as

$$\begin{aligned} g^{uu} &= \frac{a^2\sin^2\theta}{\Sigma},\ g^{u\phi}=\frac{a}{\Sigma},\ g^{ur}=-\sqrt{\frac{F_2}{F_1}}-\frac{a^2\sin 2\theta}{\Sigma}, \\ g^{rr} &= F_2+\frac{a^2\sin^2\theta}{\Sigma},\ g^{r\phi}=-\frac{a}{\Sigma},\ g^{\theta\theta}=\frac{1}{\Sigma}, \\ g^{\phi\phi} &= \frac{1}{\Sigma\sin^2\theta}. \end{aligned}$$

Using the above contravariant components, the non-zero covariant components are

$$\begin{aligned} g_{uu} &= -F_1,\ g_{ur}=-\sqrt{\frac{F_1}{F_2}},\ g_{u\phi}=a\sin^2\theta\left(F_1-\sqrt{\frac{F_1}{F_2}}\right), \\ g_{r\phi} &= a\sqrt{\frac{F_1}{F_2}}\sin^2\theta,\ g_{\theta\theta}=\Sigma,\ g_{\phi\phi}=\sin^2\theta\left[\Sigma-a^2\left(F_1-2\sqrt{\frac{F_1}{F_2}}\right)\sin^2\theta\right]. \end{aligned}$$

So new metric is

$$\begin{aligned} ds^2 &= -F_1du^2-2\sqrt{\frac{F_1}{F_2}}dudr+2a\sin^2\theta\left(F-\sqrt{\frac{F_1}{F_2}}\right)dud\phi+2a\sin^2\sqrt{\frac{F_1}{F_2}}drd\phi+\Sigma d\theta^2 \\ &+ \sin^2\theta\left[\Sigma-a^2\left(F-2\sqrt{\frac{F_1}{F_2}}\right)\sin^2\theta\right]d\phi^2. \end{aligned}$$

Finally, the EF coordinates are transformed back to BL coordinates. For this purpose the following transformation is being used

$$\begin{aligned} du &= dt+\lambda(r)dr, \\ d\phi &= d\phi'+\chi(r)dr, \end{aligned}$$

where

$$\lambda(r)=\frac{-a^2-k(r)}{A_2(r)h(r)+a^2},\ \chi(r)=\frac{-a}{A_2(r)h(r)+a^2},\ k(r)=\sqrt{\frac{A_2(r)}{A_1(r)}}h(r),$$

with

$$F_1 = \frac{A_2(r)h(r)+a^2\cos^2\theta}{\left(k(r)+a^2\cos^2\theta\right)^2}\Sigma \tag{A.4}$$

and

$$F_2 = \frac{A_2(r)h(r) + a^2\cos^2\theta}{\Sigma}. \tag{A.5}$$

Thus an RBH solution in BL coordinates turns out to be

$$\begin{aligned} ds^2 &= -\frac{A_2(r)h(r) + a^2\cos^2\theta}{\left(k(r) + a^2\cos^2\theta\right)^2}\Sigma dt^2 + 2a\sin^2\theta\frac{A_2(r)h(r) - k}{\left(k(r) + a^2\cos^2\theta\right)^2}\Sigma dt d\phi + \frac{\Sigma}{A_2(r)h(r) + a^2}dr^2 + \Sigma d\theta^2 \\ &+ \Sigma\sin^2\theta\left[1 + a^2\sin^2\theta\frac{2k(r) - A_2(r)h(r) + a^2\cos^2\theta}{\left(k(r) + a^2\cos^2\theta\right)^2}\right]d\phi^2. \end{aligned}$$

Since $A_1(r) = A_2(r)$, so $k(r) = h(r)$. Comparison of Eq. (A.4) and Eq. (A.5) gives $\Sigma = r^2 + a^2\cos^2\theta$. Hence the rotational solution of a black hole is obtained.

In Asymptotically Safe Gravity Theory

For the case taken in section (2.2.1), we have

$$A_1(r) = A_2(r) \simeq 1 - \frac{2M}{r}\left(1 - \frac{\tilde{\xi}}{r^2}\right) \text{ and } h(r) = r^2.$$

and the metric obtained from using Newman-Janis algorithm is given by

$$\begin{aligned} (ds)^2 &= -\Big(1 - \frac{2Mr}{\Sigma}\Big(1 - \frac{\tilde{\xi}}{r^2}\Big)\Big)dt^2 - \frac{4aMr\sin^2\theta}{\Sigma}\Big(1 - \frac{\tilde{\xi}}{r^2}\Big)dt d\phi + \frac{\Sigma}{\Delta}dr^2 + \Sigma d\theta^2 \\ &+ \sin^2\theta\left[r^2 + a^2 + \frac{2a^2Mr}{\Sigma}\sin^2\theta\Big(1 - \frac{\tilde{\xi}}{r^2}\Big)\right]d\phi^2, \end{aligned}$$

where $\Delta = r^2 - 2Mr + \frac{2M\tilde{\xi}}{r} + a^2$. This metric reduces to its static and spherically symmetric version when $a \to 0$.

An RDBH with Global Monopole in Perfect Fluid

For the case taken in section (5.2), we have $A_1(r), A_2(r) \to f(r)$ where

$$f(r) = 1 - 8\pi\gamma^2 - \frac{2M}{r} + \frac{Q_E^2}{r^2} + \frac{Q_M^2}{r^2} - \frac{v}{r^{3\omega+1}}. \tag{A.6}$$

The metric thus obtained from the Newman-Janis algorithm is given by

$$\begin{aligned} ds^2 &= -\left(1-\frac{r^2(1-f(r))}{\Sigma}\right)dt^2 - 2a\sin^2\theta\left(\frac{r^2(1-f(r))}{\Sigma}\right)dtd\varphi + \frac{\Sigma}{\Delta}dr^2 + \Sigma d\theta^2 \\ &+ \sin^2\theta\left[\frac{(r^2+a^2)^2 - a^2\Delta\sin^2\theta}{\Sigma}\right]d\varphi^2. \end{aligned} \tag{A.7}$$

where in order to simplify the notation we introduce the following quantity

$$\Delta = r^2 f(r) + a^2 = r^2 + a^2 - 2Mr - 8\pi r^2\gamma^2 + Q_E^2 + Q_M^2 - \frac{v}{r^{3\omega-1}}, \tag{A.8}$$

For $a = 0$, the above metric is reduced to its static and spherically symmetric counter part.

Bibliography

[1] V. Frolov, I. D. Novikov, *Black Hole Physics: basic concepts and new developments*, Springer Science & Business Media (2012).

[2] I. D. Novikov, *Black Holes and the Universe*, Cambridge University Press (1990).

[3] K. Schwarzschild, General Relativity and Gravitation, **35**, 5 (2003).

[4] Y. Hagihara, Japanese Journal of Astronomy and Geophysics, **8**, 67 (1931).

[5] H. Reissner, Annals of Physics , **355**, 9 (1916).

[6] G. Nordström, Koninklijke Nederlandsche Akademie van Wetenschappen Proceedings, **20**, 2 (1918).

[7] J. Lense and H. Thirring, Physical Journal, **19**, 156 (1918).
B. Mashhoon, F. W. Hehl and D. S. Theiss, Gen. Relat. Gravit. **16**, 711 (1984).

[8] R.P. Kerr, Physical Review Letters, **11**, 5 (1963).

[9] B. Carter, Physical Review, **174**, 5 (1968).

[10] B. Carter, General Relativity and Gravitation, **41**, 12 (2009).

[11] S. Chandrasekhar, *The Mathematical Theory of Black Holes*, Oxford University Press (1998).

[12] G. Slezáková, *Geodesic Geometry of Black Holes* (Doctoral dissertation, The University of Waikato).

[13] E. Hackmann, *Geodesic Equations in Black Hole Space-times with Cosmological Constant*, doctoral dissertation, Universität Bremen (2010).

[14] P. Pradhan, Class. Quant. Grav. **32**, 16 (2015).

[15] M. Sharif, S. Iftikhar, European Physical Journal Plus, **131**, 12 (2016).

[16] J. L. Synge, Monthly Notices of the Royal Astronomical Society, **131**, 463 (1966).

[17] J. M. Bardeen, In Black Holes (Les Astres Occlus), p. 215-239 (1973).

[18] J. P. Luminet, Astronomy and Astrophysics, **75**, 228 (1979).

[19] J. P. Luminet, arXiv:1902.11196 (2019).

[20] A. de Vries, Classical and Quantum Gravity, **17**, 123 (2000)

[21] K. Hioki and K. I. Maeda, Physical Review D **80**, 2 (2009).

[22] A. Abdujabbarov, F. Atamurotov, Y. Kucukakca, B. Ahmedov, and U. Camci, Astrophysics and Space Science, **344**, 429 (2012).

[23] L. Amarilla, E. F. Eiroa, and G. Giribet, Physical Review D, **81**, 12 (2010).

[24] L. Amarilla and E. F. Eiroa, Physical Review D, **85**, 6 (2012).

[25] L. Amarilla and E. F. Eiroa, Physical Review D, **87**, 4 (2013).

[26] S.W. Wei and Y.X. Liu, Journal of Cosmology and Astroparticle Physics, **2013**, 063 (2013).

[27] M. Amir, K. Jusufi, A. Banerjee and S. Hansraj, Classical and Quantum Gravity, **36**, 21 (2019).

[28] M. Amir, B. P. Singh and S. G. Ghosh, European Physical Journal C, **78**, 399 (2018).

[29] R. Shaikh, Physical Review D, **98**, 024044 (2018).

[30] R. Shaikh, P. Kocherlakota, R. Narayan and P. S. Joshi, Monthly Notices of the Royal Astronomical Society, **482**, 52 (2019).

[31] G. Gyulchev, P. Nedkova, V. Tinchev and S. Yazadjiev, European Physical Journal C, **78**, 544 (2018).

[32] G. Gyulchev, P. Nedkova, V. Tinchev and Stoytcho Yazadjiev, American Institute of Physics Conference Proceedings, **2075**, 040005 (2019).

[33] A. Abdujabbarov, M. Amir, B. Ahmedov and S. G. Ghosh, Physical Review D, **93**, 104004 (2016).

[34] A. Abdujabbarov, B. Juraev, B. Ahmedov and Z. Stuchlík, Astrophysics and Space Science, **361**, 226 (2016).

[35] M. Amir, A. Banerjee and S. D. Maharaj, Annals of Physics, **400**, pp-198 (2019).

[36] C. Bambi and K Freese, Physical Review D, **79**, 043002 (2009).

[37] A. E. Broderick, T. Johannsen, A. Loeb and D. Psaltis, The Astrophysical Journal **784**, 7 (2014).

[38] T. Johannsen, A. E. Broderick, P. M. Plewa, et al., Physical Review Letters, **116**, 031101 (2016).

[39] Y. Mizuno, Z.Younsi, C. M. Fromm, et al., Nature Astronomy, **2**, 585 (2018).

[40] P. V. P. Cunha and C. A. R. Herdeiro, General Relativity and Gravitation, **50**, 42 (2018).

[41] B. P. Abbott et. al. Physical Review Letters, **116**, 6 (2016).

[42] R. Abbott et. al. arXiv:2010.14527 (2020).

[43] M. Volonteri, P. Madau, E. Quataert and M. J. Rees, The Astrophysical Journal, **620**, 69 (2005).

[44] R. D. Blandford and R.L. Znajek, Monthly Notices of the Royal Astronomical Society, **179**, 433 (1977).
A.C. Fabian, Annual Review of Astronomy and Astrophysics, **50**, 455 (2012).

[45] M. C. Miller and J. M. Miller, Physics Reports, **548**, 1 (2015).

[46] C. Bambi, "*Astrophysical Black Holes: A Review*". arXiv:1906.03871. (2019)

[47] X. Hou, Z. Xu, M. Zhou, J. Wang, Journal of Cosmology and Astroparticle Physics, **2018**, 07 (2018).

[48] B. Pratap Singh, arXiv:1711.02898 (2017).

[49] A. Abdujabbarov, B. Toshmatov, Z. Stuchlík and B. Ahmedov, International Journal of Modern Physics D, 26, 1750051 (2017).

[50] R. A. Konoplya, Physics Letters B, **795**, 01 (2019).

[51] K. Jusufi, M. Jamil, P. Salucci, T. Zhu and S. Haroon, Physical Review D, **100**, 4 (2019).

[52] K. Akiyama *et al.* [Event Horizon Telescope Collaboration], The Astrophysical Journal, **875**, no. 1, L1 (2019).

[53] K. Akiyama *et al.* [Event Horizon Telescope Collaboration], The Astrophysical Journal, **875**, no. 1, L6 (2019)

[54] B. P. Abbott et al., Physical Review Letters, **119**, 16 (2017).

[55] B. P. Abbott et al., The Astrophysical Journal Letters, **848**, 2 (2017).

[56] B. P. Abbott et al., Physical Review X, **9**, 3 (2019).

[57] Y. Aso, Y. Michimura, K. Somiya, M. Ando, O. Miyakawa, T. Sekiguchi, D. Tatsumi, H. Yamamoto, et al., Physical Review D, **88**, 4 (2013).
P. Amaro-Seoane, H. Audley, S. Babak, J. Baker, E. Barausse, P. Bender, E. Berti, P. Binetruy, M. Born, D. Bortoluzzi, et al., arXiv:1702.00786 (2017).
J. Hough, Progress in Particle and Nuclear Physics, **66**, 2 (2011).

[58] J.E. McClintock, R. Shafee, R. Narayan, R.A. Remillard, S.W. Davis, L.X. Li, The Astrophysical Journal, **652**, 518 (2006).

[59] E. Berti, M. Volonteri, The Astrophysical Journal, **684**, 2 (2008).

[60] C. S. Reynolds, arXiv:2011.08948 (2020).

[61] S. Haroon, M. Jamil, K. Lin, P. Pavlovic, M. Sossich and A. Wang, The European Physical Journal C, **78**, 6 (2018).

[62] S. Haroon, M. Jamil, K. Jusufi, K. Lin, R. B. Mann, Physical Review D, **99**, 4 (2019).

[63] S. Haroon, K. Jusufi, M. Jamil, Universe, **6**, 4 (2020).

[64] A. Grenzebach, V. Perlick, and C. L*ä*mmerzahl, Physical Review D, **89**, 124004 (2014).

[65] A. Grenzebach, V. Perlick, and C. L*ä*mmerzahl, International Journal of Modern Physics D, **24**, 1542024 (2015).

[66] A. Grenzebach, Equations of Motion in Relativistic Gravity, **179** (2015).

[67] O. Yu. Tsupko, Physical Review D, **95**, 104058 (2017).

[68] A. Grenzebach, V. Perlick and C. Lämmerzahl, Physical Review D, **89**, 124004 (2014).

[69] C. Rovelli, Living Reviews in Relativity, **11**, 5 (2008).

[70] D. W Chiou, Journal of Modern Physics D, **24**, 1 (2015).

[71] K. R. Dienes, Physics Report, **287**, 447 (1997).

[72] S. Mukhi, Classical and Quantum Gravity, **28**, 153001 (2011).

[73] S. Nojiri, S. D. Odintsov, International Journal of Geometric Methods in Modern Physics, **04**, 115 (2007).

[74] T. Clifton, P. G. Ferreira, A. Padilla, C. Skordis, Physics Report, **513**, 1 (2012).

[75] K. Koyama, Report on Progress in Physics, **79**, 046902 (2016).

[76] Z. Bern, Living Reviews in Relativity, **5**, 5 (2002).

[77] S. Weinberg, S. W. Hawking and W. Israel, eds. *In General Relativity: An Einstein Centenary Survey*, Cambridge University Press, 790-831 (1979).

[78] M. Niedermaier, M. Reauter, Living Reviews in Relativity, **9**, 5 (2006).

[79] Y. F. Cai, D.A. Easson, Journal of Cosmology and Astroparticle Physics, **09**, 002 (2010).

[80] A. Bonanno, M. Reuter, Physical Review D, **60**, 084011 (1999)

[81] A. Bonanno, M. Reuter, Physical Review D, **73**, 083005 (2006)

[82] C. Gonz*á*lez, B. Koch, International Journal of Modern Physics A, **31**, 26 (2016).

[83] Á. Rincòn, B. Koch, I. Reyes, Journal of Physics: Conference Series, **831**, 1 (2017).

[84] K. Falls, D. F. Litim, A. Raghuraman, International Journal of Modern Physics A, **27**, 5 (2012).

[85] F. Saueressig, N. Alkofer, G. D'Odorico, F. Vidotto, Proc. Sci. FFP **14**, 174 (2015).

[86] K. Falls and D. F. Litim, Physical Review D, **89**, 8 (2014).

[87] D. F. Litim and K. Nikolakopoulos, Journal of High Energy Physics, **4**, 21 (2014).

[88] K. Falls, D. F. Litim, K. Nikolakopoulos and C. Rahmede, Physical Review D, **93**, 10 (2016).

[89] M. Azreg-Aïnou, Physical Review D, **90**,6 (2014).

[90] M. Reuter and E. Tuiran, Physical Review D, **83**, 4 (2011).

[91] V. C. Rubin, Jr. W. K. Ford and N. Thonnard, The Astrophysical Journal, **238**, 471 (1980).

[92] F. Zwicky, Helvetica Physica Acta, **6**, 110 (1933).

[93] Planck Collaboration: P. A. R. Ade, N. Aghanim, et al., Astronomy and Astrophysics, 571, A16 (2014).

[94] T. W. B. Kibble, Journal of Physics A, **9**, 1387 (1976).

[95] M. Barriola and A. Vilenkin, Physical Review Letters, **63**, 341 (1989).

[96] K. Jusufi, M. C. Werner, A. Banerjee and A. Ovgun, Physical Review D, **95**, 104012 (2017).

[97] T. Ono, A. Ishihara and H. Asada, Physical Review D, **99**, 12 (2019).

[98] M. P. Hobson, G. P. Efstathiou and A.N. Lasenby, *General Relativity: An Introduction for Physicists*, Cambridge University Press (2006).

[99] Z. Xu, X. Hou and J. Wang, Classical and Quantum Gravity, **35**, 115003 (2018).

[100] H. Goldstein, C. Poole and J. Safko, *Classical Mechanics* (2002).

[101] M. Reuter, Physical Review D, **57**, 02 (1998).

[102] A. Bonanno and M. Reuter, Physical Review D, **62**, 043008 (2000).

[103] B. Toshmatov, Z. Stuchlik, B. Ahmedov, European Physical Journal Plus, **132**, 98 (2017).

[104] M. Sharif, S. Iftikhar, European Physical Journal Plus, **131**, 427 (2016).

[105] J.B. Hartle, *Gravity: An Introduction to Einstein's General Relativity*, Pearson, Upper Saddle River, (2009).

[106] S. J. Clark and R. W. Tucker, Classical and Quantum Gravity, **17**, 19 (2000).

[107] C. Chakraborty and P. Majumdar, Classical and Quantum Gravity, **31**, 7 (2014).

[108] C. Chakraborty, P. Kocherlakota and P. S. Joshi, Physical Review D, **95**, 4 (2017).

[109] C. Chakraborty, P. Kocherlakota, M. Patil, S. Bhattacharyya, P. S. Joshi, A. Królak, Physical Review D, 95, 8 (2017).

[110] W. G. Ramírez and A. A. Deriglazov, Physical Review D, **96**, 12 (2017).

[111] Gravity Collaboration, Astronomy and Astrophysics, **602**, 94 (2017).

[112] V. V. Kiselev, Classical and Quantum Gravity, **21**, 13 (2004).

[113] M. H. Li and K. C. Yang, Physical Review D, **86**, 123015 (2012).

[114] B. Carter, Communications in Mathematical Physics, **10**, 280 (1968).

[115] G. W. Gibbons and M. C. Werner, Classical and Quantum Gravity, **25**, 235009 (2008).

[116] M. C. Werner, General Relativity and Gravitation, 44, 3047 (2012).

[117] K. Jusufi, International Journal of Geometric Methods in Modern Physics, **14**, 12 (2017).

[118] K. Jusufi, Physical Review D, **98**, 064017 (2018)

[119] K. Jusufi, Physical Review D, **98**, 044016 (2018)

[120] K. Jusufi, F. Rahaman and A. Banerjee, Annals of Physics, **389**, 219 (2018)

[121] K. Jusufi, N. Sarkar, F. Rahaman, A. Banerjee and S. Hansraj, European Physical Journal C, **78**, 349 (2018)

[122] K. Jusufi, M. C. Werner, A. Banerjee and A. Ovgun, Physical Review D, **95**, 10 (2017).

[123] R. M. Teixeira Filho and V. B. Bezerra, Phyical Review D, **64**, 084009 (2001).

[124] S. Haroon, M. Jamil, K. Jusufi, K. Lin and R. B. Mann, Physical Review D, **99**, 044015 (2019).

[125] Z.Xu, X. Hou and J. Wang, Journal of Cosmology and Astroparticle Physics, **10**, 046 (2018).

[126] H. Erbin, Universe, **3**, 1(2017).

[127] E. T. Newman and A. I. Janis, Journal of Mathematical Physics, **6**, 915 (1965).

[128] N. Dadhich, K. Narayan and U. A. Yajnik, Pramana – Journal of Physics, **50**, 307 (1998).

[129] S. Haroon, M. Jamil, K. Lin, P. Pavlovic, M. Sossich and A. Wang, European Physical Journal C, **78**, 519 (2018).

[130] Y. Heydarzade and F. Darabi, Physics Letters B, **771**, 365 (2017).

[131] Suvankar Dutta, Akash Jain, Rahul Soni, Journal of High Energy Physics, **2013**, 60 (2013).

[132] S. E. Vazquez and E. P. Esteban, Nuovo Cimento B Serie, **119**, 489 (2004).

[133] S.M. Carroll, *Spacetime and Geometry*, Cambridge University Press (2019).

[134] T. Johannsen, The Astrophysical Journal, **777**, 2 (2013).

[135] J. B. Griffiths, J. Podolskỳ, *Exact Space-Times in Einstein's General Relativity*, Cambridge University Press, (2009).

[136] C. Bambi, European Physical Journal C, **75**, 1 (2015).

[137] J.M. Bardeen, Nature **226**, 64 (1970).